# A $LiNbO_3$ OPTICAL PARAMETRIC SYSTEM: DESIGN, CONSTRUCTION AND PERFORMANCE.

by

A.J.Turner

This thesis submitted for the Degree of Doctor of Philosophy.

May 1980.

# A $LiNbO_3$ PARAMETRIC SYSTEM: DESIGN, CONSTRUCTION AND PERFORMANCE.

by

A.J.Turner

Ph.D. Thesis 1980

UNIVERSITY OF SOUTHAMPTON

ABSTRACT

FACULTY OF ENGINEERING

ELECTRONICS

Doctor of Philosophy

# A $LiNbO_3$ OPTICAL PARAMETRIC SYSTEM: DESIGN, CONSTRUCTION AND PERFORMANCE.

by Andrew James Turner

This thesis describes the design and operation of a flexible optical parametric oscillator based system, which provides a tunable coherent source of near and middle infrared radiation. The system is suitable for use in applications such as high energy spectroscopy and photo-excitation.

The system design has concentrated on obtaining a narrow linewidth and high output energy from the Nd:YAG laser pumped $LiNbO_3$ OPO throughout its tuning range, with the ability to extend operation to longer wavelengths by down-conversion. An important consideration has been to make control and tuning of the system as simple as possible for the experimenter; this has been achieved by the use of motorised tuning mechanisms and programmed digital-processor based electronics. Several features, including the non-linear characteristics of the tuning elements, have been incorporated into the processor software, allowing a simplification of the design of the drive mechanisms and interface electronics to be made.

Included are measurements of the performance of the system, including those of the output energy, linewidth, beam divergence and the effects of incorrect tracking between tuning elements. With grating tuning alone, the OPO produces millijoule output pulses of $\sim 3cm^{-1}$ linewidth from 1.45μm to 4μm, while the down-converter produces microjoule outputs from 4μm to 24μm. The linewidths of the OPO and down-converter are reduced to $\sim 0.1\ cm^{-1}$ by the addition of an etalon.

The results of some demonstration experiments using the source are also presented, these giving indirect indications of the whole system performance.

LIST OF CONTENTS

# CHAPTER 1

## Introduction

The Optical Parametric Oscillator (OPO) was one of the earliest devices capable of generating widely tunable coherent radiation in the visible and near infra-red regions. However, in the period following the first demonstration (1), the device has gained a reputation for being costly, difficult to use and unreliable. Many of the reported OPOs have been plagued by materials problems, and been short lived. The non-linear material which has proved the most successful is lithium niobate ($LiNbO_3$), and between 1969 and 1975, many devices were successfully built using this material, usually using non-critical phase-matching in conjunction with a suitable visible pump laser. Such a device is described by Wallace (2); it was manufactured commercially by Chromatix Inc. of California. These OPOs were primarily limited by the low visible pump beam intensities which can be handled by $LiNbO_3$ without refractive index damage (3) or non-linear absorption (4), and also by the slow scan rate arising from the use of temperature tuning, although the use of tunable dye laser pumping (5) later removed this particular limitation.

Pumping of $LiNbO_3$ at reasonable temperatures by the 1.06$\mu$m line of the Nd:YAG laser, rather than by its visible second harmonic requires a phase-matching angle of about $45^\circ$- $50^\circ$. Until 1974, the longest available $45^\circ$ $LiNbO_3$ crystals were only 1 or 2 cm long, but in 1974 it was realised (6) that high quality boules of $LiNbO_3$ could be grown perpendicular to the (01.4) or (01.3) crystallographic planes. Much longer $45^\circ$ crystals could be cut from these boules, approximately parallel to the growth direction, and this increase in crystal length made efficient and reliable infra-red pumping of $LiNbO_3$ possible. At 1.06$\mu$m, the problems of refractive index damage and non-linear absorption do not occur, and the material can safely handle single pass intensities of $4J/cm^2$ ($200MW/cm^2$) or greater. This results in high parametric gain and large conversion efficiencies, making up more than adequately for the reduction in the gain coefficient for 1.06$\mu$m pumping, as compared to that for visible pumping of equal intensity.

Simple 2 mirror single-resonant parametric oscillators constructed using this material and pumped at 1.06$\mu$m (e.g. (7)) can have thresholds of oscillation a factor of 20 below the threshold of optical damage.

The main drawback to this simple OPO configuration is the large linewidth of the output, as determined solely by the phase-matching characteristics of the $LiNbO_3$, and which near degenerate can be greater than 50 $cm^{-1}$.

The system described in this thesis is the result of further development of the basic 1.06$\mu$m pumped $LiNbO_3$ OPO, allowing efficient conversion of the pump energy into signal and idler outputs in the range 1.45$\mu$m to 4$\mu$m, but with a linewidth throughout the tuning range of 0.1 $cm^{-1}$. Energies of millijoules per pulse have been obtained on both the signal and idler. Figure 1.1 shows a block diagram of the complete system. Narrowing of the linewidth of the OPO is achieved by the use of a diffraction grating and an angle-tuned etalon as tuning elements in the OPO cavity. The angles of the grating and etalon, and also those for the phase-matching of the $LiNbO_3$ and down-converter crystals, are set by a mini-computer, which allows the OPO to be re-tuned between pump laser pulses in applications such as differential LIDAR or spectroscopic scanning. The system has provision for a crystal down-conversion stage, which generates an output of frequency equal to the difference in frequency between the signal and idler, and therefore allows the basic OPO tuning range to be extended. Using proustite ($Ag_3AsS_3$) or cadmium selenide (CdSe) as the mixing crystals, outputs, generally of microjoules per pulse, are obtainable between 4$\mu$m and 24$\mu$m. Figure 1.2 gives a general impression of the system's output power throughout the complete tuning range of 1.45$\mu$m to 24$\mu$m.

The OPO system described was constructed at Southampton between 1975 and 1978, following the abandonment of the earlier proustite OPO programme (8), because of problems in obtaining proustite of high enough quality. During 1977, a second OPO, based on the design described in this thesis was built at Southampton for the Central Electricity Research Laboratories, Leatherhead. The computer-based tuning control of this OPO is much more sophisticated than that in the original system, to permit faster re-tuning. The mechanical design has also been improved. Following construction of the CERL OPO, the electronic circuits of the original system were rebuilt and rationalised. At the same time, a manually tuned $LiNbO_3$ OPO was designed in collaboration with J K Lasers Ltd of Rugby, and built by them for the Physical Chemistry Department of Cambridge University. This device incorporates several new design features, and is well adapted for commercial manufacture. The description in this thesis refers to the Southampton system, except where stated otherwise.

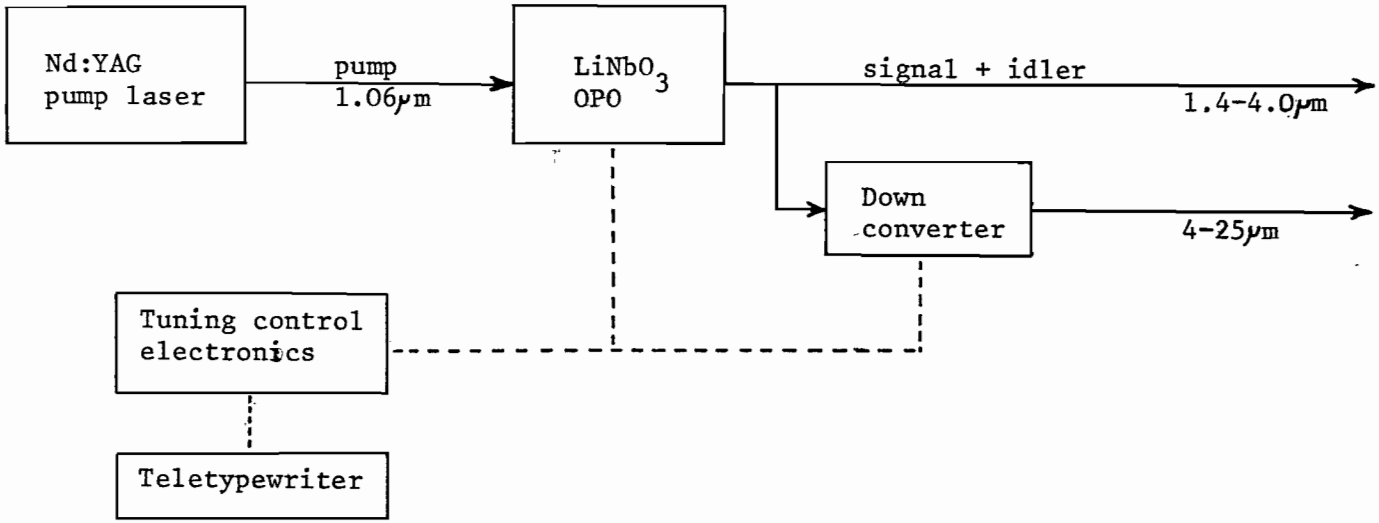


FIGURE 1.1

Block diagram of tunable OPO system.

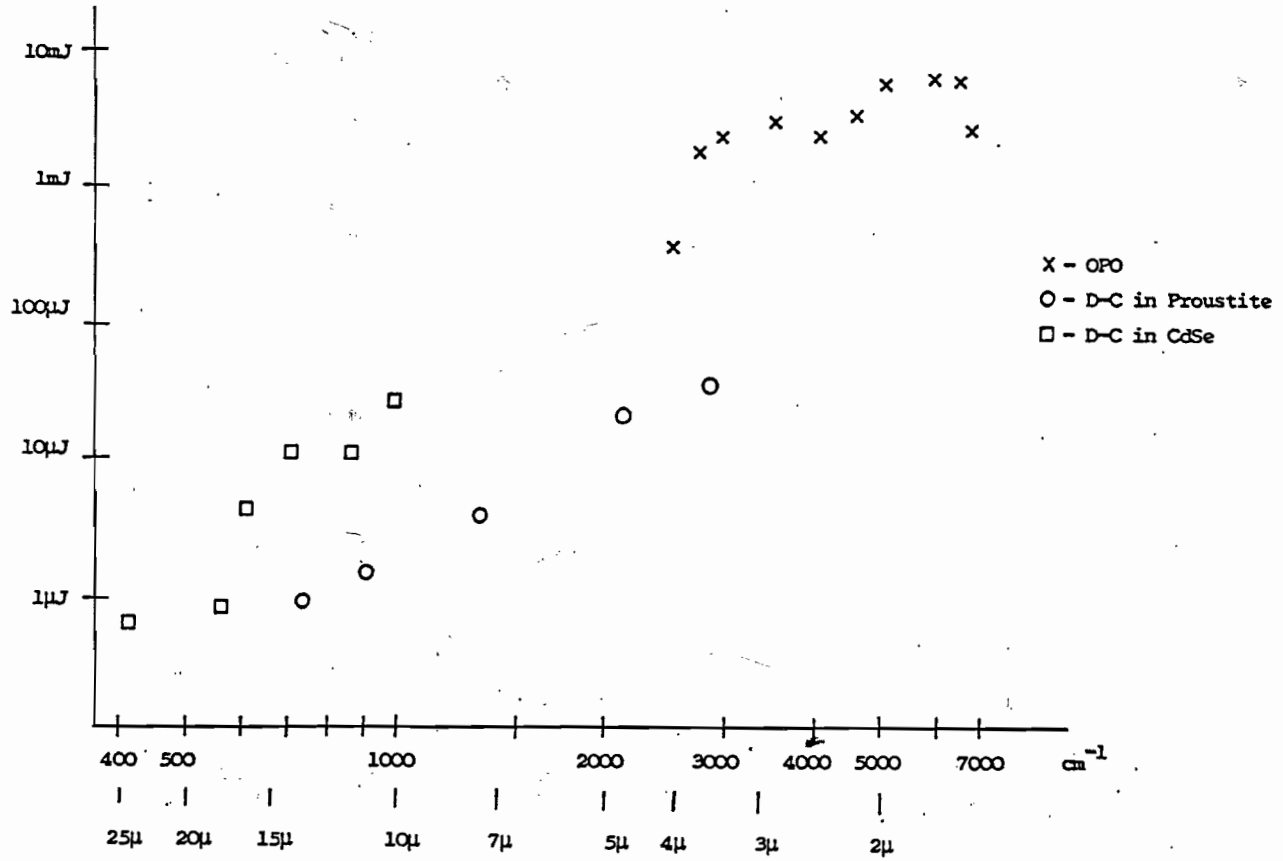


FIGURE 1.2

Composite plot of OPO and down-converter output, as a function of output frequency.

Similar $LiNbO_3$ OPOs, some with down-converters, have been constructed in various parts of the world. Most have been built for use at a fixed wavelength in particular applications and rely on manual tuning. At Stanford University, a computer controlled OPO is in use for atmospheric pollution studies (9). In contrast, the Southampton system has been designed and built as a general purpose source, with ease of use a particular consideration, and it has been used in a number of spectroscopic and photochemical experiments (10).

This thesis deals primarily with the design of the OPO system, and with performance tests carried out on it. Mention is made of some of the demonstration experiments carried out using the tunable outputs; these provided additional information on the characteristics.

Chapter 2 gives an overall view of the system. This is followed, in chapter 3, by a detailed consideration of the design of each part of the system, including the pump laser and control electronics. Chapter 4 deals with the actual performance, particularly measurement of the output beam parameters. Finally, chapter 5 describes some further developments which have been implemented and indicates others which could be investigated. Appendices on the optical alignment of the OPO and on the computer commands are included.

# CHAPTER 2

## System Description

The objective in building the OPO system was to produce a reliable, simple to use tunable source capable of producing coherent outputs in the range 1.45 $\mu$m to 24$\mu$m, with ~0.1 $cm^{-1}$ resolution, and with sufficient energy over the whole range to allow the use of room temperature detectors (such as pyroelectric) in spectroscopic applications. The millijoule outputs obtained in the 1.5 $\mu$m to 3.5 $\mu$m region are adequate for photochemical excitation work.

Figure 2.1 shows a detailed block diagram of the whole system.

The principal element of the system is the OPO, which converts the fixed frequency pump from the Nd:YAG laser chain into a pair of outputs, both tunable in frequency. The basic principles of parametric oscillation and related non-linear optical processes are given in several review papers, including (11) and (12).

The $LiNbO_3$ OPO itself is formed into an 'L' shaped cavity, with the 45° mirror (M1) designed to transmit the pump (1.06 $\mu$m) and totally reflect the resonant signal (1.45 $\mu$m to 2.13 $\mu$m). This arrangement prevents the pump radiation hitting the etalon and grating, both of which are likely to suffer damage if exposed to the full intensity of the pump. The OPO output mirror (M2) is designed to transmit the pump and the idler (2.13 $\mu$m to 4 $\mu$m) and only partially reflect the resonant signal. The third OPO mirror (M3) separates the residual pump from the signal and idler outputs, but, more significantly, returns the unconverted pump back through the $LiNbO_3$. This provides additional signal gain in the 'backward' direction through the crystal, enhancing performance. Alternatively, with such double-pass pumping, the efficiency at a fixed pumping level is increased. It appears, however, that the optical components in the OPO cavity may be more susceptible to optically induced damage, due to standing pump waves. The backward travelling pump is transmitted through the 45° mirror with minimum reflection, and is rejected by the Faraday isolator. The functions of the two mirrors M2 and M3 (figure 2.1) could probably be combined into a single, specially designed coating. The inevitable partial reflection of the idler from these mirrors could give rise to frequency instabilities in the output of the device (e.g. 13), but no observed instability has been attributed to this cause.

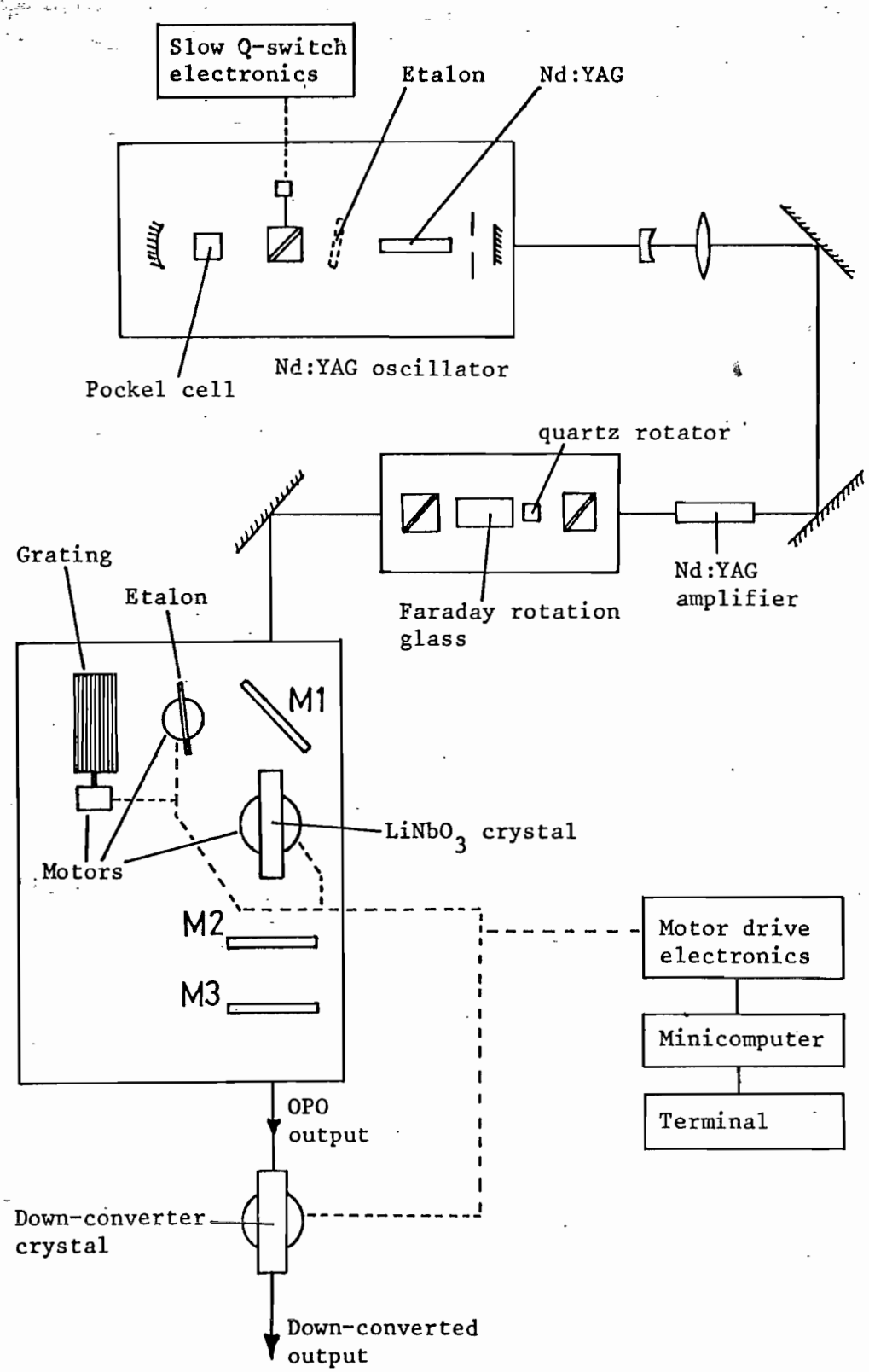


FIGURE 2.1

OPO system : detailed block diagram

The $LiNbO_3$ crystal* is 50mm long and 10mm in diameter, and anti-reflection coated to reduce the reflection losses of the signal to below 2% per surface. The crystal is mounted in a constant temperature oven, set to about 32°C. The calculated plane-plane dynamic threshold of a single-resonant parametric oscillator with such a crystal is about $0.2J/cm^2$. Further calculations show that for cavity losses in the range 10-90%, pump pulses in the range 10-25ns produce the lowest energy threshold. To obtain a usable conversion efficiency, the pump requires to be several times above threshold, and in a beam of diameter large enough to overcome the effects of walk-off over the length of the crystal. A single Nd:YAG $TEM_{oo}$ laser oscillator produces insufficient energy to meet these requirements. The pumping system therefore consists of a Q-switched $TEM_{oo}$ oscillator and a single Nd:YAG amplifier stage, with a Faraday rotation isolator to prevent parasitic oscillation of the amplifier and reject the on axis pump beam reflected from the OPO. The linewidth of the laser oscillator can be reduced as required to less than $0.05cm^{-1}$ by the insertion of an intracavity etalon, assisted by a slow Q-switching arrangement (14).

Setting of the OPO frequency is achieved by fixing the angles of the grating and etalon to correspond to the required signal frequency, and by setting the angle of the $LiNbO_3$ to obtain phase-matching for this frequency. In effect, phase-matching in the $LiNbO_3$ can be considered as an additional tuning element. Its bandwidth is however wavelength dependent, and only induces a narrowing effect when well away from degenerate. The grating, and the $LiNbO_3$ and down-converter crystals, are rotated by drives incorporating stepper motors, connected to a Computer Automation LSI 3/05 minicomputer, while the etalon is similarly rotated by an analogue galvanometer drive. The minicomputer is programmed to calculate the angles of the tuning components corresponding to the frequency requested by the user, and to then set the motors to these positions. The use of the minicomputer eliminates the need for the operator to manually set and optimise the angle of each of the tuning elements whenever the OPO frequency is changed. The timing connection from the laser allows automatic tuning of the OPO to occur between laser pulses.

* $LiNbO_3$ crystals have been obtained from Crystal Technology Inc., California, and from Barr and Stroud Ltd, Glasgow.

The tuning range of the OPO is limited at the long wavelength end to about 4$\mu$m. The high output power from the OPO near degenerate is however well suited to be the input to further non-linear-optical mixing stages, and these can be used to generate wavelengths outside the range covered directly by the OPO. A variety of such mixing stages have been investigated in conjunction with OPO sources by several laboratories; these include second harmonic generation (15) and 3-wave mixing in crystals (16) which together can give coverage from the visible to 25$\mu$m, and 4-wave mixing (17) and stimulated Raman scattering in liquids and gases (18) for which more limited tuning ranges have so far been achieved. In all of these devices, the tunability of the converted output is of course derived from the tunability of the OPO.

The process of difference frequency generation (down-conversion) in crystals is the most interesting of these processes, since the output can cover the spectroscopically important range of 4-24$\mu$m. With an OPO working near degenerate, the signal and idler of a single OPO can be used as the two inputs to the difference frequency mixing stage, thus dispensing with the need for an additional coherent source, as is required when most other forms of tunable laser are used for an input. The linewidth of the down-converted output replicates those of the OPO outputs. The output power is however typically only 0.1% or less of that of the OPO.

The output wavelengths of the signal and idler of the 1.06$\mu$m pumped OPO are suitable for down-conversion in several infra-red non-linear optical materials. Table 2.1 gives the potential tuning range of the more important of these. The system has been designed around two materials, CdSe (10-24$\mu$m) and proustite (4-12$\mu$m), as suitable crystals of these already existed in the Laboratory. Other crystals, including those for S.H.G. can be used by simply changing the computer's internal tuning tables and, if necessary, changing the focusing conditions.

Details of the design of the OPO, pump laser, down-converter and control electronics are given in the next chapter.

TABLE 2.1

| | | |
|---|---|---|
| CdSe | 9.5 - 24μm | 40mm crystals available commercially |
| Proustite | - 12.5μm | 10mm crystals available commercially |
| $AgGaSe_2$ | - 17μm | 40mm crystals have been grown |
| $AgGaS_2$ | - 12μm | Difficult to grow |
| $AgSbS_3$ | - 13μm | Not available commercially |
| $ZnGeP_2$ | - 12μm | Difficult to grow |
| $Tl_3AsSe_3$ | - 17μm | Not available commercially |
| $LiIO_3$ | - 5.5μm | 30mm crystals available commercially |
| $LiNbO_3$ | - 4.5μm | 50mm crystals available commercially |

Down-conversion tuning range of various materials from a 1.06μm pumped OPO. The tuning range quoted for each material is that limited by phase-matching and absorption. Where no short wavelength limit is given, the range overlaps with that of the OPO idler.

# CHAPTER 3

## System Design

### 3.1 Pump Laser

The laser system for pumping the OPO consists of a Q-switched $TEM_{oo}$ Nd:YAG oscillator, a single Nd:YAG amplifier and a Faraday isolator (figure 2.1). The oscillator, which had been previously used as the pump source in the proustite OPO programme, is of a fairly standard design (Laser Associates Model 252), consisting of a 3" x ¼" flashlamp pumped Nd:YAG rod and a KD*P Pockel cell for Q-switching. The oscillator's output energy is typically 8mJ per pulse, and the pulse length is about 15ns (FWHM). The unnarrowed linewidth is $\sim 0.5 cm^{-1}$. The pulse repetition rate of the laser oscillator, and hence the whole system, is limited to about 3 p.p.s. by thermal problems in the pumping chamber and the power supply of the laser oscillator.

Although the pump acceptance linewidth of $LiNbO_3$ is large enough for the OPO to be efficiently pumped by the unnarrowed Nd:YAG output, the linewidth of the pump is replicated by the idler, and also by the down-converted output. Narrowing of the pump linewidth to less than about $0.05 cm^{-1}$ is required if idler linewidths of $\sim 0.1 cm^{-1}$ are to be obtained. The technique employed to obtain such narrow pump linewidths involves the use of a combination of an angle-tuned intracavity etalon of $0.33 cm^{-1}$ free spectral range, and a slow Q-switch (14), in which the Pockel cell is held partially open until the circulating field reaches a threshold level, at which time it is opened completely. This technique can reduce laser oscillation to just one longitudinal mode, although this is not necessary for pumping the OPO.

For satisfactory operation of the OPO, the pumping system is required to be stable in both amplitude and frequency. The latter requires that the laser etalon temperature drift be less than $0.02 cm^{-1}$, equivalent to $0.2^{\circ}C$, while the temperature of the Nd:YAG rod must be held constant to about $\pm 2^{\circ}C$. The closed loop cooling of the pumping chamber provides adequate control over the laser rod temperature, but no control of the temperature of the laser etalon has been provided. This leads to a drift in laser frequency of $\sim 0.1 cm^{-1}/^{\circ}C$, with the eventual possibility of oscillation on two adjacent laser etalon modes. Since the minimum linewidth of the OPO is equivalent to about 100 laser longitudinal modes,

no fine control over the laser cavity length is needed.

The beam from the laser oscillator is passed through a 2:1 magnifying telescope so as to give an adequate filling of the beam in the amplifier rod. The amplifier (J K Lasers Ltd Series 2000) uses a 3" x ¼" Nd:YAG rod. In passing through the telescope and amplifier, the beam tends to be spatially distorted, with concentric interference rings arising from the uncoated lenses of the telescope in addition to the effects of saturation and thermal focusing in the amplifier rod.

The Faraday isolator is used to prevent reflections from the OPO re-entering the amplifier, and upsetting the laser amplifier or oscillator. Constructed by J K Lasers Ltd to Southampton University designs, it consists of a 50mm long rod of Hoya FR-5 glass mounted in a pulsed solenoid with two dielectric stack polarisers set at 45° to each other, and a 7mm long block of crystalline quartz, which counteracts the 45° rotation in the isolator glass. Calcite polarisers were originally used in the isolator, but were found to badly distort and attenuate the transmitted beam.

The pump energy available to the OPO is varied by changing the energy to the amplifier flashlamp. The maximum energy available following a single pass of the amplifier is 80mJ, with an effective spot size (full width to $1/e^2$ intensity) of ~1.8mm.

Many of the tests and experiments involving the OPO system used the above single-pass amplifier arrangement. In some instances, when more pump energy was required, two passes of the amplifier rod were made. Such an arrangement is shown in figure 3.1, with the isolator separating the forward and reverse beams as well as performing its isolation duties. The output from this double-pass amplifier is up to 150mJ, but spatial distortions of the amplified beam are considerably greater than with the single pass amplifier. The highest measured OPO output energies were obtained using such a double-pass amplifier arrangement.

An alternative pump source, used mainly during tests of the CERL OPO, was an unstable resonator Nd:YAG laser. Both near-field and far-field pumping were tried; only the latter proved satisfactory (19). Unstable resonator laser pumping was not however adopted for the system because a suitable laser was not available in the long term. Some doubts also remained regarding the alignment stability of the unstable resonator laser.

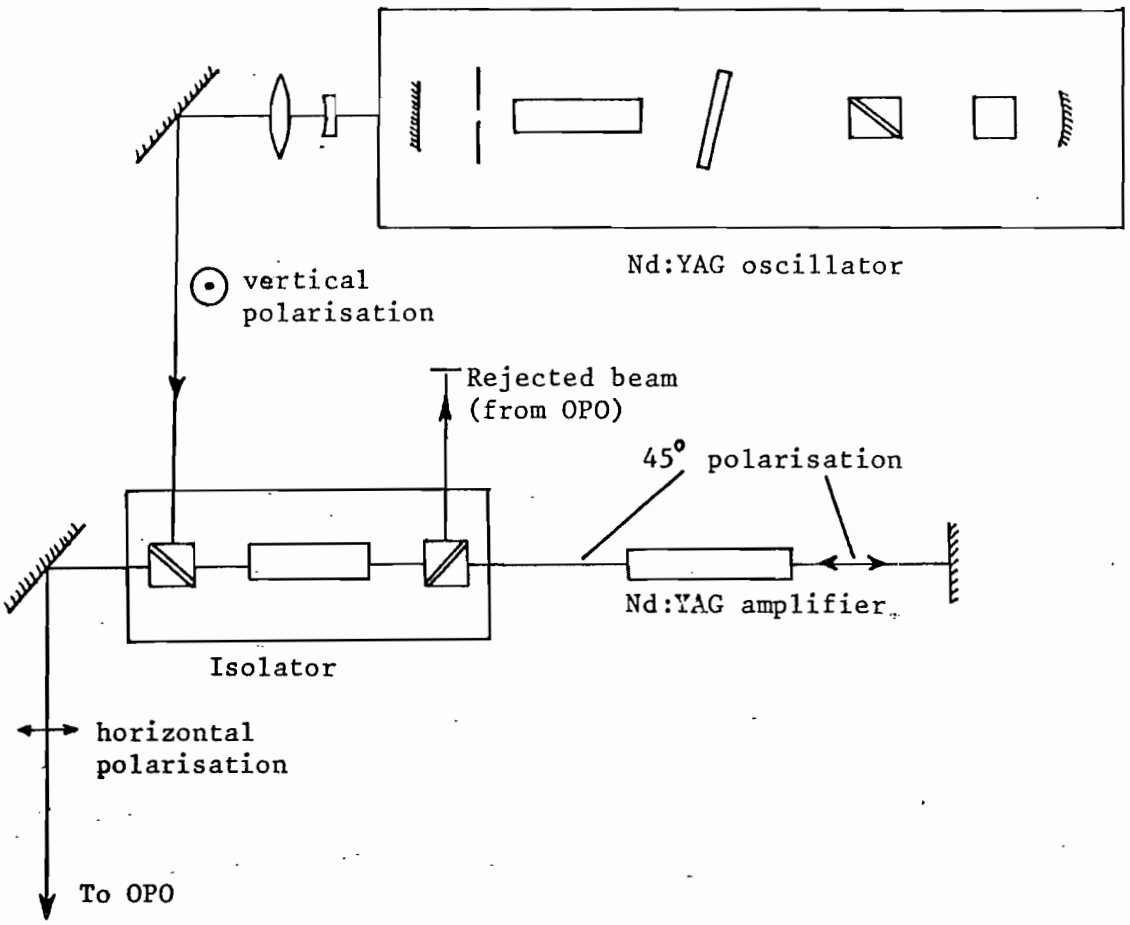


FIGURE 3.1

Double-pass amplifier arrangement.

## 3.2 OPO Cavity Design and Characteristics

### 3.2.1 Design of OPO cavity

The gain-bandwidth and tuning characteristics of $LiNbO_3$ for type I phase-matching are shown in figure 3.2. Type II phase-matching is also possible, but the non-linear coefficient ($d_{eff}$) is too low to allow single-resonant parametric oscillation. When the OPO is operated without any tuning elements, the output linewidth is determined solely by the $LiNbO_3$ phase-matching conditions, and is typically $\frac{1}{3}$ of the gain-bandwidth (12), as a result of the multiple passes through the crystal (gain-narrowing).

Several line narrowing elements have been considered and demonstrated in OPOs, including etalons (20), diffraction gratings and birefringent filters (12). The tuning elements define the operating frequency of the device, although in the case of etalons and birefringent filters, the free spectral range of the filter must be large enough to prevent oscillation on more than one mode of the filter. This requires a F.S.R. of greater than $\sim 50cm^{-1}$ if the OPO is to be used near degenerate, where the $LiNbO_3$ bandwidth is at its greatest. This problem does not occur with diffraction gratings operated in first order. Gratings also have the advantage of being readily available as stock items from suppliers.

One problem with all the tuning elements mentioned above is that they are liable to optically induced damage at the $1.06\mu m$ intensities required to pump the OPO. This means that the resonated signal beam must be physically separated from the pump radiation either by the use of polarising elements or by a dichroic beam splitter.

Because of the availability of replica diffraction gratings, the cavity has been designed to use commercially available 600 lines/mm gold or aluminium overcoated replica gratings, blazed for either $1.9\mu m$ or $1.6\mu m$. Such gratings* are specified by the manufacturers as having a high reflectivity ( >80%) over most of the signal range when the ruled grooves are perpendicular to the signal polarisation. The splitting of the signal from the pump beam (see figure 3.3) is achieved by using a standard quarter-wavelength dielectric stack mirror, made from zinc sulphide and cryolite. The mirror is orientated such that the reflectivity

* obtained from Bausch and Lomb, and from PTR Optics Ltd.

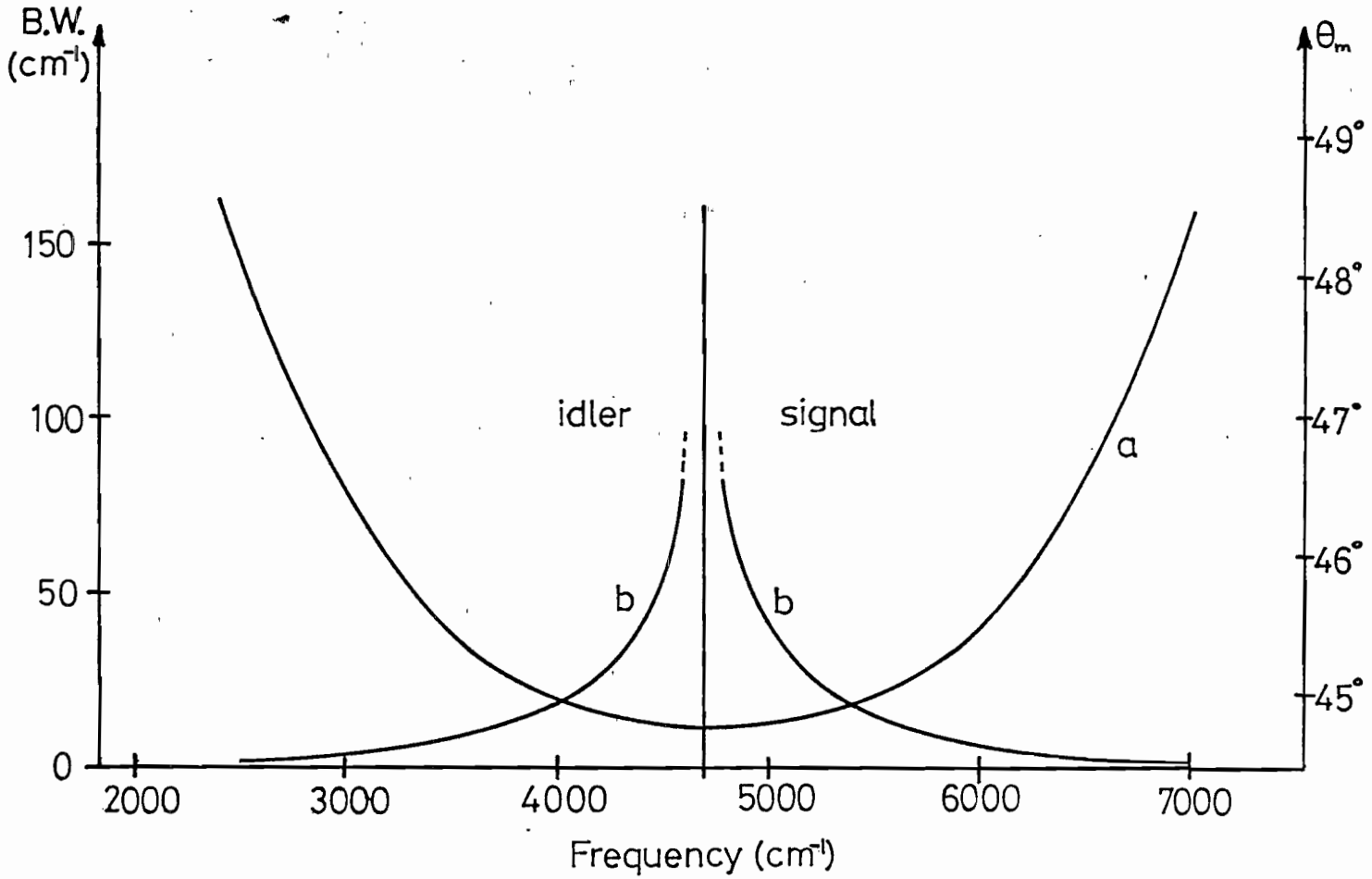


FIGURE 3.2
Phase-matching angle (a) and small signal Gain-Bandwidth (b) of 1.06μm pumped $LiNbO_3$.

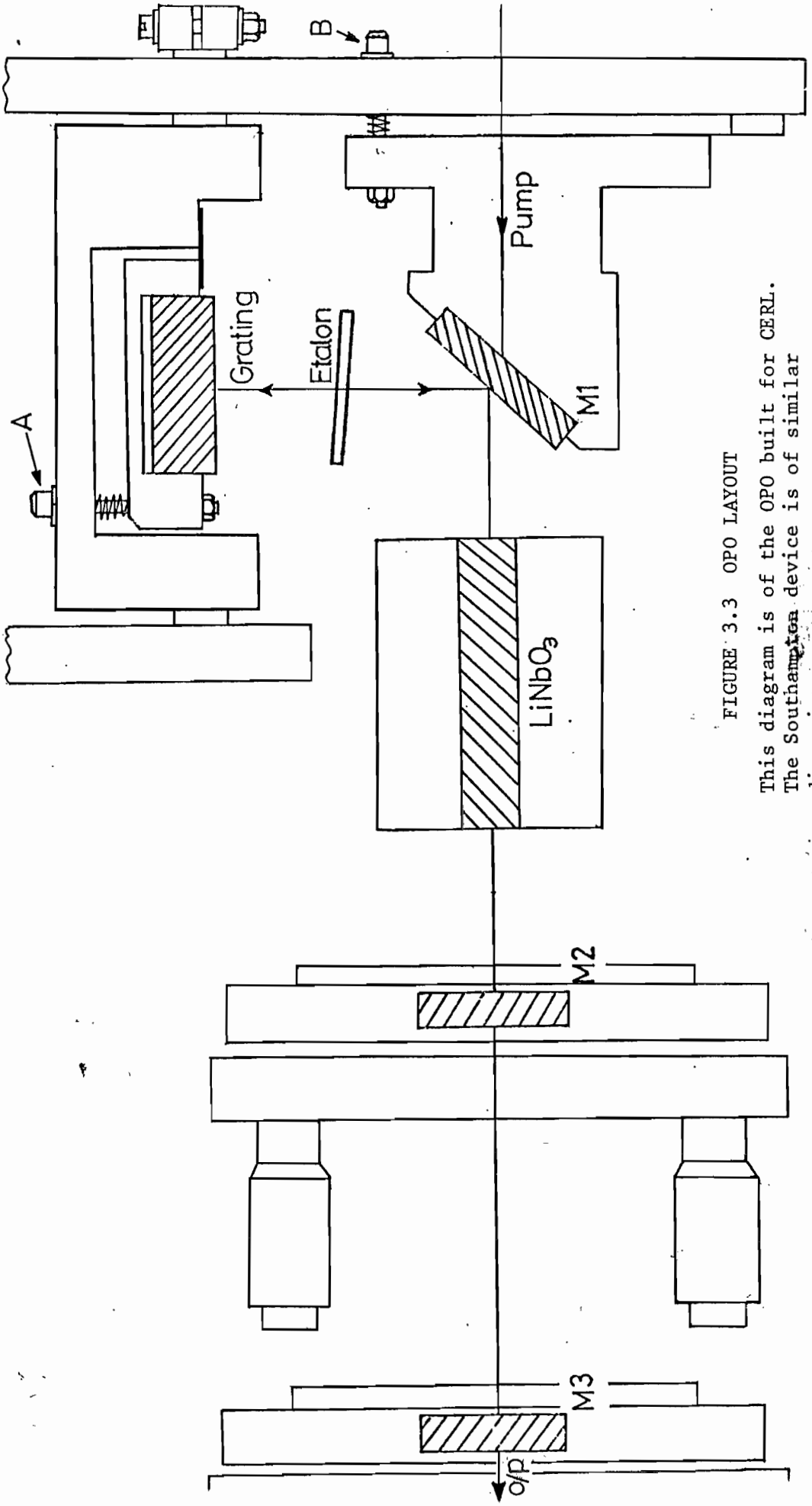


FIGURE 3.3 OPO LAYOUT

This diagram is of the OPO built for CERL. The Southampton device is of similar dimensions.

A & B are for the adjustment of the grating and 45° mirror alignments.

and spectral bandwidth for the s-polarisation signal are both greater than those of normal incidence, while the reflectivities of the pump at both coated and uncoated surfaces of the beam-splitter are less than 1%.

Cryolite and ZnS are both 'soft' coating materials, and are not preferred by commercial manufacturers. However, the ratio range of refractive indices of the 'harder' infra-red coating materials is reduced, making it difficult to manufacture a single $45^{\circ}$ incidence mirror with the wide bandwidth required to cover the whole signal range, without recourse to a 'staggered' stack. An alternative (21) is to use an in-line cavity with the pump radiation coupled into the $LiNbO_3$ by a $45^{\circ}$ mirror pitched to reflect 1.06$\mu$m (s-polarisation) and transmit the signal (p-polarisation). This allows a standard 1.06$\mu$m mirror to be used, provided this has a high transmission between 1.45$\mu$m and 2.13$\mu$m.

The OPO output mirror is required to transmit the pump and idler, and reflect a fraction of the signal. Its reflectivity can be 100% if only the idler output is required, but is normally less to allow some of the signal to be coupled out. The mirror has to have the same reflection bandwidth as the beamsplitter mirror (i.e. 1.45$\mu$m - 2.13$\mu$m) and should ideally have a sharp edge at 2.13$\mu$m, to avoid idler reflection. Because of the high gain in the $LiNbO_3$, and other losses within the cavity, the output energy is not strongly dependent on the actual reflectivity of the output mirror, over a wide range of reflectivities. Two designs have been used for this mirror. For low reflectivities, allowing a high output coupling of the signal, a standard $\lambda/4$ two-layer cryolite/ZnS (SLHA) stack is used although near degenerate this gives a high reflectivity for the idler. The alternative design (SLLHLHA), also constructed from cryolite and ZnS, has a larger signal reflectivity and gives a slightly lower OPO threshold. An extra half-wavelength layer is included to widen the reflection bandwidth and to increase the transmission of the idler.

### 3.2.2 Cavity characteristics

As constructed, the cavity is plane-plane. The gain region of the $LiNbO_3$ is however well defined by the $TEM_{oo}$ pump beam. Due to the effect of 'gain focusing', where the finite diameter of the gain region in the $LiNbO_3$ results in a reduction of the signal beam diameter during amplification, the cavity is effectively stable, although the Fresnel number is such that a multi-transverse mode output is to be expected. The transverse mode structure of the amplified signal beam is affected by the loss experienced by wavefronts of high divergence as a result of phase-mismatch.

With normal single pass pumping, gain is obtained in the $LiNbO_3$ in the direction of pump propagation, while the return pass for the signal through the crystal is purely passive. It has been shown (22) that if the remaining pump is reflected back through the crystal, gain is also obtained in this reverse direction, leading to a reduced threshold of oscillation, and a higher conversion efficiency. In practice, with 1.75μm pitched anti-reflection coatings on the crystal, 10% of the pump is lost by reflection from each crystal face, and the returning pump is therefore of much reduced intensity.

Double-passing of the pump reduces the OPO threshold to 60% of the single-pass pump threshold, and for a given pump power well above threshold raises the output by about 50%. One problem with double-passing is that optical components in the cavity are more susceptible to damage due to standing pump waves, especially when the coherence length of the pump is greater than twice the 1.06$\mu$m mirror to crystal spacing, as a result of narrowing of the pump linewidth. Measurements made on uncoated $LiNbO_3$ showed that the damage threshold of greater than $\sim 5J/cm^2$ is reduced to $\sim 2J/cm^2$ when the pump is reflected back through the crystal.

A single quarter wavelength layer $SiO_2$ coating on $LiNbO_3$ pitched at 1.75$\mu$m has a reflectivity of less than 2% over the whole signal range, but the reflectivity at the pump wavelength is $\sim$10%. This reduces the intensity of the pump and leads to powerful stray 1.06$\mu$m beams. Pitching of the anti-reflection coatings at a shorter wavelength (figure 3.4) reduces the reflection at 1.06$\mu$m, and also at the shorter signal wavelengths, where any improvement in OPO performance is desirable. The OPO has used crystals anti-reflection coated at 1.4$\mu$m, as well as at 1.75$\mu$m.

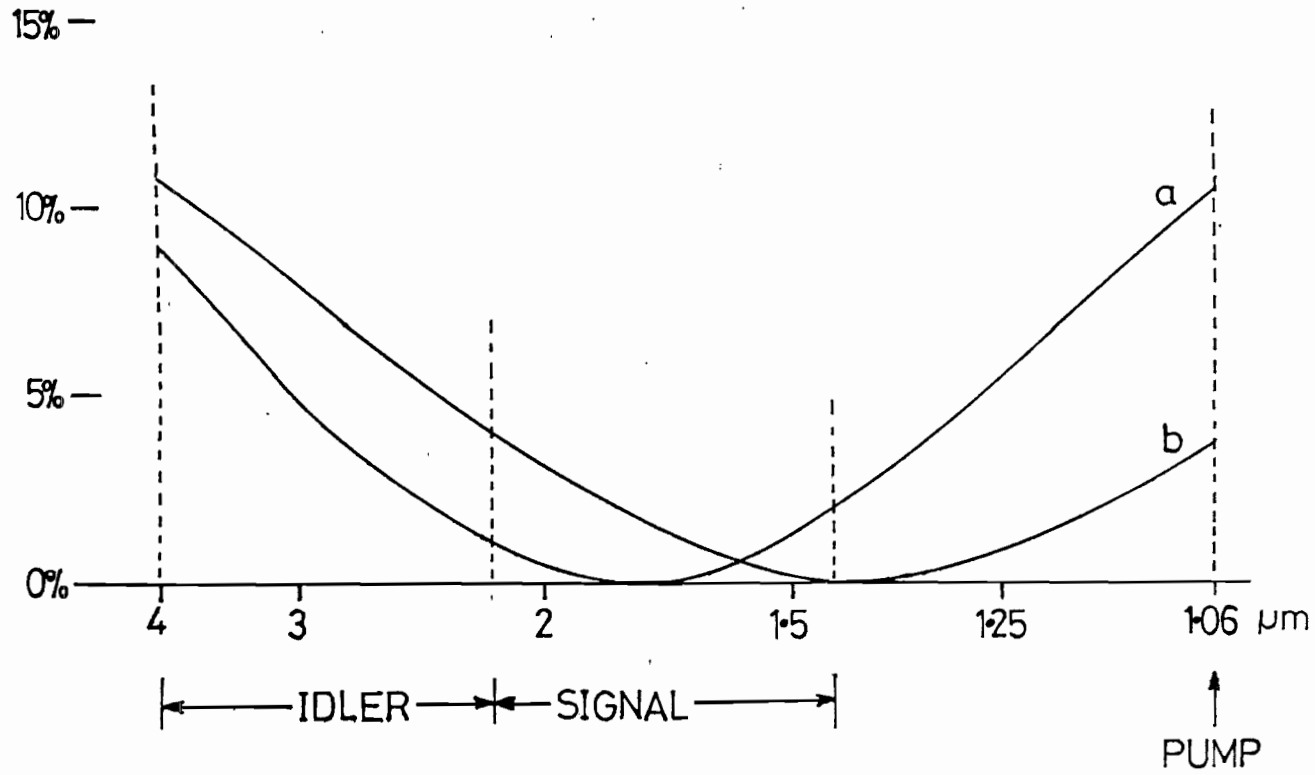


FIGURE 3.4

Reflection of a single layer antireflection coating on $LiNbO_3$.

a - pitched at 1.75μm

b - pitched at 1.4μm

## 3.3 Tuning Characteristics

### 3.3.1 $LiNbO_3$ Tuning characteristics

The tuning characteristics of the $LiNbO_3$ crystal are determined by phase-matching of the coupled pump, signal and idler waves; this in turn depends on the refractive indices of the material at the three frequencies. The most accurate published data for the refractive indices of stoichiometric $LiNbO_3$ is that presented by Hobden and Warner (23) as Sellmeier equations, dependent on both wavelength and temperature. This data was used to generate the OPO tuning curve shown in figure 3.5 (a).

The $LiNbO_3$ used in the OPO is grown from a congruent mixture, producing material deficient in lithium. The refractive indices of congruent material have been measured between UV and $3\mu m$ (24), and this data has been converted to Sellmeier equations to simplify phase-matching calculations (25). The calculated tuning curve for the OPO using this data is given as figure 3.5 (b), while the experimentally obtained tuning curve (using a C.T.I. crystal) is shown as figure 3.5 (c). The three tuning curves on figure 3.5 are all drawn relative to the angle of degenerate oscillation. The uncertainty of $\pm 0.0001$ in the measurement of the refractive indices of the congruent $LiNbO_3$ (24) can account for the deviation between curves 3.5 (b) and (c) from degenerate to $3\mu m$, while the deviation between $3\mu m$ and $4\mu m$ can be attributed to errors in extrapolation of the refractive index values beyond $3\mu m$. The most satisfactory fit between the experimental and calculated tuning curves was obtained by using the congruent Sellmeier equations, but with the birefringence used in the calculations reduced by about 9%. It should be noted that the error is most likely in measurement of o-ray dispersion, and not in the birefringence.

The rate of change of phase-mismatch with angle within the $LiNbO_3$ remains constant at about $80cm^{-1}$/degree (internal), throughout the tuning range, despite the change in tuning rate. The gain-bandwidth curve in figure 3.2 assumes a phase mismatch of $\frac{\Delta kl}{2} = \pm 1$, with a 5cm long crystal. This means that the $5cm^{-1}$ crystal must be set by the stepper motor drive to an accuracy better than $\pm 1/100^{o}$ external. Using the same criterion, the pump beam wavefront must have a radius of curvature of at least 10 metres so as to avoid phase mismatch at the edges of the beam (figure 3.6 (a)).

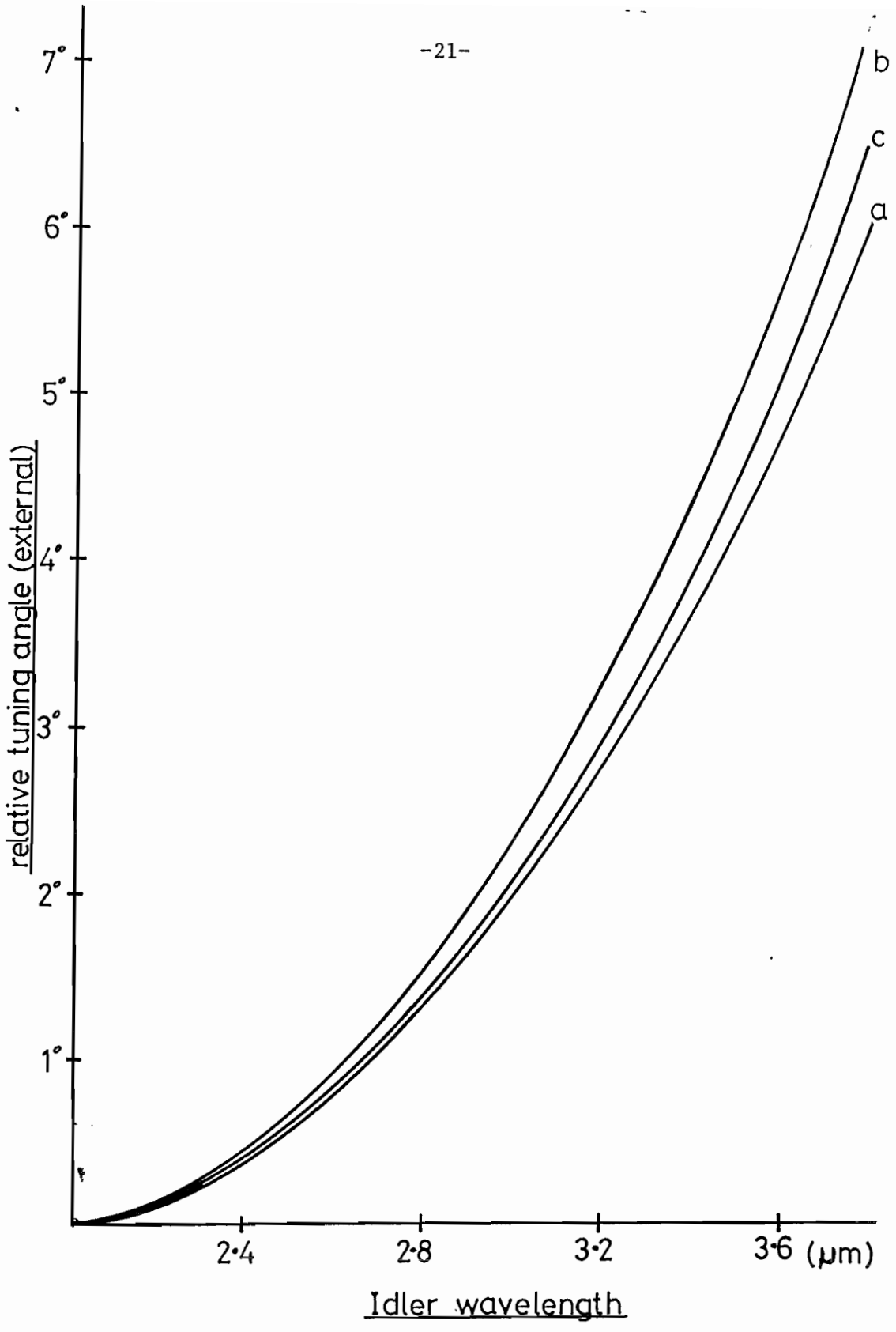


FIGURE 3.5

$LiNbO_3$ Tuning Curves (300°K)

a - calculated from stoichiometric refractive index data. $\theta_m = \sim 44.7°$

b - calculated from congruent refractive index data. $\theta_m = \sim 45.0°$

c - experimental (CTI crystal) $\theta_m = 45° \pm 0.5°$

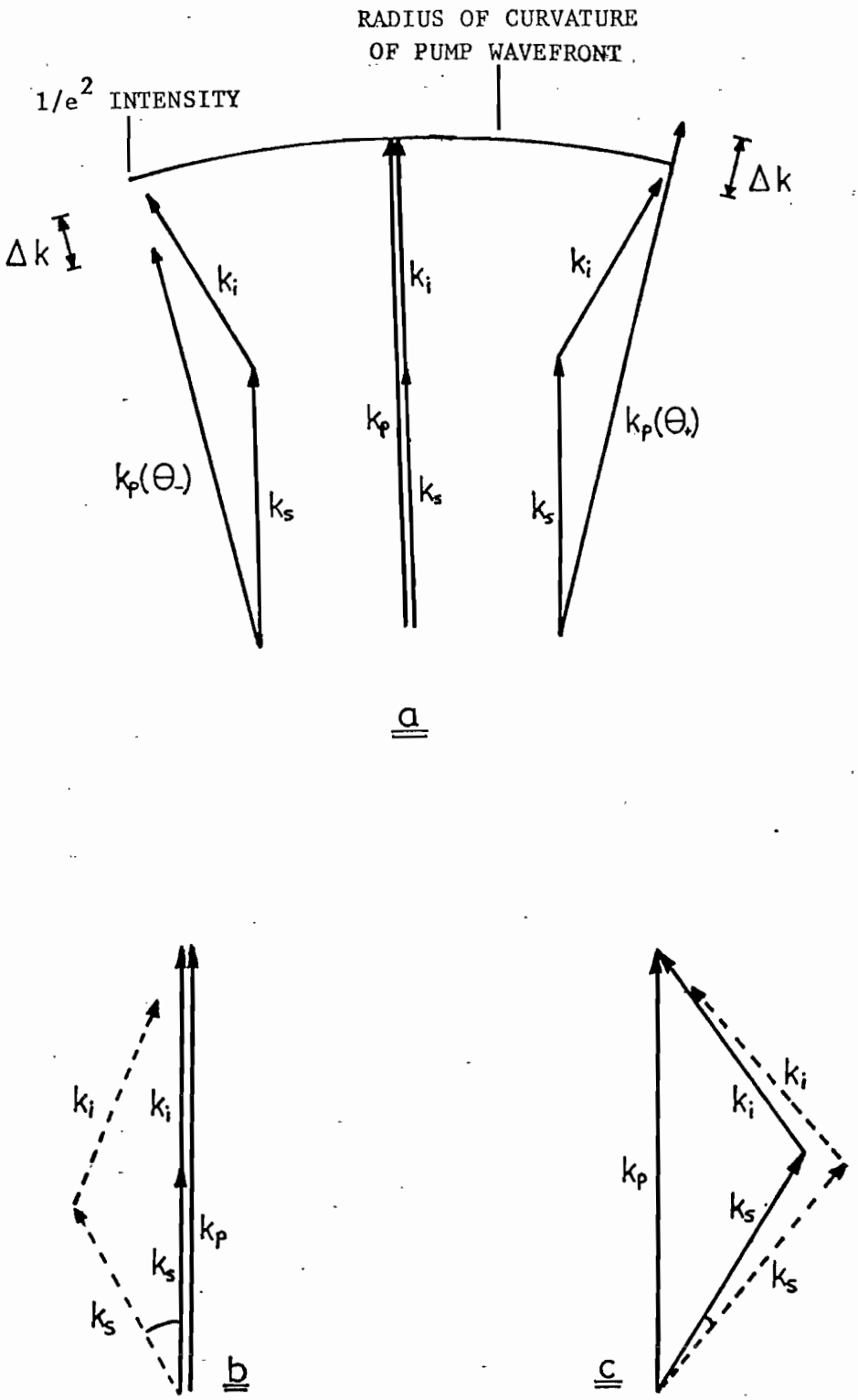


FIGURE 3.6

a - Effects of birefringence and pump beam divergence (or convergence) on phase-matching

b - Vector diagram showing signal acceptance angle for collinear phase-matching

c - Vector diagram showing reduced signal acceptance angle for noncollinear phase-matching

Phase-matching also determines the input acceptance angle for parametric gain of the signal to the $LiNbO_3$ crystal. For an OPO cavity collinear with the pump, the acceptance angle (figure 3.6(b)) is about 4 mrad half angle, this being comparable to the observed divergence of the output beam. With non-collinear operation of the OPO, the acceptance angle is reduced within the plane. For a 5 mrad angle between the signal and the pump, the acceptance angle is then of the order of 2 mrad (see figure 3.6(c)).

### 3.3.2 Grating tuning characteristics

The diffraction grating is used as the principal tuning element in the OPO cavity, both to fix the frequency of operation and provide a narrow linewidth. It is operated in the 1st order Littrow mode.

The tuning curve of the grating is derived from the standard grating equation. The OPO linewidth resulting from the line-narrowing effects of the grating is more difficult to estimate. Following the procedure described by Hanna et al (26), for a 1mm diameter signal beam near to degenerate, a value of about $4cm^{-1}$ is obtained. This value does not include the effects of multimode operation of the OPO or of gain-narrowing. In dye lasers the latter effect can reduce the output linewidth by a factor of ~5 (26). A signal linewidth of $3cm^{-1}$, resulting from the narrowing effects of the grating, was used in the determination of the required etalon FSR, this being typical of the linewidth obtained from OPOs operated with such a grating tuned cavity, e.g. in (12).

### 3.3.3 Etalon tuning

The angle-tuned etalon is used to further reduce the linewidth of the OPO output from that determined by the grating alone. The relationship between etalon tilt angle and frequency is multivalued, as illustrated in figure 3.7(a).

The OPO uses a 1mm thick fused silica plate etalon, with dielectric coatings on the parallel faces giving a finesse of 7 over most of the signal tuning range. The $3.5cm^{-1}$ free spectral range of the etalon was chosen to allow the generation of a narrow linewidth while being large enough to cause etalon modes adjacent to the oscillating mode to be outside the gain-narrowed linewidth determined by the grating. This situation is depicted in figure 3.7 (b). If the centre frequency of the grating pass-band does not however correspond exactly to an etalon mode,

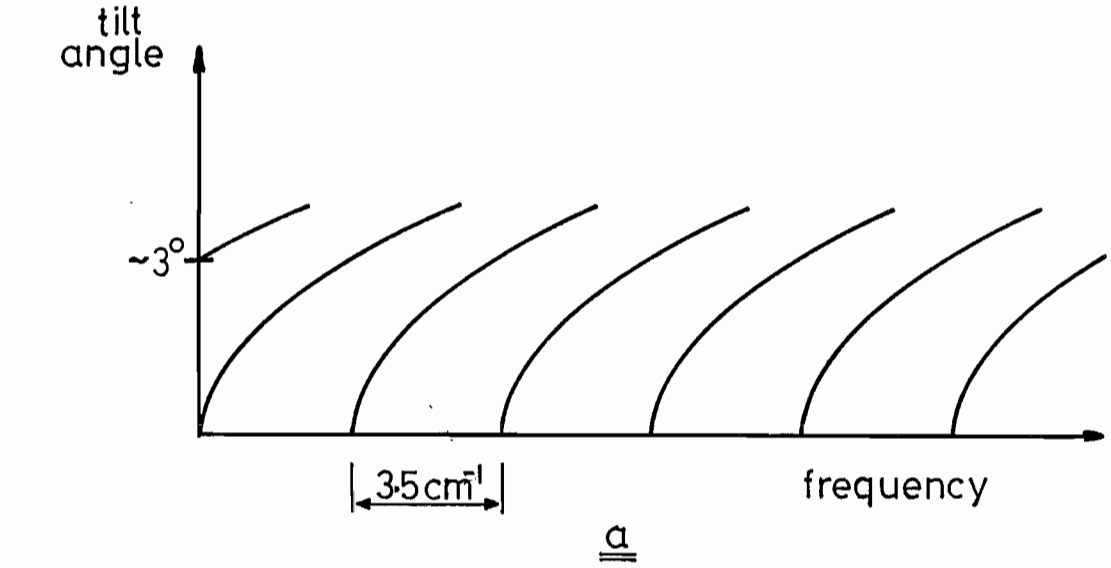


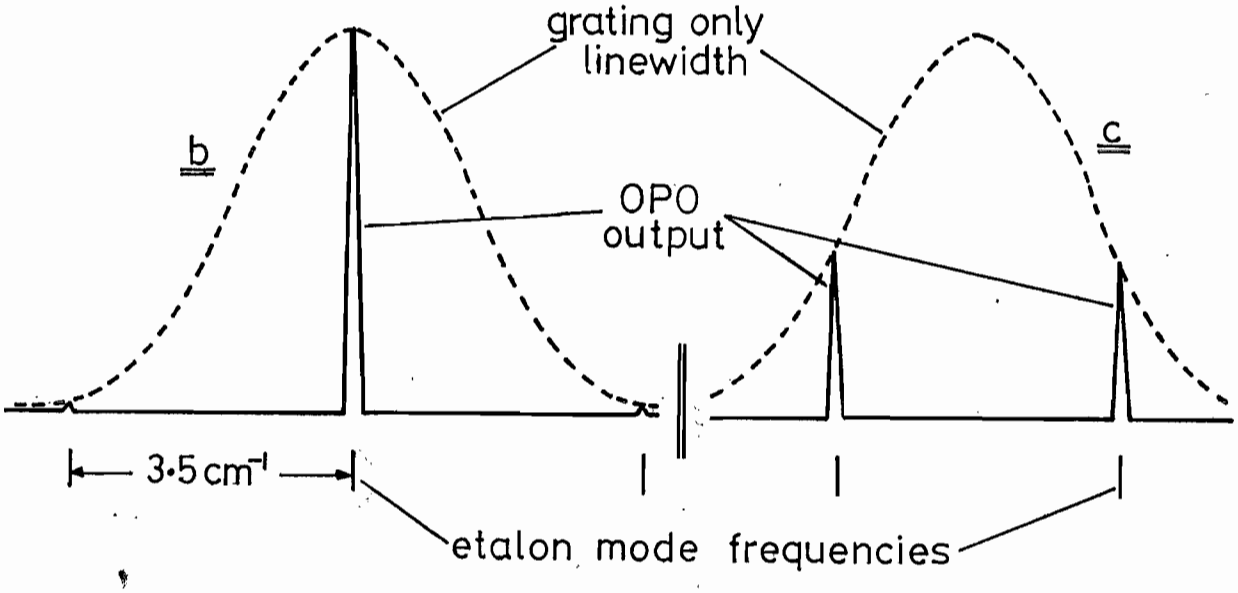


FIGURE 3.7

a - Tuning characteristics of a 1mm silica etalon.

b - Narrowing of the OPO linewidth by use of the intracavity etalon. With the etalon accurately tuned to the grating, the output is almost totally in one etalon line.

c - Detuning of the etalon results in an output consisting of two strong frequencies.

the output of the OPO may consist of two frequencies, as a result of significant simultaneous oscillation on two adjacent etalon modes. This condition is depicted in figure 3.7 (c). It is avoided by accurate tuning of the etalon and grating.

The single pass bandwidth of each transmission order of the etalon is $0.5cm^{-1}$. Two passes are made during each round trip of the cavity, so with gain-narrowing, a signal linewidth of $\sim 0.1cm^{-1}$ can be calculated.

## 3.4 Down Conversion

The down-conversion stage consists of the appropriate crystal mounted on a stepper motor drive connected to the minicomputer to adjust phase-matching, and a filter to remove the unconverted signal and idler. The angular resolution required by both proustite and CdSe is much less severe than that of the OPO $LiNbO_3$ crystal, and a simple gear box has been used to reduce the angular step size of the motor to a more suitable value (measurements indicate that the particular gearbox used is just linear enough, see section 3.6.2). Temperature control of the proustite or CdSe crystals is not required since both materials have low temperature tuning rates. The outputs from the OPO are usually sent through the mixing crystal without focusing, since this gives the highest conversion in the CdSe or proustite, without damage to the crystal.

The 1.06 $\mu$m total reflector in the OPO prevents unconverted pump radiation from reaching the down-converter crystal and therefore reduces the risk of 1.06 $\mu$m induced crystal damage or non-linear absorption (27).

### 3.4.1 Cadmium Selenide Down Converter

The class structure and birefringence of CdSe is such that phase-matching is possible only over a restricted range of wavelengths. Figure 3.8 shows a complete plot of phase-matching angles for CdSe, derived from the Sellmeier equations of Bhar (28). The broken line, which corresponds to the signal of a 1.06 $\mu$m pumped OPO, shows that this pump frequency allows a wide tuning range, between 9.5 $\mu$m and the onset of infra-red lattice absorption at about 25 $\mu$m. In contrast, the mixing of the outputs of a ruby or 0.659$\mu$m pumped OPO could only be used to generate outputs from 15 $\mu$m to 25 $\mu$m, and it is likely that the output powers would be significantly reduced by free-carrier effects (27).

Figure 3.9 shows the tuning curve for down-conversion in CdSe from the signal and idler of a 1.06 $\mu$m pumped OPO. For a 2.4cm crystal, as used in the system, the signal and idler acceptance bandwidths are greater than $1cm^{-1}$, while the external angle requires to be set to an accuracy of better than $\pm 0.07^{o}$ to obtain maximum output.

The threshold of optically induced damage of CdSe is quoted by various authors as being between 18 and 60 $MW/cm^2$, for various wavelengths,

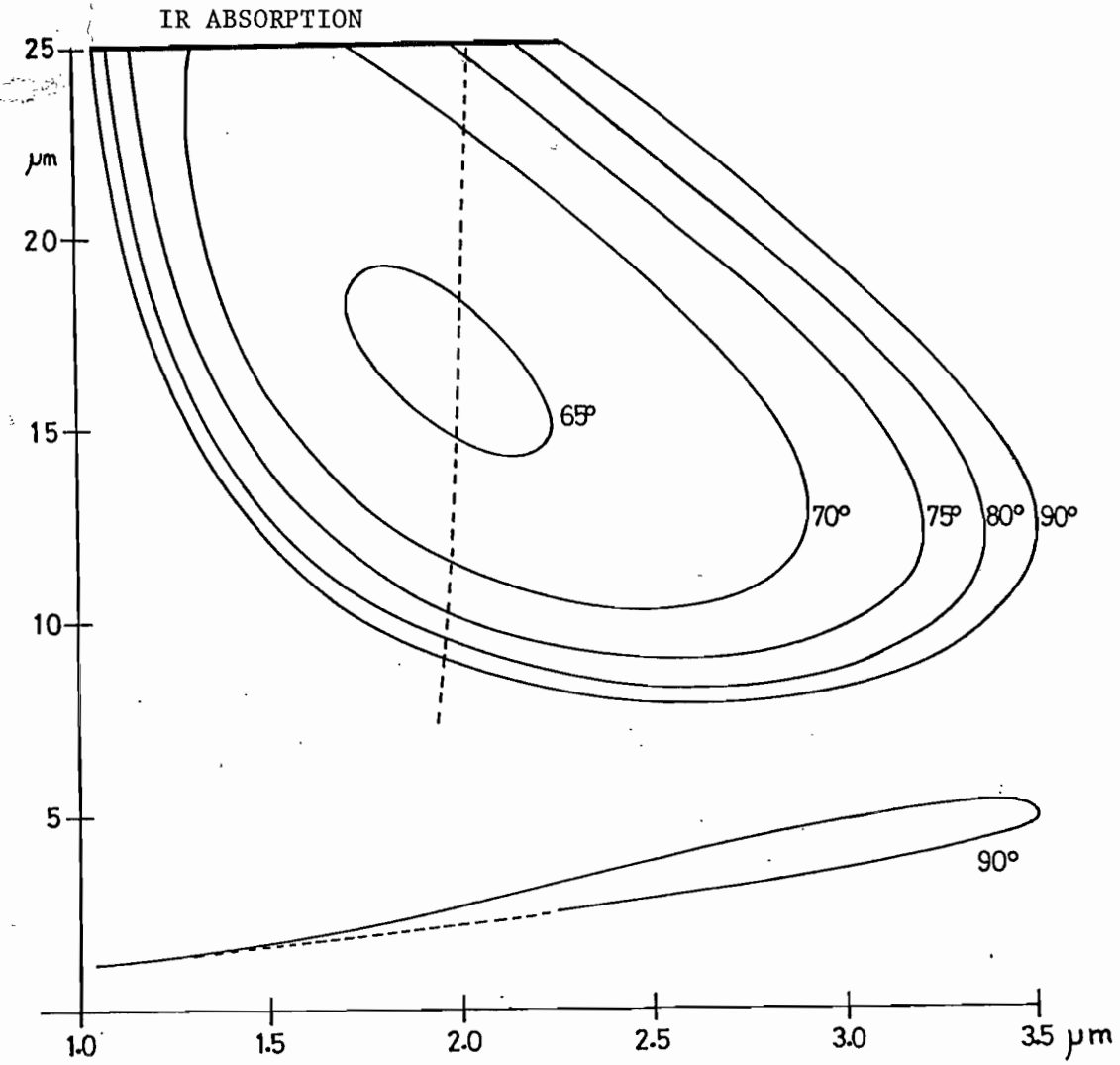


FIGURE 3.8 3-WAVE PHASE-MATCHING PLOT FOR CdSe

These traces show the phase-matching angle for type 2b interactions in CdSe as contours. The horizontal axis corresponds to the wavelengths of the shortest wave involved (an o-ray); the vertical axis in the top trace corresponds to the wavelength of the longest wave (also o-ray). Phase-matching is not possible outside the 90° contour. The lower trace shows the corresponding 90° contour for the e-ray, with the vertical axis now corresponding to the wavelength of the e-ray wave. The broken line corresponds to the output generated by mixing the signal and idler of a 1.06μm pumped OPO.

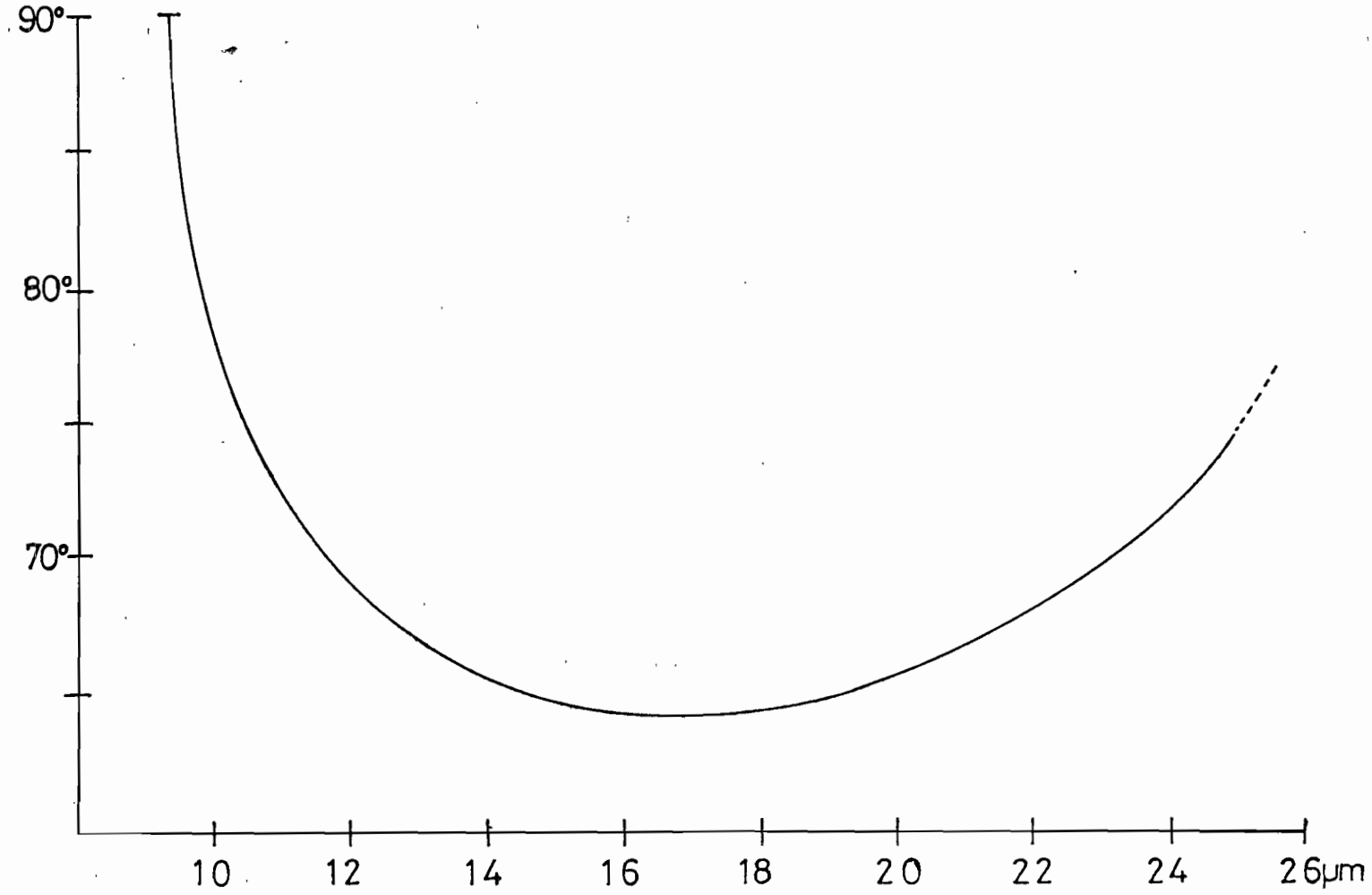


FIGURE 3.9

Phase-matching angle of CdSe down-converter,
pumped by the signal and idler of a 1.06μm pumped OPO.

pulse lengths and surface finishes. For signal and idler intensities greater than 10 MW/cm$^2$, high conversion efficiencies, close to pump depletion, are indicated by simple theory in a 2.4cm crystal, but such high efficiencies have not been observed experimentally.

The type II phase-matching of CdSe requires that the two inputs to the down-converter crystal be orthogonally polarised, with the signal entering the CdSe as an o-ray, and the idler as an e-ray. It is possible to split and then recombine the signal and idler following rotation of one of these waves by 90$^o$ using edge filters centred at 2.1$\mu$m but this requires special components and introduces additional complexity. In the simpler method, used in the system, the crystal is set at 45$^o$ to vertical, and the vertically polarised signal and idler waves divide equally between e and o-rays within the crystal. The result of this is that only half of the total OPO output is the correct polarisation within the CdSe crystal to be of use in the conversion process, and the small signal gain is therefore reduced by a factor of four, leading to a reduced output. Double refraction walk-off in CdSe is sufficiently small to be neglected.

### 3.4.2 Proustite Down-converter

The birefringence and class structure of proustite are such that all three types of phase-matching for down-conversion are possible (29). The tuning curves for all three types are shown in figure 3.10. Type IIa ($k^e_{ir} = k^e_s - k^o_i$) is of little interest, because it has a relatively low effective non-linear coefficient, and like CdSe, requires the two inputs to be orthogonally polarised. Of the remaining two types of phase-matching, type I ($k^o_{ir} = k^e_s - k^o_i$) has the higher non-linear conversion coefficient, but again requires orthogonally polarised inputs. Once the factor of four reduction in the type I conversion gain, due to the splitting of both signal and idler between o and e-rays, is taken into account, type I and type IIb ($k^o_{ir} = k^e_s - k^e_i$) have approximately equal gain coefficients, that of type I being less wavelength dependent. Type I phase-matching involves a smaller rotation of the crystal during tuning, and since CdSe also requires a 45$^o$ mounted motor, type I is preferable, to avoid adjustment of the down-converter motor axis when changing crystals.

The largest available proustite crystals of suitable quality are 1cm long, and the measured threshold of optical damage is 0.4J/cm$^2$ (30).

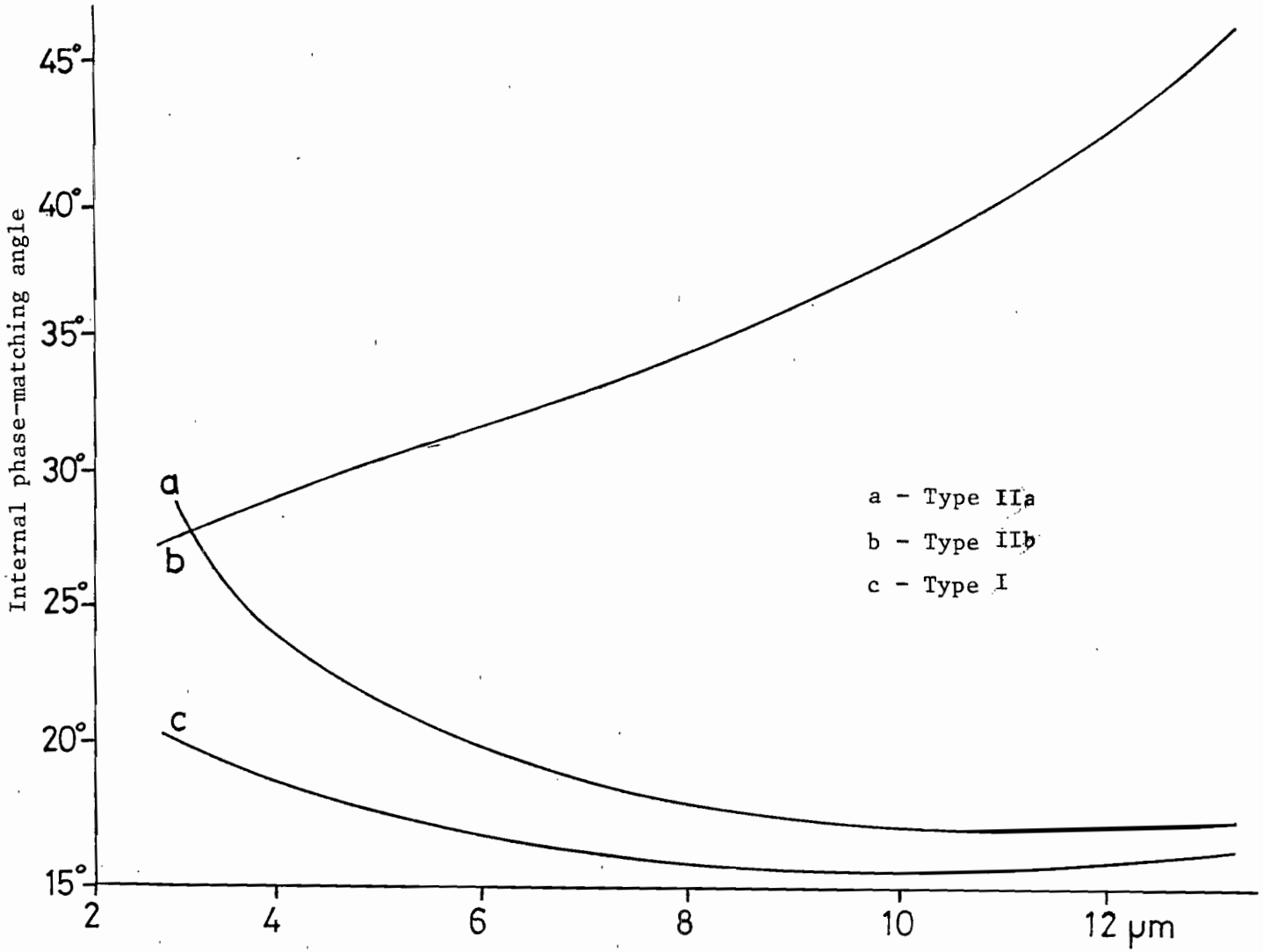


FIGURE 3.10

Down-conversion phase-matching in proustite
(from the signal and idler of a 1.06μm pumped OPO)

## 3.5 Temperature control of Optical Components

Each of the three OPO tuning elements is temperature sensitive. For the grating, the temperature dependent mechanism is that of thermal expansion of the glass substrate. For the $LiNbO_3$, the refractive indices (particularly for the e-ray pump) are temperature sensitive, affecting the phase-matching conditions. In the etalon, both refractive index changes and thermal expansion of the silica are involved. To obtain a drift free output from the OPO, these three components are best maintained at constant temperature. The alternative of compensating temperature variations by equivalent changes in the tuning angles is much more complex.

Table 3.1 lists the temperature stability requirements of the grating, $LiNbO_3$ and etalon, and the criteria used in obtaining these values. The $LiNbO_3$ is the most temperature sensitive of the components; a change of $1^{o}C$ affects phase-matching such that the parametric gain at the frequency reflected by the grating will be too small to support oscillation. The temperature rise within the $LiNbO_3$ crystal due to direct absorption of a small fraction of the pump, signal and idler is believed not to be large enough to cause a significant change in phase-matching at the energy levels involved in the OPO.

To maintain the $LiNbO_3$ crystal at a constant temperature, it is mounted in a temperature regulated aluminium block, heated to about $32^{o}C$. The control for this consists of a temperature sensing thermistor within the block, and a remote proportional control circuit, with the required heat being generated by power transistors bolted onto the side of the block. Thermal lagging of the block was found unnecessary. Limited measurements of the $LiNbO_3$ temperature stability (including using crossed polarisers) indicated that the control is adequate. No drift in OPO performance has been attributed to changes in $LiNbO_3$ temperature.

For accurate work, the etalon temperature has also to be controlled. Unfortunately lack of time prevented the completion of a temperature controller for this component, or for the grating, although space has been provided in the electronics rack for the necessary control circuits. In the CERL OPO however, the etalon holder is controlled in temperature in a manner similar to the $LiNbO_3$, although the effectiveness of this has yet to be confirmed. The baseplate of the CERL instrument is maintained to $\pm 2^{o}C$ by a heater system, with the cover and bottom lagged

TABLE 3.1

| | Temperature dependence | Max. allowable error | Max. temperature deviation |
|---|---|---|---|
| Etalon | $\frac{\partial n}{\partial T} = 11*10^{-6}/°C$ | $\pm 0.03\ cm^{-1}$ | $\pm 0.5°C$ |
| Grating | $\frac{1}{\ell}\frac{\partial \ell}{\partial T} = 6*10^{-6}/°C$ | $\pm 0.2\ cm^{-1}$ | $\pm 6°C$ |
| $LiNbO_3$ | $\frac{\partial}{\partial T}\left(\frac{\Delta k \ell}{2}\right) = 3.5/°C$ | $\frac{\Delta k \ell}{2} = \pm 1$ | $\pm 0.3°C$ |

Temperature dependence of tuning components

with foam polystyrene to reduce the thermal loss as well as to even out temperature variations. This reduces drift effects due to thermal expansion in the various mechanical assemblies, and in particular, maintains the grating at near constant temperature.

## 3.6 OPO Mechanical Structure

The OPO mechanical structure has the optical components positioned above a metal base plate, and the stepper motors and drive mechanisms for the grating, $LiNbO_3$ and etalon below. There is no provision for the down-conversion stage on the base; when used this is mounted externally.

### 3.6.1 Grating assembly

Of the tuning elements, the grating has the greatest number of resolvable points (table 3.2) and hence its drive presents the greatest problem in design, with respect to linearity and mechanical accuracy. For this reason, the baseplate, grating drive and $45^{\circ}$ mirror mount have been designed as an integral assembly, meeting the requirements of the grating drive, while the $LiNbO_3$ crystal and etalon drives, and the stepper motors, are built as separate sub-assemblies, attached to the baseplate.

Figure 3.11 shows the baseplate, grating assembly and the $45^{\circ}$ mirror holder. The U-shaped grating holder allows the face of the grating to be positioned on the grating's axis of rotation, to prevent the resonant beam tracking over the face of the grating as it is tuned. The two shafts at either end of the U-shaped holder and the bearings are accurately aligned, so that the whole rotation mechanism is well defined. The bracket under the baseplate on which the leadscrew is mounted is positioned to form a rigid structure with the baseplate and one of the grating support blocks.

The linear movement of the leadscrew is converted into rotary motion of the grating by the vertical arm (figure 3.12). The required angular accuracy of the grating of $\pm$ 3 seconds of arc ($\pm \frac{1}{4} cm^{-1}$) corresponds to a movement of $\pm$ 2.5$\mu$m at the end of the arm. The leadscrew linearity and resetability are not specified by the manufacturer, but measurements (including the performance of the OPO) suggest that they are adequate. The stepper motor is connected to the leadscrew via a pinned belt; this introduces little longitudinal force on the leadscrew. The computer software responsible for driving both this and the other stepper motors eliminates the effects of backlash in the drive mechanism by always approaching the final position from the same direction, deliberately overshooting and then returning by the same amount, if necessary. The computer calculated angle takes into account all of the trigonometric relationships between leadscrew position and grating frequency, when setting the motor.

TABLE 3.2

| | Total rotation | Resolution angle |
|---|---|---|
| OPO etalon | 4° | 0.018° |
| Grating | 15° | 0.002° |
| $LiNbO_3$ (50mm) | 8° | 0.01° |
| CdSe (24mm) | 50° | 0.07° |
| Proustite Type I (10mm) | 10° | 0.05° |
| Proustite Type IIb (10mm) | 50° | 0.05° |

Angular range of tuning components.

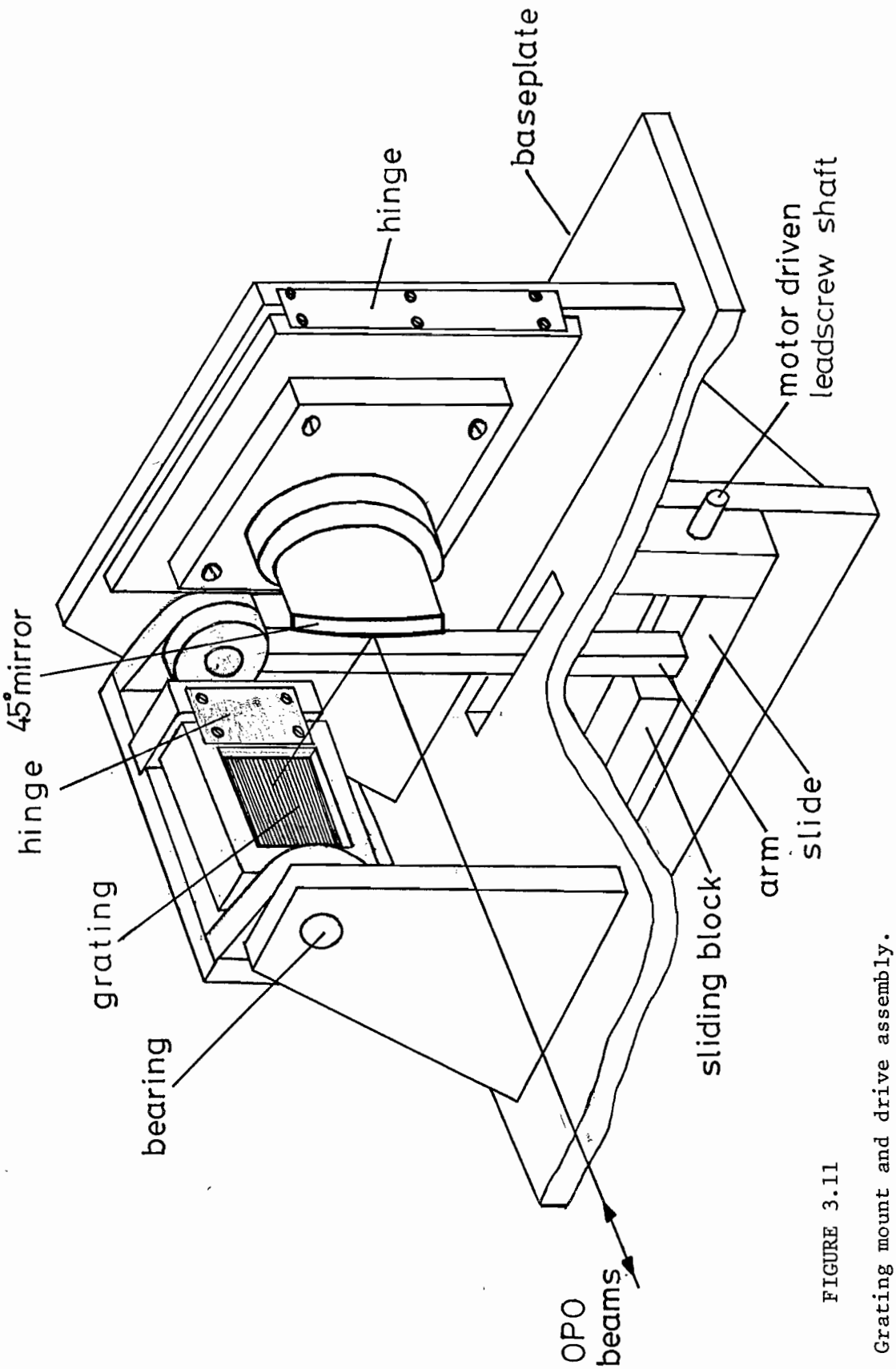


FIGURE 3.11

Grating mount and drive assembly.

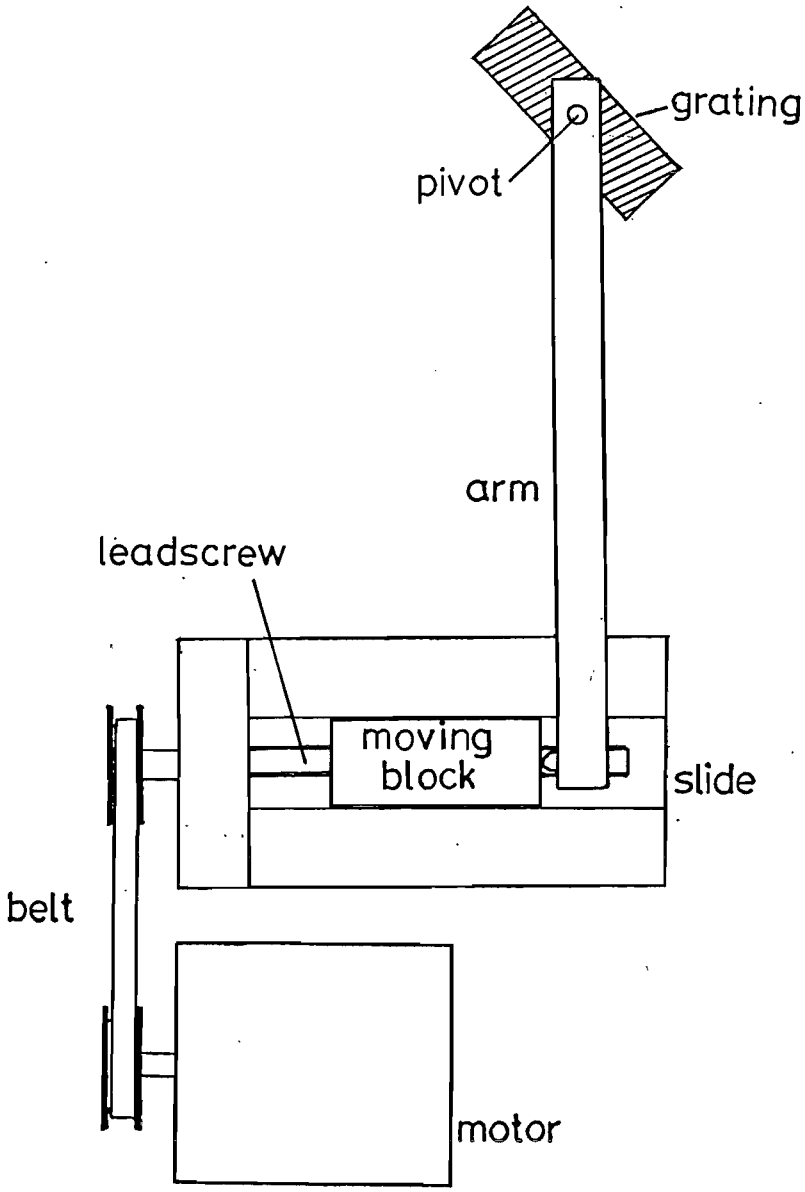


FIGURE 3.12 Diffraction grating drive mechanism. The pinned belt drive eliminates belt slip problems.

The grooves of the grating require to be accurately aligned parallel to the grating's axis of rotation, so that the grating remains in alignment with the OPO cavity as the grating is tuned. This necessitates alignment around two axes (figure 3.13). Calculations show, however, that if one of these angles is fixed, the effects of an error in this plane on the cavity alignment can be counteracted over the limited range of angles ($15^{o}$ - $40^{o}$) to which the grating is set, by a related deliberate misalignment in the other plane. This allows only one fine adjustment for the grating to be provided (figure 3.13). Coarse rotation of the grating round its face normal axis can be achieved by adjustment of the leaf spring.

The $45^{o}$ mirror has only one fine adjustment; that which enables horizontal alignment of the resonant beam. Coarse positioning and tilting of this mirror are also possible, to enable the signal beam to be placed on a suitable region of the grating.

### 3.6.2 $LiNbO_3$ drive

The $LiNbO_3$ crystal is driven by an assembly mounted under the baseplate. Originally, following the previous practice in the laboratory (8), the crystal was mounted on the output shaft of a stepper motor gearbox, with limited facilities for centering the crystal onto the pump beam. Although this system gave the required resolution and resetability, the deviation from true linearity over the $8^{o}$ tuning range used was found to be excessive. Initially, this non-linearity was hidden by the inaccuracies in the calculated tuning curves of the $LiNbO_3$ (section 3.3.1), and was only recognised once the tuning problem was understood. Figure 3.14 shows the measured deviation from linearity for the gearbox used on the $LiNbO_3$ drive. The $7\frac{1}{2}$ minutes of arc error corresponds to a cutting inaccuracy of 0.001" (25$\mu$m) in the position of the teeth on the output gears. There may also be a contribution from fine irregularities of motion as teeth engage and disengage. These problems cancel out over $360^{o}$, but are significant when only a fraction of a revolution is considered. A gearbox using the highest quality of commercial gears is still unlikely to be linear enough to be used satisfactorily with the $LiNbO_3$ crystal.

Because of the above problem, an alternative drive assembly was designed. Limitations were imposed by the available space, and also by the low torque output of the stepper motor used. The capacity of the stepper motor power supply could not easily be increased to take another high power stepper motor.

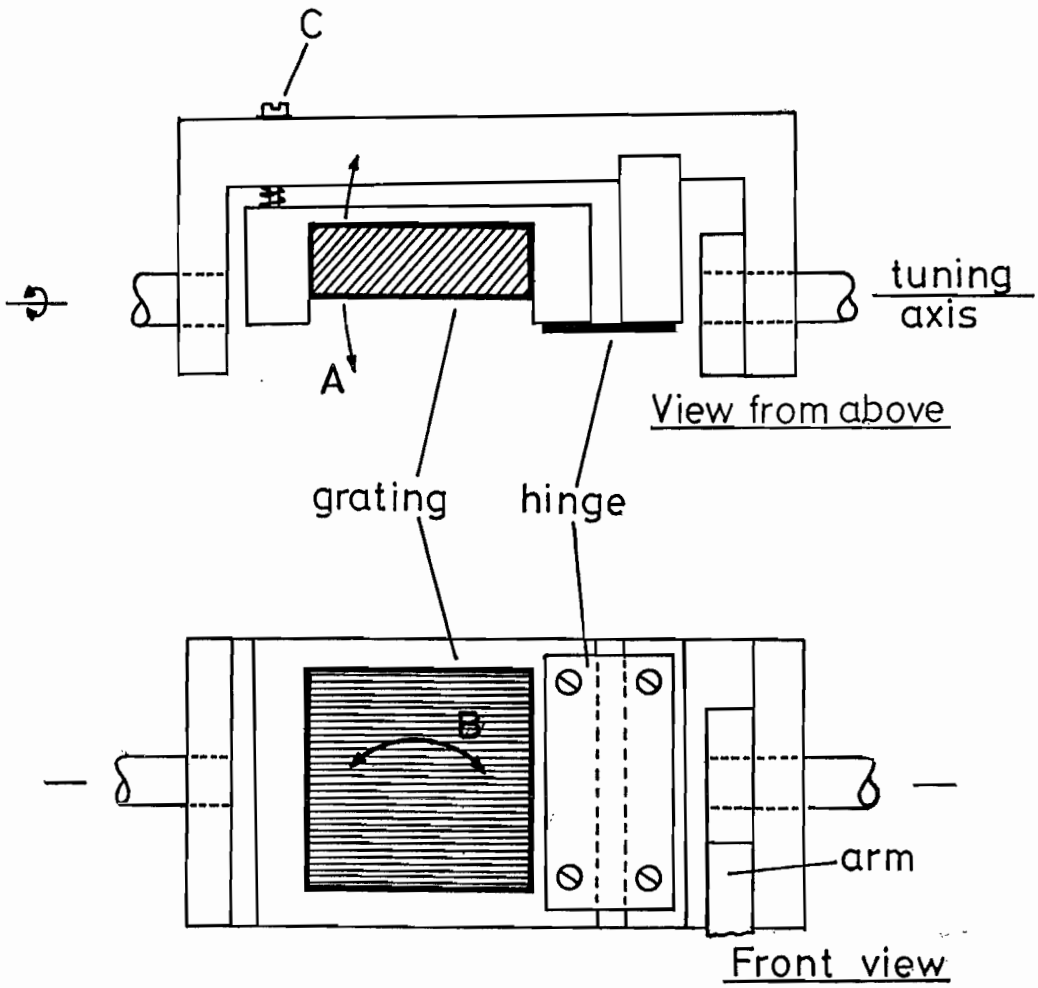


FIGURE 3.13

The grooves of the grating require to be exactly parallel to the axis of rotation to maintain alignment as the grating is tuned. This requires alignment of the grating in the two directions A & B shown above.

In the OPO, screw C provides for alignment in the direction A, while adjustment in direction B can only be obtained by coarse positioning of the hinge and a compensating mis-alignment in direction A to reduce remaining errors.

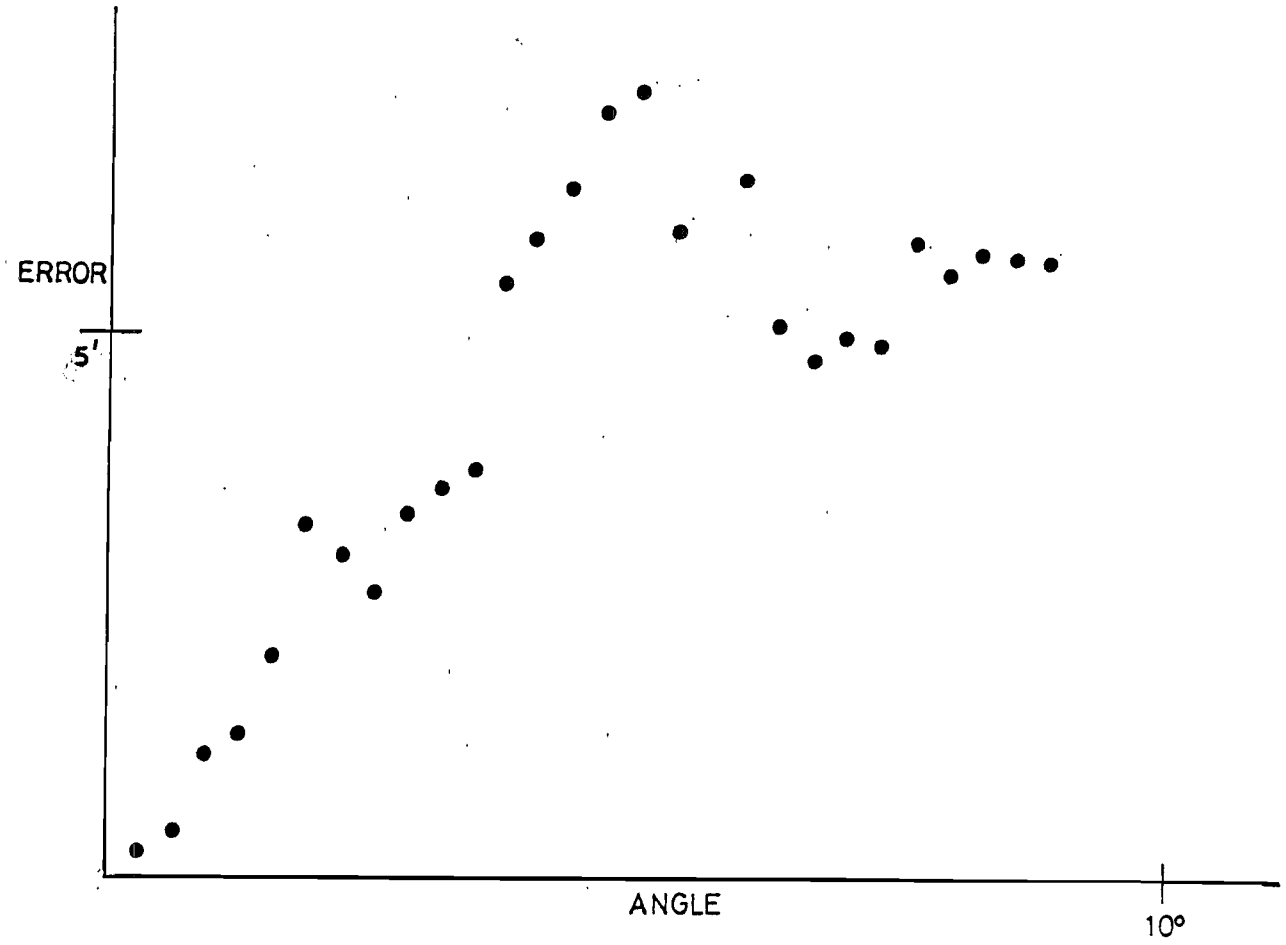


FIGURE 3.14 Non-linearity of a stepper motor gearbox.

The trace shows the deviation from true (vertical axis) plotted against the output angle (horizontal axis) of the AM5020D stepper motor gearbox.

The modified $LiNbO_3$ drive (figure 3.15) consists of a micrometer head driven from the stepper motor via gearing and a sliding coupling. Although this gives adequate accuracy in position, the arrangement of components tends to enhance the resonances of the stepper motor and is very noisy. This may be due to inaccurate machining of the components and can probably be corrected by using a different form of coupling. Like the grating drive, the software driving the $LiNbO_3$ stepper motor accounts for the trigonometric relationships in the drive mechanism, and also executes backlash correction.

### 3.6.3 Other OPO components

The galvanometer drive is mounted through a hole in the baseplate, with the lightweight etalon holder mounted directly onto the shaft. The etalon is positioned in the tight space between the grating and the $45^{o}$ mirror.

The OPO output and the $1.06\mu m$ total reflection mirror mounts are both based on the laboratory standard design, this giving sufficient resolution, although displaying an annoying hysteresis behaviour when being finely adjusted.

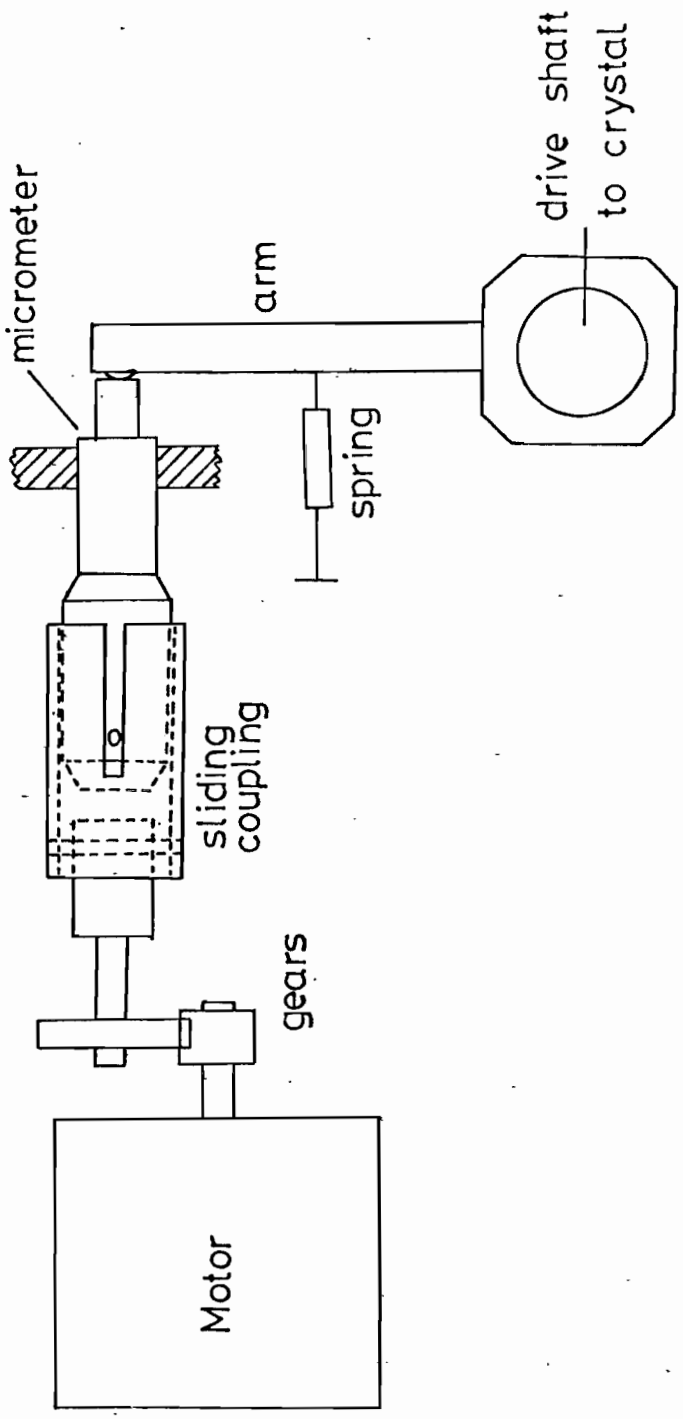


FIGURE 3.15

Re-designed $LiNbO_3$ drive mechanism.

## 3.7 Electronic Control Circuits

The tuning control system is centred around the minicomputer, with motors to drive the optical tuning elements, interface electronics and a teletypewriter. Figure 3.16 gives a block diagram of this system. The approach taken with the electronics has been to include as many features as possible in the computer software, allowing a reduction of electronic circuits to a minimum, and reducing mechanical complexity.

The minicomputer used (Computer Automation LSI 3/05) is a simple and low cost 16 bit machine, with a semiconductor memory (RAM) of 8 k words. The control program, which uses most of the available memory, was written in assembly code, this being the only language available, and it includes some mathematical routines written by the manufacturer.

Stepper motors are one of the simplest ways of converting digital information into movement, and are used in the drives to the grating and non-linear optical crystals. The etalon could also have been driven by a stepper motor, but although it is more expensive, an analogue galvanometer drive has been used. This has the advantage over a stepper motor drive of being physically more convenient to mount in the cavity, and, since the relationship between mechanical angle and electrical drive is absolute, rather than multivalued, as in a stepper motor, there is no ambiguity of position.

The stepper motors, which are all 4-phase types with full step drive* are used in open loop, with no feedback from the OPO output or the mechanics to validate the motor position. The system therefore relies on the stepper motor drives having been set up properly, and on the motors responding accurately to the movements dictated by the computer at all times.

Initially, commercial stepper motor drive cards, with series current limiting resistors, were used to drive the motors. The effective circuit of such a drive is shown in figure 3.17. The problem encountered with them is that the effective 2 bit counter on the drive card may not remain in step with the computer in the open loop situation. Pickup of R.F. interference (from the laser flashlamps) on the step line can cause changes in the drive card counter, and therefore move the motors. The

* Motor types: Slo-Syn M061 and Imnex PD14/16

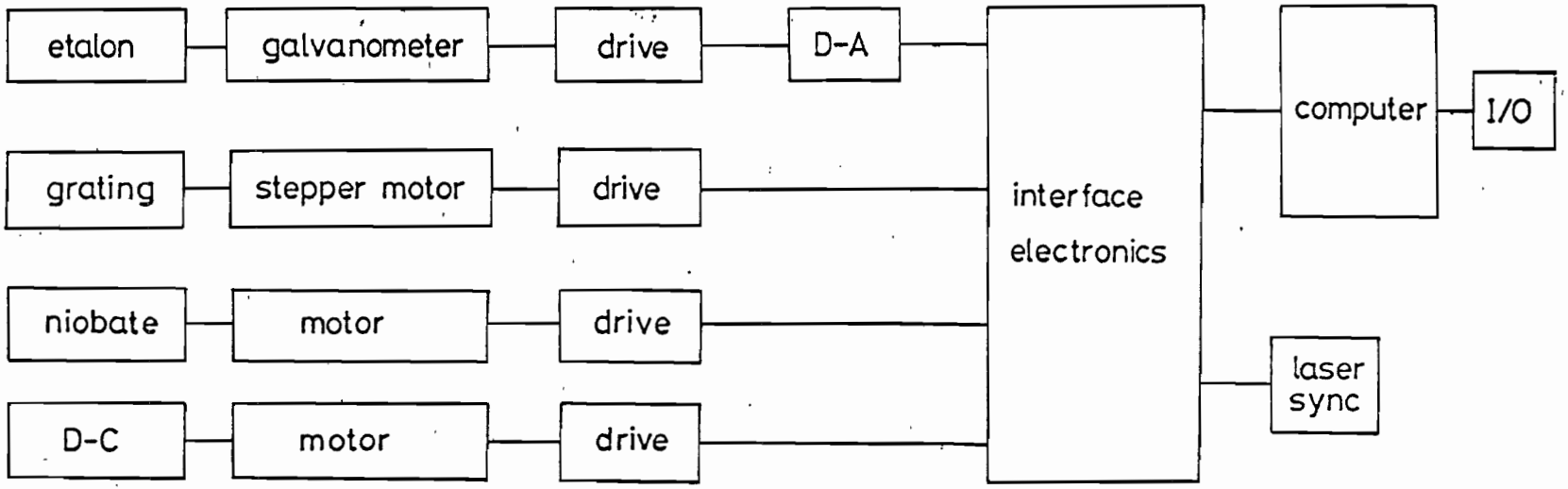


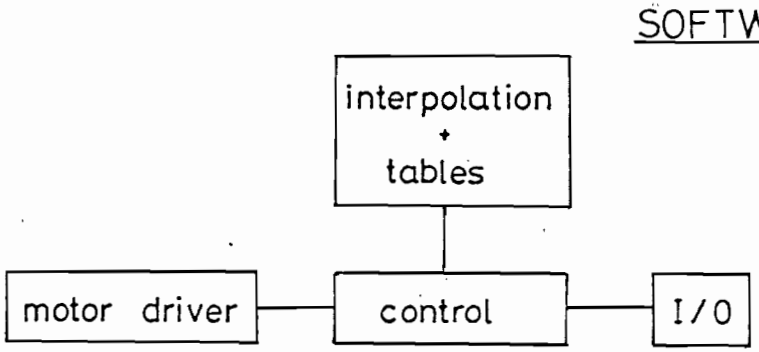


FIGURE 3.16

Electronics block diagram.

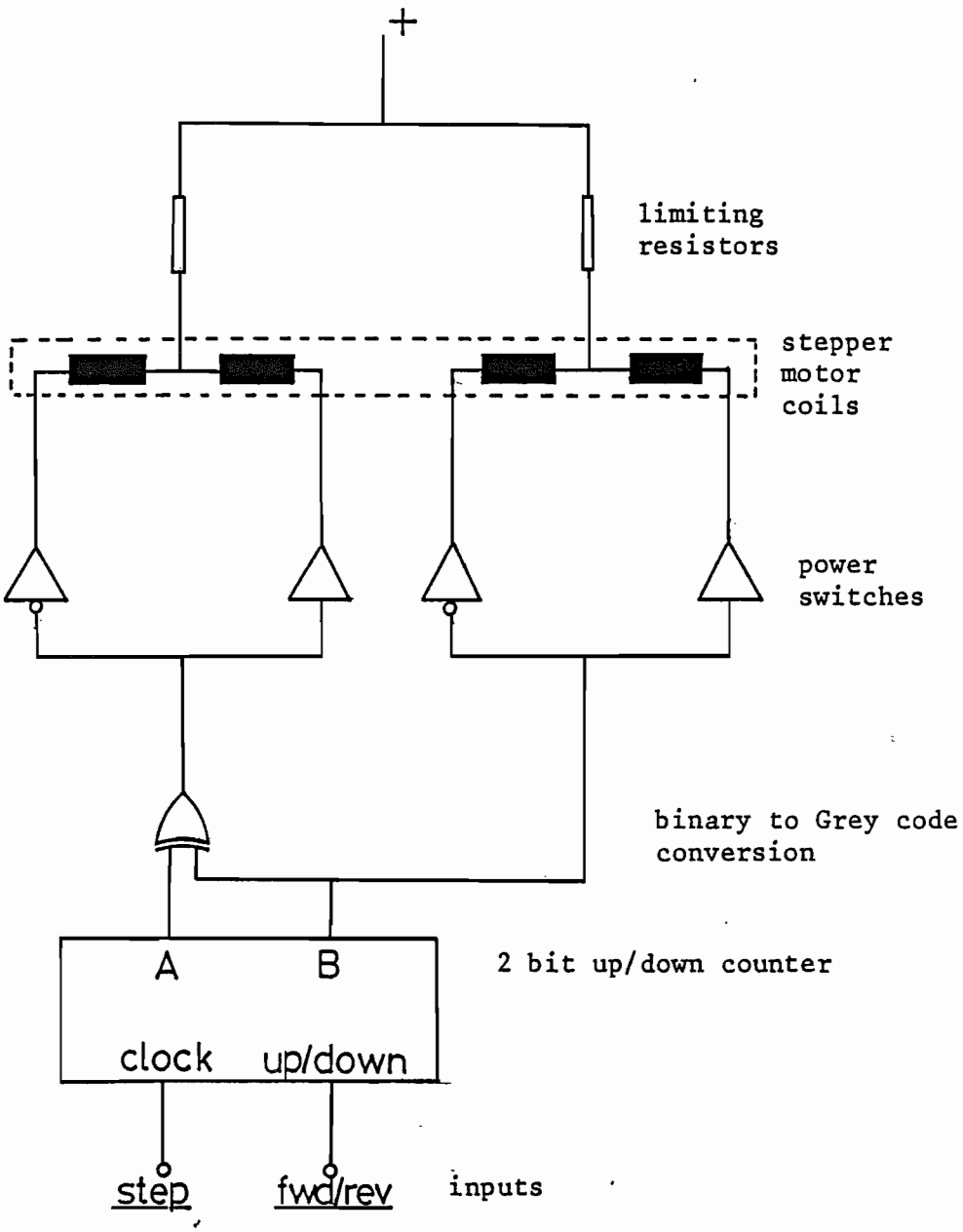


FIGURE 3.17

4-phase stepper motor circuit using commercial drive card.

In practice, the counter and binary to Grey code encoder are combined by using a ring-counter circuit.

motor positions can then only be brought back into line with the computer by human intervention.

When power is removed from the coils of a motor, friction and a slight magnetic holding torque prevent the rotor from moving more than about one step, so that if, when power is restored, the original drive condition is re-established, the motor returns to its original position. On commercial motor drives, the two bit counters do not necessarily restart on the correct phase, and the motors may therefore gain or lose one or two steps in the process. On the CERL OPO, a single line of feedback from each stepper motor drive to the computer enables the computer to search for the correct driving phase at the drive card before switching the supply to the motor coils on. This requires considerable extra hardware and software.

The drive system finally adopted uses specially designed electronic current switches, which are driven directly by an output port on the computer, and do not themselves contain counting or latching circuits. The computer software determines which coils are to be energised, and this information is output to the drive circuits directly. Following system power-up, the computer turns on power to the motors only after the previous driving phases have been established.

The three stepper motors are all run at a constant stepping rate from a common oscillator running at about 250Hz. This speed is set by necessity to be within the start-stop capability of each of the motors, and also be away from their natural resonances. In contrast, the grating, $LiNbO_3$ and down-converter crystal motors on the CERL OPO are driven by independent oscillators, each being capable of being ramped up to a high slew-rate (about 1.5kHz), to permit much faster tuning of this OPO. The CERL control computer again is responsible for counting motor steps, and for controlling acceleration and deceleration, with communication between the motors and computer being in this case by interrupt. Both the hardware and software on the CERL design are considerably more complex than on the Southampton system, but the increase in tuning rate is essential for applications such as time resolved atmospheric pollution studies, particularly when used with a high repetition rate Nd:YAG pump laser.

The tuning behaviour of the etalon is different from that of the grating and non-linear optical crystals, in that it need not be tilted beyond an angle corresponding to detuning of one free spectral range, at which point the next mode is selected. The accuracy to which

the angle of the etalon needs to be specified to give an OPO output accurate to $0.03cm^{-1}$ or better is therefore only 1/150 or better of the etalon's total movement. The analogue galvanometer* driving the etalon, with its internal position feedback, is capable of achieving the required resolution, while being physically smaller, quieter and faster than a stepper motor assembly. The angle to which the etalon is to be set is calculated by the computer, and output via a digital to analogue converter to the galvanometer drive amplifier, this being much simpler than the driving of a stepper motor.

* General Scanning Inc. type G100-PD

## 3.8 Control Software

While the electronic and mechanical hardware provides the minimum necessary framework for tuning of the optics, it is the mini-computer software which provides the details of the control system and presents a suitable communication interface between the user of the system and the tuning motors. Figure 3.18 gives the functional relationship between the various software blocks which together form the computer program.

The user's commands relating to tuning and calibration are entered on the teletypewriter terminal, which is also used for status reporting. Appendix 2 contains a list and explanation of the more commonly used commands. Many checks are made throughout the program for error conditions, such as illegal commands and incorrect hardware conditions. In the event of an error being recognised, a message is printed on the terminal and the current operation is aborted.

### 3.8.1 Command interpretation

The command interpretation block of the program accepts the user's commands from the teletypewriter and, depending on the command entered, executes the relevant coding. Since the terminal communicates by program control rather than by interrupt, commands can only be entered when the computer is free from other tasks.

Figure 3.19 shows, as an example, a flow diagram depicting the operations involved in scanning in frequency. The form is similar to a Fortran 'Do Loop', with the OPO frequency as the control variable. The scan is one of two commands which requires time synchronisation with an external device, usually the laser. Tuning occurs in discrete frequency jumps immediately following OPO pulses. In some experimental cases, the synchronisation pulse can come from data processing instruments, to indicate that, for example, sufficient data has been obtained at the one frequency.

The directions of the grating and $LiNbO_3$ motors are defined so that when the OPO is tuning in one direction, no backlash correction is given. This results in a fast scanning direction. If a down-converter crystal such as CdSe is also used, both directions may be slow over part of the range, because of the change in the direction of tuning of the down-converter crystal (e.g. in figures 3.9 and 3.10(c) ).

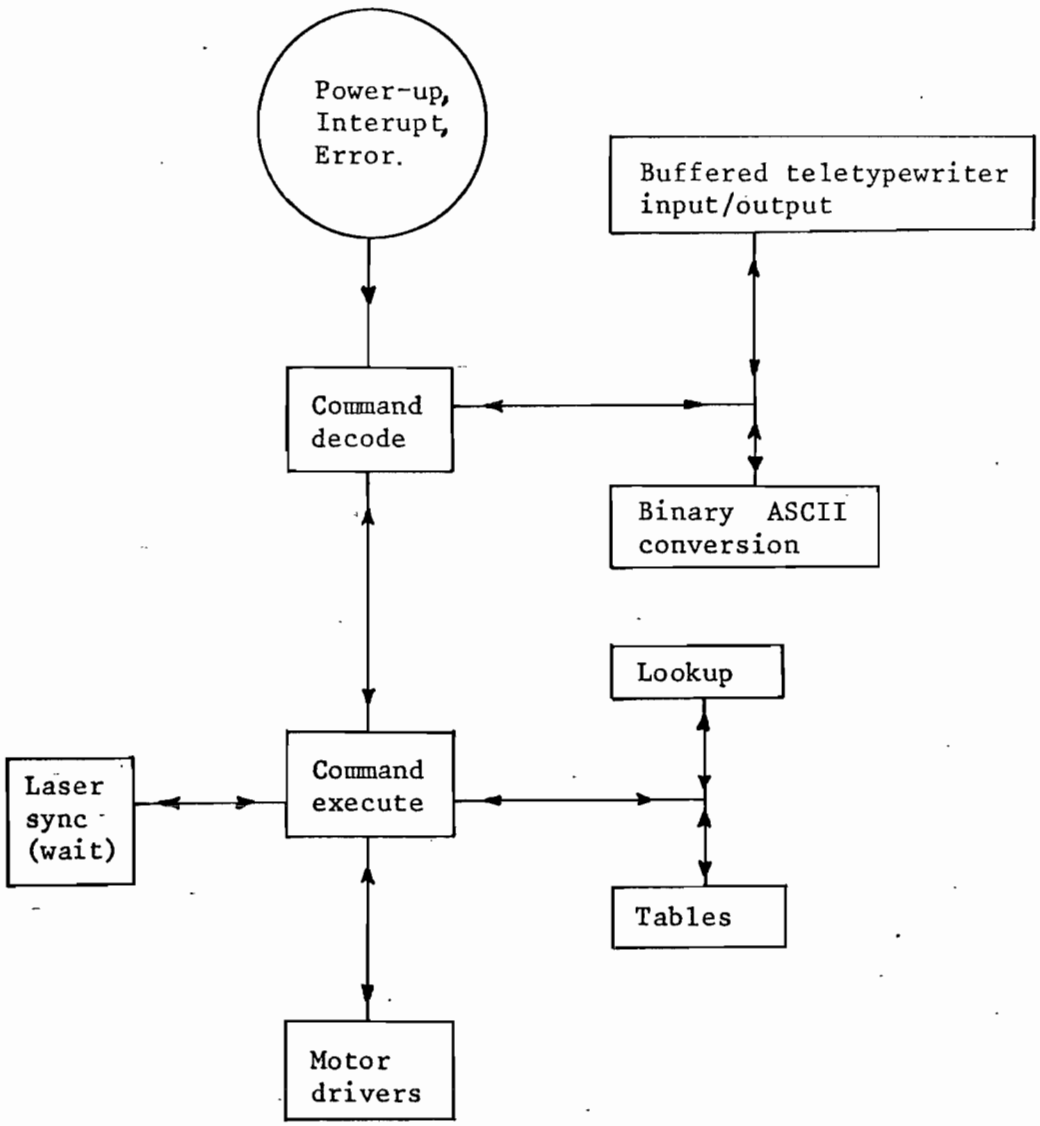


FIGURE 3.18

Software block diagram of system

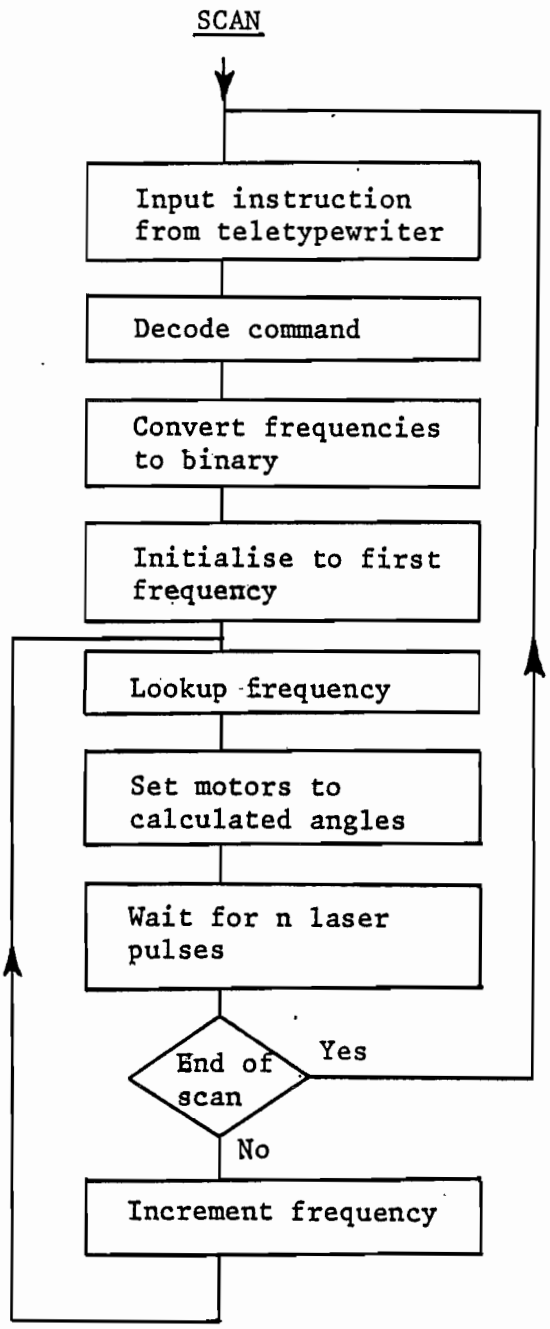


FIGURE 3.19

Flow diagram of real time scan

3.8.2 Table Lookup

This section calculates the motor angle from a frequency or wavelength either specified by the user, or generated by the computer, such as during a scan. The routine internally uses signal frequency (in $cm^{-1}$), but accepts an input in either frequency (in $cm^{-1}$) or wavelength (in $\mu m$) in the ranges of the signal, idler or down-converted outputs, converting to the corresponding signal frequency as necessary.

The routine contains a set of 6 stored data tables, one for each of the stepper motors and three for the etalon. For the stepper motors, the tables contain the actual positions in motor steps (relative to an arbitrary origin) of the motors, specified at intervals of $20cm^{-1}$ in and slightly beyond the signal range. For a given intermediate frequency, the position is calculated by linear interpolation between the two nearest table entries. This gives an equivalent accuracy of better than $0.1cm^{-1}$. The use of polynomials, rather than stored tables, was considered for calculation of the motor positions, but an eighth order polynomial would be required to define the movements of the non-linear crystals to sufficient accuracy, and this would require considerable calculation time on a machine without hardware multiply and divide. The use of tables takes up more memory within the computer than would polynomials, but the tables permit small corrections to the tuning curves to be made fairly easily. Real-time calculations from the basic physical principles were considered impractical.

The etalon position is also derived from data tables with entries every $20cm^{-1}$. The method used to obtain the angle is more complex, because of the discrete jumps as the etalon transfers from one mode to the next, and the greater accuracy involved. The actual function calculated is related to the square of the etalon angle, this being linearly proportional to frequency. To calculate the etalon tilt angle, two parameters of the tuning curve need to be known or easily derived as a function of frequency. These are the absolute frequency of each of the modes (at normal incidence) and the tuning rate (tilt versus frequency). Like the stepper motors, these values could be calculated from first principles (using Sellmeier equations for the refractive index) or by polynomials, but again this was considered impractical. Three 16 bit tables are used for the calculation of etalon position. One contains the value of the tuning rate and the second contains the free spectral range

of the etalon. The third table contains the difference in frequency between that of the $20cm^{-1}$ point and the frequency of the nearest (but lower) etalon mode (at normal incidence), this form being used since it enables the absolute frequency of the etalon mode to be compressed into one word of computer memory, while still maintaining accuracy. The values of the tuning rate and free spectral range are also compressed into one 16 bit word, and are the average values over the $20cm^{-1}$ range. Calculation of the etalon angle (see figure 3.20) consists of determining the difference in frequency between the required OPO frequency and the nearest (lower) etalon mode, which is found by adding multiples of the free spectral range to the frequency stored in the tables. This difference frequency is multiplied by the tuning rate and the square root of the result taken, to convert it to the angle. The errors introduced in this approach are less than $0.03cm^{-1}$. The etalon is always positioned in the free spectral range starting $0.5cm^{-1}$ away from face normal, to avoid problems arising from direct reflection, and to minimise losses at higher angles.

Being able to set the etalon to an accuracy of $0.1cm^{-1}$ over the total tuning range of about $2500cm^{-1}$ involves knowing the refractive index and thickness of the etalon to a higher accuracy than is easily measured. The effect of temperature changes on the etalon leads to drift and, because of the lack of temperature control, this must be capable of correction. To allow for both these effects, extra tuning commands, relating to an offset frequency, are provided. These allow the etalon to be fine tuned by a few wavenumbers by the user during set up, therefore allowing the etalon frequency to be made to coincide with the frequency determined by the grating and $LiNbO_3$. Similar commands are also provided to give a software definition of the angle of normal incidence of the etalon.

Figure 3.21 shows a complete flow diagram for the lookup routine.

### 3.8.3 Motor driving software

This section is responsible for control of the galvanometer and stepper motors. It is called when the motors are required to move, and control is returned once all the motors have reached their final destination.

On entry, the etalon angle is output immediately to the D-A converter, to allow the galvanometer to swing round to its new position,

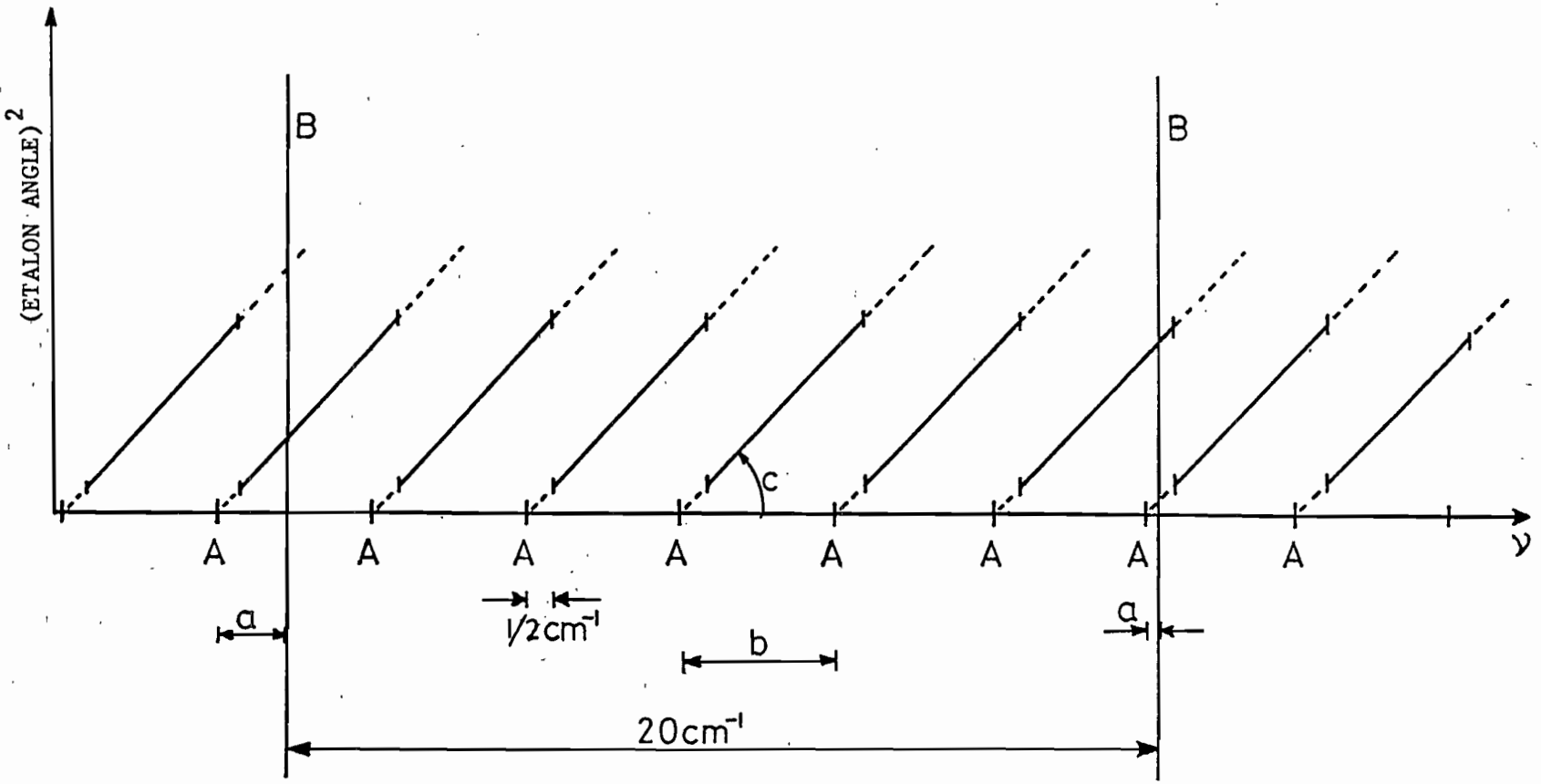


FIGURE 3.20 Calculation of etalon angle.

a - offset frequency (table 1)
b - free spectral range (table 2)
c - slope ($rad^2/cm^{-1}$) (table 3)

A - etalon normal incidence modes
B - table entry frequencies (every 20 $cm^{-1}$)

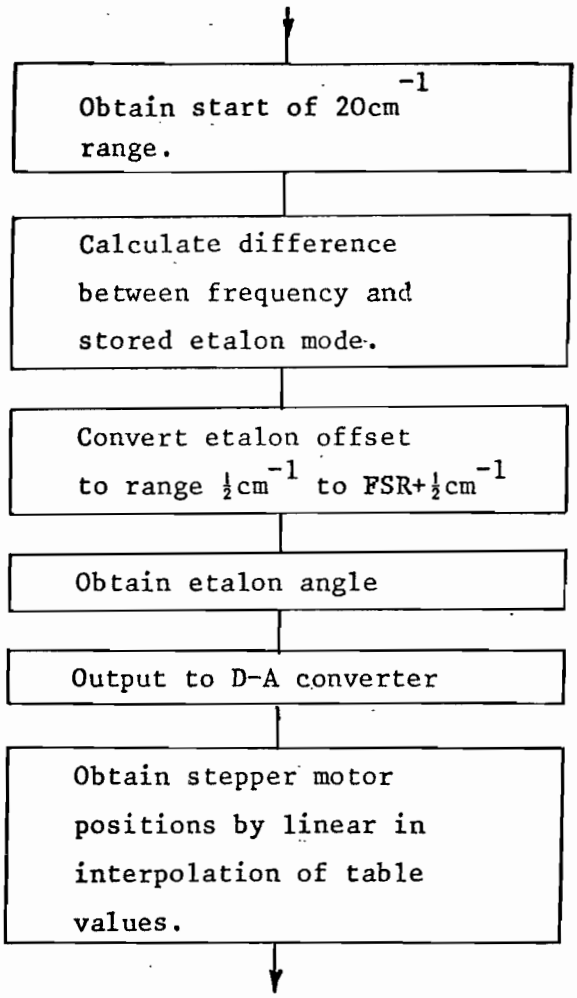


$$\nu_{20} = 20*\mathrm{INT}\left(\frac{\nu}{20}\right)$$

$$\Delta\nu = (\nu-\nu_{20})+\nu_{\mathrm{TABLE1}}+\mathrm{FBIAS}$$

$$\Delta\nu = \Delta\nu \pm m*\mathrm{FSR}$$

$$\theta_{\mathrm{EXT}} = (\mathrm{SLOPE}*\Delta\nu)^{\frac{1}{2}}+\mathrm{EBIAS}$$

$$N = N(\nu_{20}) + \left(N(\nu_{20}+20)-N(\nu_{20})\right)\left(\frac{\nu-\nu_{20}}{20}\right)$$

FIGURE 3.21

Flow diagram for the 'LOOKUP' routine.

while the stepper motors are moving.

The difference between the current and desired future positions of each of the motors indicates the number of steps and in which direction it is required to move. If the motor is to reverse, the number of backlash steps (40) is added to the reverse count, and note is taken, so that the final forward part of the sequence can be made later.

Before any of the motors are moved, the computer waits for 8 periods of the common stepper motor clock oscillator (32ms). This is done to ensure that such a delay exists between the end of the previous stepper motor run and the beginning of the next, to avoid the possibility of restarting a lightly damped motor during an overshoot following a previous halt.

The sequence on the two lines to each motor drive takes the form of a two bit Grey-encoded count, this corresponding to the distribution of current in the 2 pairs of coils. On each clock oscillator pulse, the two phase drive information for each of the three motors is output and is also stored in memory for further use. The memory locations storing the current step count of the motors are also adjusted to keep the computer in step with the motors, in case of an interrupt or other sudden halt.

When a motor has executed the required number of steps, it is held in its position until the other motors have finished. If any of the motors were reversing, there is a second delay of 8 clock periods before they are moved forwards by the appropriate number of steps.

## 3.9 Generation of Tuning Tables

The stored data tables used in the calculation of the angles of the various tuning elements were generated on a computer more suited to arithmetic calculation, and transferred to the control computer using paper tape. The tables are included with the OPO control program in a binary dump for easy reloading. In the event of one of the tuning elements being changed, the tuning angles can be easily re-calculated and a new table generated.

The tables were generated from the calculated tuning characteristics of the appropriate optical component, and from a knowledge of the mechanical linkage between the motor and the component. For the grating, the relationship between angle and frequency is the normal grating equation for Littrow operation. By working backwards from the calculated angle, using the appropriate trigonometric relationships, the displacement of the lead-screw slide was found, and from this the number of stepper motor steps was obtained. The calculations assume a fixed angle of $35^{o}$ between the grating face normal angle and the arm, and any variance in this angle, beyond about $1^{o}$, leads to errors in linearity. The largest uncertainty in the calculations was the actual machined length of the arm. The effective length was obtained indirectly by measurement of the actual OPO frequency generated near the extreme ends of the grating slide, and by comparison of these with the values calculated using the nominal length. This effective length was then used in subsequent calculations to give more accurate table entries.

A similar approach was used to calculate the tables relating to the non-linear crystals. In these cases the fundamental relation between frequency and angle was calculated from phase-matching, using Sellmeier equations to define the refractive indices. For $LiNbO_3$, Sellmeier equations for congruent material were used (25), but as mentioned in section 3.3.1, these require modification to give an adequate fit to the experimentally observed tuning curves, while the equations of Bhar (28) and Hobden (31) were used without such difficulties for CdSe and proustite respectively. The calculated internal angle was converted to an external angle using Snell's equation.

The calculations involved in generation of the etalon tables followed a similar pattern to those above, but the calculated values were scaled and compressed into the 16 bit form used in the lookup.

Figure 3.22 shows the flow diagram of the programs, which were written in both Fortran and Basic, and run on ICL 1907 and CAI LSI-2 computers.

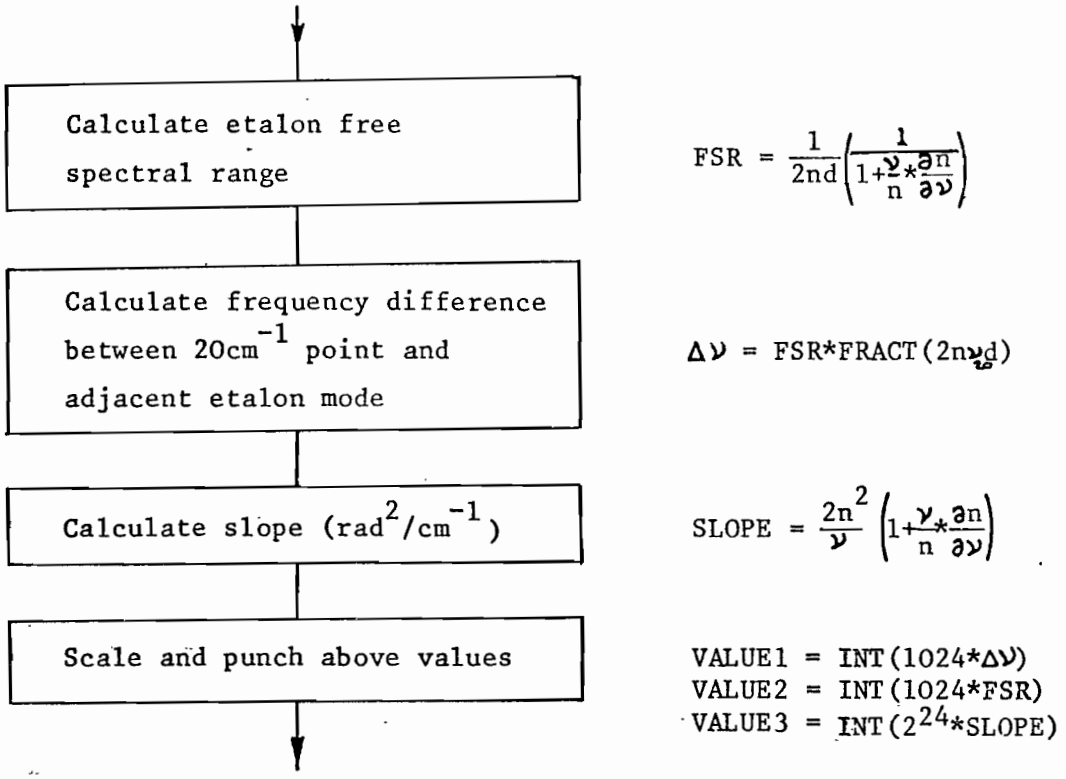


FIGURE 3.22

Etalon table generation sequence.

This sequence is repeated at 20cm$^{-1}$ intervals between 4680cm$^{-1}$ and 7220cm$^{-1}$. The free spectral range (FSR) and the tuning rate in radians$^2$/cm$^{-1}$ (SLOPE) are calculated using the mid-frequency of the 20cm$^{-1}$ interval.

CHAPTER 4

# System Performance

## 4.1 Energy and Tuning Range

A plot of OPO output energy as a function of wavelength is shown in figure 4.1. In this case, the pump energy was 150mJ ($\sim$2J/cm$^2$ at the centre of the beam) obtained by using the double-pass laser amplifier configuration. Both the pump laser and OPO were operated without etalons, so the linewidths of the signal and idler were about 3cm$^{-1}$. The OPO was pumped in a double-pass configuration. The energies plotted in figure 4.1 were derived from measurements of the total signal and idler energy, with a few independent measurements at spot frequencies to determine the relative proportions of signal and idler in the output.

With single-pass pumping of the $LiNbO_3$, the idler is generated in the forward direction in the $LiNbO_3$ only, and in the ideal is totally coupled to the output beam. In contrast, a significant fraction of the signal is reflected by the output coupler to maintain oscillation. Some of this signal energy is subsequently lost, particularly at the grating. With double-passing of the pump beam through the OPO crystal, the interaction between signal and pump in the reverse direction results in additional amplification of the signal. It also results in the generation of idler waves travelling towards the pump source. Measurements have shown that this backward travelling idler wave contains slightly more energy than the normal forward travelling wave (32) but in the present design, the reverse beam is usually lost by absorption in the substrate of the 45$^o$ mirror. Double-passing of the pump does however lead to significant overall increases in the resonant signal and the forward travelling idler, and hence also in the output beam energy.

The conversion of energy from the pump to the OPO output beams in figure 4.1 is of the order of 10-15% throughout much of the tuning range. The actual conversion from the pump is much higher than this, with part of the generated idler being lost in the reverse beam and reflections at the crystal surfaces, and some of the signal being lost within the cavity. Pump depletion of up to 50% has been observed in the centre of the pump beam after its double pass through the OPO.

The changes in output energy as a function of frequency, as shown in figure 4.1, are due to two factors: the decrease in photon energy at longer wavelengths and wavelength-dependent losses within the cavity.

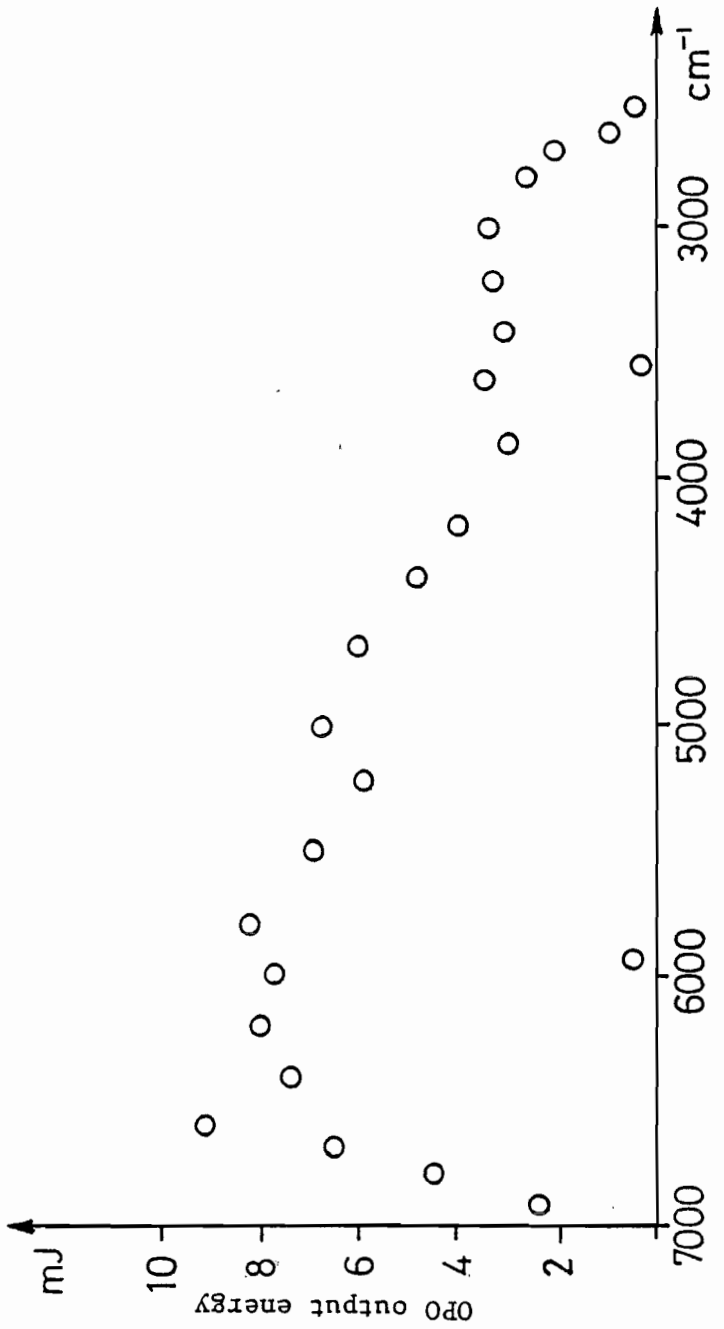


FIGURE 4.1

Output energy as a function of frequency.

Output energies up to 50% higher than those shown above have been obtained more recently.

The wavelength dependent losses within the cavity arise from changing output coupling, off-axis reflections of the signal from the grating and crystal faces, and from optical absorption within the $LiNbO_3$, particularly of the idler, which leads to a reduction in parametric gain. Two $LiNbO_3$ absorptions are prominent, and significantly affect the output of the OPO at certain wavelengths. The increasing absorption for wavelengths longer than about 3.8$\mu$m is due to lattice absorption, and this, being a fundamental property of $LiNbO_3$, determines the long wavelength limit of any $LiNbO_3$ OPO. The sharp falls in output around 2.87$\mu$m and 1.69$\mu$m are due to absorption of the idler at 2.87$\mu$m by OH impurity present in the $LiNbO_3$. The infra-red transmission of one of the OPO crystals is shown in figure 4.2. OPO crystals obtained from various sources have shown the OH absorption to varying extents. For all the crystals tested in the system, the OH absorption has been strong enough to prevent oscillation over 25$cm^{-1}$ bands around the idler wavelength of 2.87$\mu$m and the corresponding signal wavelength of 1.69$\mu$m, with reduced outputs over bands of 150$cm^{-1}$. Claims have been made for $LiNbO_3$ crystals free from OH impurity. With crystals containing the impurity, the tuning gaps can be covered by down-conversion or second harmonic generation, although with an inevitable loss in power.

At a signal frequency of about 6650$cm^{-1}$, the 46.5° cut crystal is set close to face normal, depending on the vertical tilt angle of the crystal. The near-axis reflections of both signal and idler from the crystal faces can lead to a noticeable increase in OPO output power, although no significant change in the linewidth or absolute frequency has been observed. The effect is more pronounced with uncoated $LiNbO_3$, or crystals anti-reflection coated for 1.4$\mu$m. This effect can be of use in initial alignment of the OPO.

Plots of the OPOs output away from any $LiNbO_3$ absorptions as a function of pump power are shown in figure 4.3. The pump limit of 2$J/cm^2$ is set to prevent crystal damage. The outputs compare well with those obtained by other workers (e.g. (18) ) under similar conditions. When the cavity losses increase due to absorption or misalignment, the threshold rises and the efficiency decreases.

Figure 4.4 shows the down-converted outputs obtained using a 10mm long crystal of proustite (type IIb phase-matching) and a 24mm long crystal of CdSe. The outputs produced from both crystals are lower than calculated.

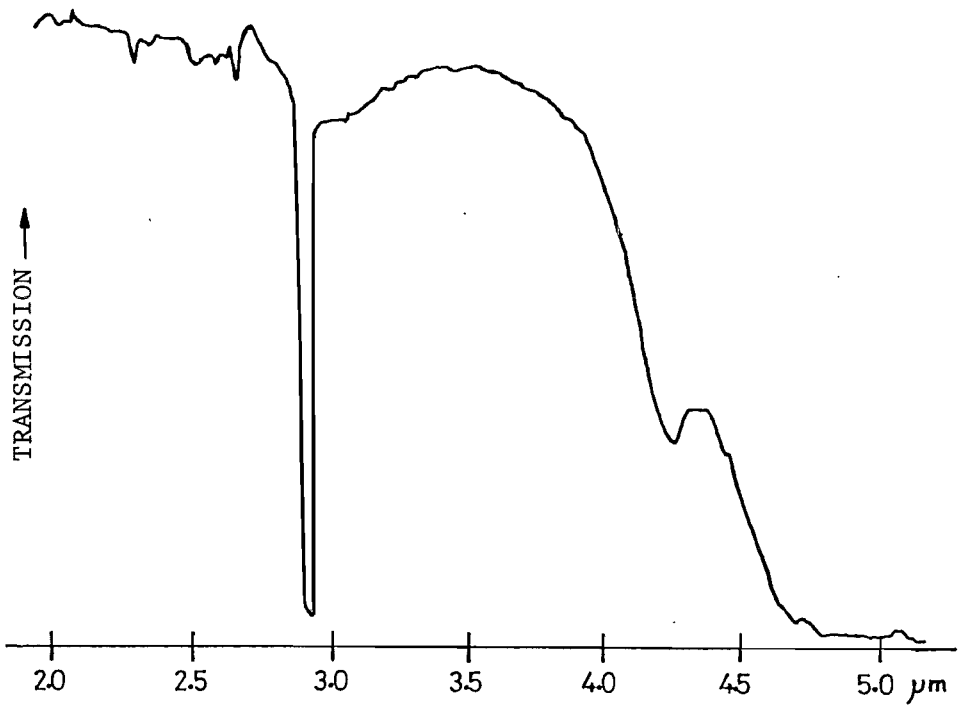


FIGURE 4.2

Infrared transmission of a typical 5cm long $LiNbO_3$ OPO crystal.

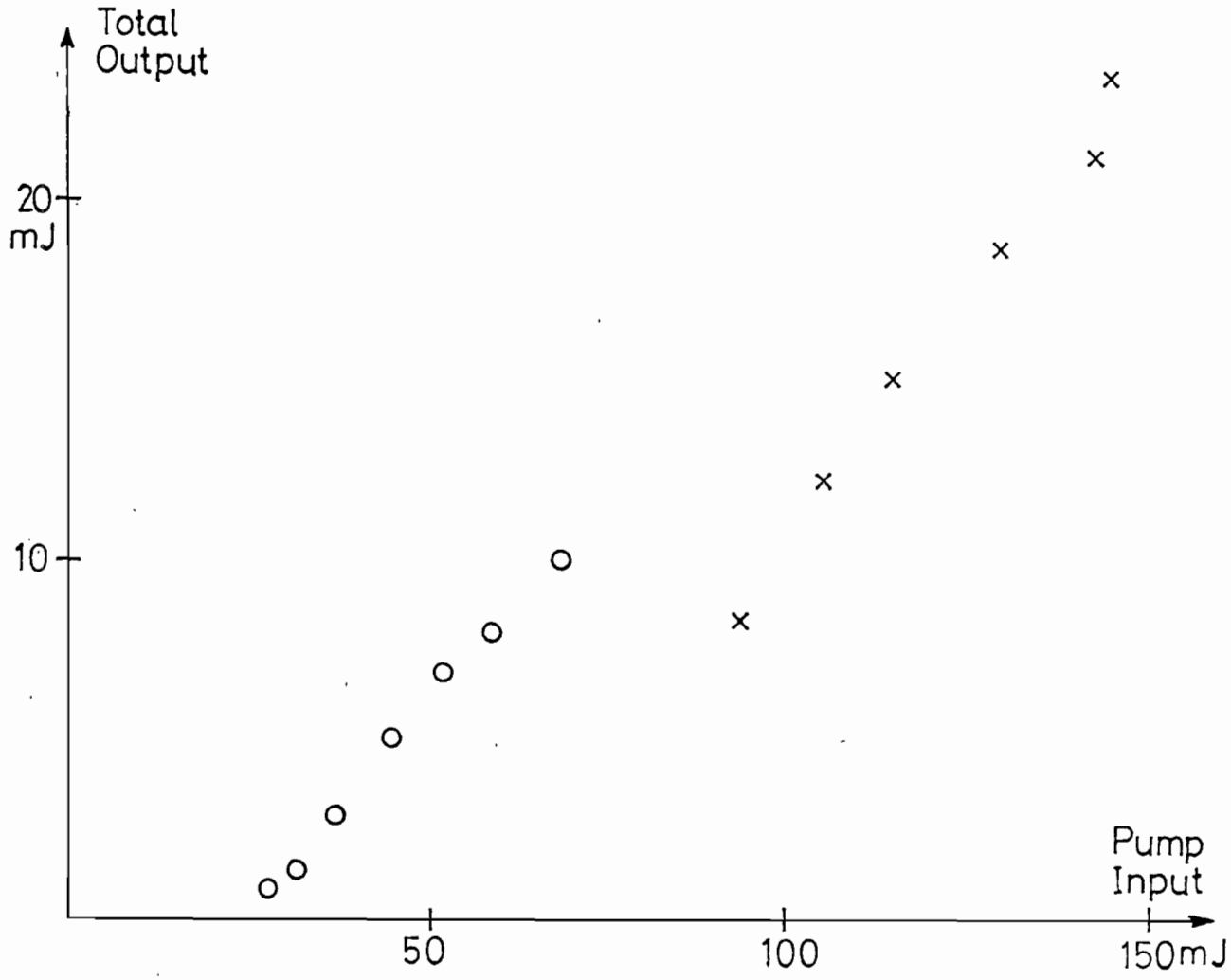


FIGURE 4.3 OPO output as a function of pump input energy.

O - single pass Nd:YAG amplifier.

× - double pass Nd:YAG amplifier, larger diameter pump beam.

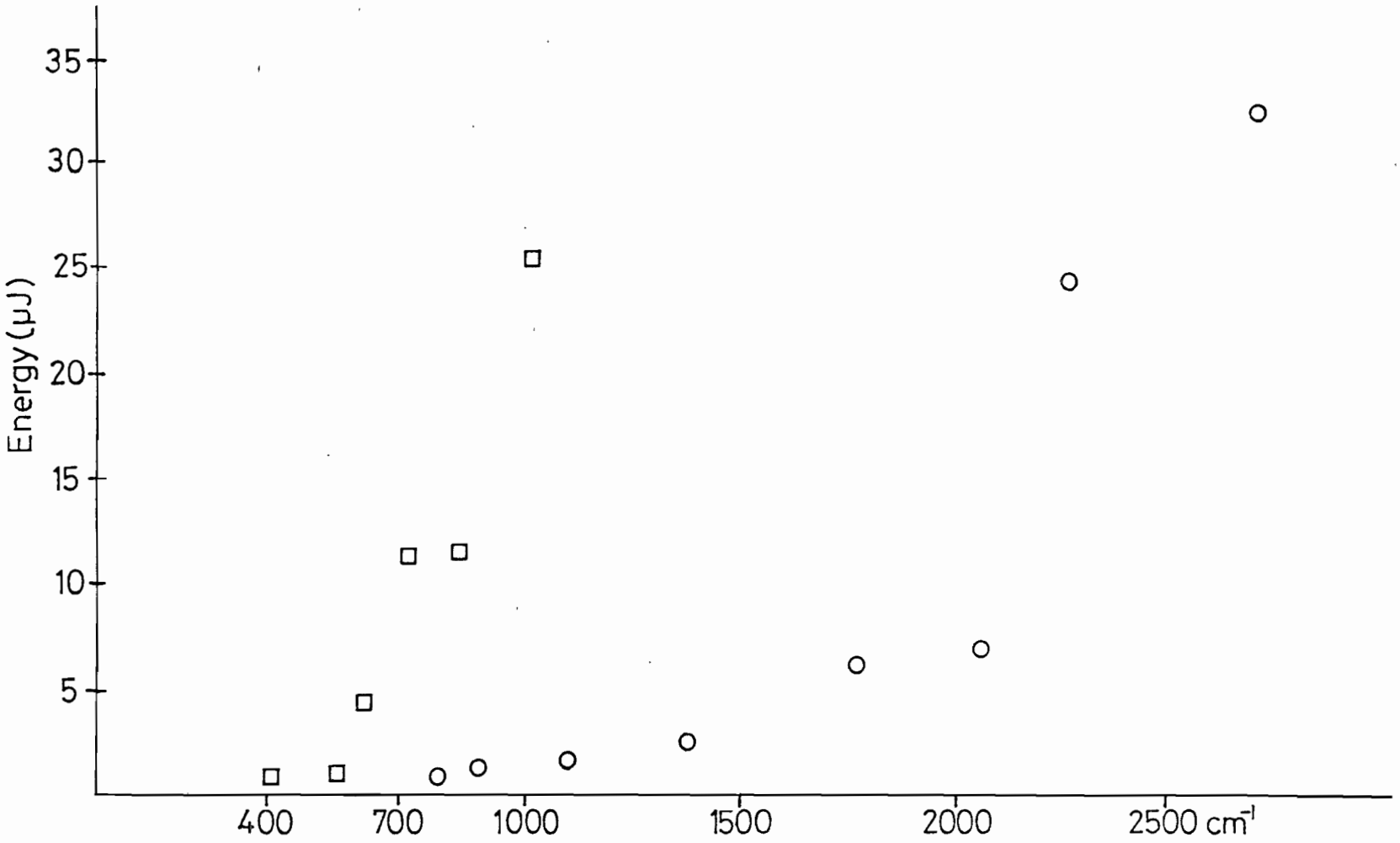


FIGURE 4.4 Down-converted output energy

○ - in 1cm proustite crystal (type IIb)

□ - in 2.4cm CdSe crystal

Insertion of the etalon into the OPO to narrow the linewidth results typically in a 10-30% drop in output energy from both the OPO and down-converter, and also a slight reduction in tuning range.

## 4.2 Linewidth and Beam Divergence

Like the output energy, the linewidth of the signal idler or down-converter output is easily measured at spot frequencies. Most of the linewidth measurements made on the system have involved either observing the transmission of one of the outputs through a scanning monochrometer, or scanning the OPO while measuring transmission through a fixed optical filter or absorption line. Since information is acquired point by point, many pulses are required to obtain the linewidth profile, and pulse to pulse variations in profile or frequency may not show up properly.

When operated without an etalon, the linewidths of the signal and idler are usually in the range 3-4$cm^{-1}$ (FWHM). The pulse to pulse frequency stability has been determined to be better than 0.5$cm^{-1}$. Operation of the OPO with the intracavity etalon reduces the linewidth of the signal to around 0.1$cm^{-1}$, and the linewidth of the idler is reduced to a similar value when the pump is suitably narrowed. Figure 4.5 shows the idler linewidth, as monitored by manually tuning the OPO etalon over a narrow gas absorption line.

No attempt has been made to control the length of the OPO cavity, and hence fine tune the longitudinal modes of the cavity, since the mode spacing, at 0.02$cm^{-1}$, is several times smaller than the etalon narrowed linewidth of the device. Fine tuning of the cavity modes is unintentionally achieved by rotation of the $LiNbO_3$ crystal. Theory (e.g. 33) tends to indicate that the longitudinal modes of the OPO will not develop strongly, at least during the build up phase of the resonant field, because of the high gain and small number of cavity transits involved. If cavity modes do appear, as has been seen with dye lasers (26), they may present problems if the OPO is being used to investigate samples which have fine structure of the order of 0.02$cm^{-1}$.

The linewidth of the down-converted output is determined by those of the signal and idler. Figure 4.6 shows an absorption scan of $CO_2$ gas, taken with the down-converted output, although with a 0.5$cm^{-1}$ linewidth since in this case the linewidth of the pump was not narrowed.

The measured beam divergences of about 4 milliradians (full angle to half intensity) are several times the diffraction limit of 1mm diameter beams at the signal and idler wavelengths. Details of some of the

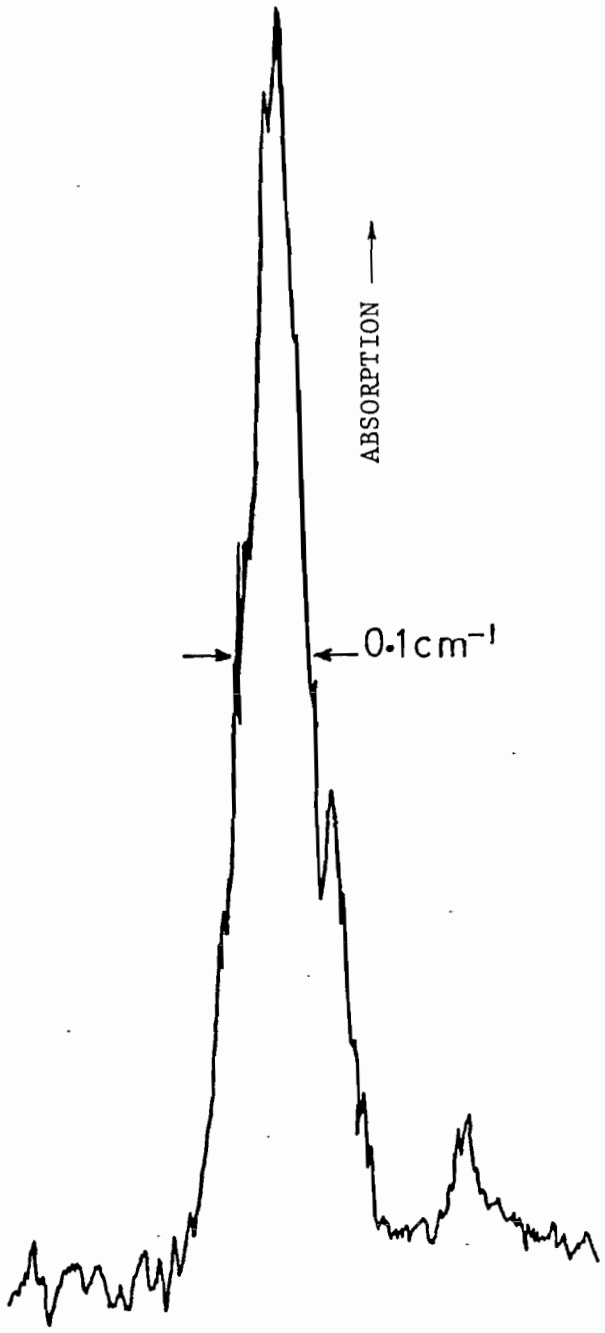


FIGURE 4.5

0.1 $cm^{-1}$ resolution scan of an absorption line in methane gas, taken using the idler output of the OPO, with manual tuning of the etalon.

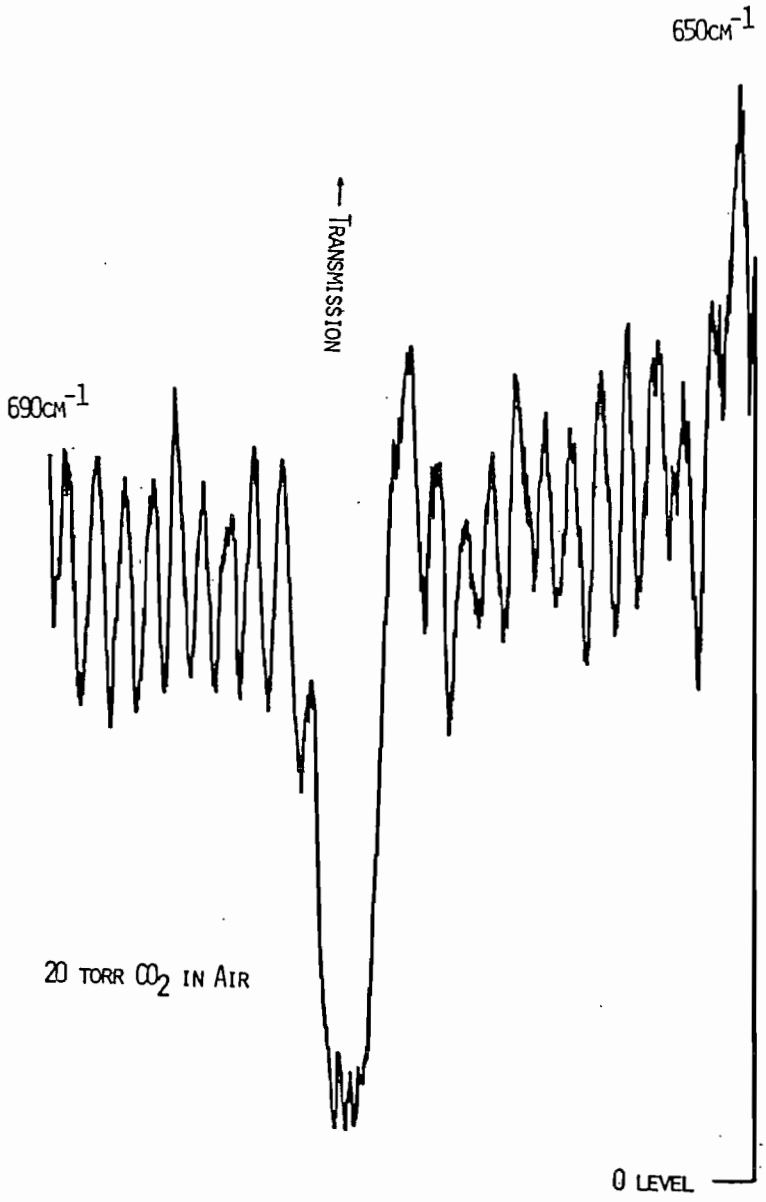


FIGURE 4.6

Double beam absorption spectrum of $CO_2$ gas, between 650 $cm^{-1}$ and 690 $cm^{-1}$, taken using the output from the CdSe down-converter.

measurements are given in (32). The signal beam profile, as observed by burns on 'Polaroid' film, is very irregular, much more so than the irregularly shaped pump beam. The CERL OPO however produces near circular burns on 'Polaroid', and has a measured beam divergence of 2.7 mrad (vertical) x 1.1 mrad (horizontal) (34).

## 4.3 Tuning Control Performance

The main problem encountered in tuning control was that of mistracking, while scanning, between the $LiNbO_3$ crystal phase-matching, the grating and the etalon. The major uncertainties responsible for the differences between the calculated tuning curves and those actually observed were in the values of the refractive indices of the $LiNbO_3$, the length of the arm in the grating drive mechanism and in the thickness, and hence the free spectral range, of the etalon. In each case, more accurate tables for use in the internal tuning calculations were generated on an external computer; these new values incorporated corrections derived from the observed errors.

Imperfect tracking between the grating and $LiNbO_3$ crystal results in phase mis-match, and hence a fall in output, and also in a pulling in frequency towards that of perfect phase-matching. Conditions may also favour a slightly non-collinear interaction in the $LiNbO_3$, with resulting distortion of the output beam profile. These effects can be corrected by manual adjustment of the $LiNbO_3$ angle. In contrast, imperfect tracking between the etalon and grating (and $LiNbO_3$) results in the oscillation appearing periodically on two adjacent modes as the OPO is tuned. The spectral output of the etalon narrowed OPO is shown in figures 4.7 and 4.8. In figure 4.7, the tuning rates of the grating and etalon differ by about 1%, due to an error in the value of etalon thickness used in the calculations of the tuning tables, and the transfer of output energy between adjacent modes can be clearly seen. When two etalon modes are approximately equally spaced from the grating frequency, the division of energy into each mode varies from pulse to pulse. The etalon tuning rate was corrected in the trace shown in figure 4.8.

With the final versions of the data tables, the tracking between the grating, $LiNbO_3$ and CdSe down-converter is such that following accurate alignment and calibration of the system the non-linear crystals do not require additional adjustment to obtain maximum output throughout the tuning range, and the OPO output frequency is accurate to better than $\pm$ 2cm$^{-1}$. With the etalon, a tuning range in excess of 400cm$^{-1}$ near degenerate is possible without the appearance of unwanted etalon modes. The tuning range with an etalon is smaller further away from degenerate, because of frequency pulling resulting from slight inaccuracies in the $LiNbO_3$ angle. A 300cm$^{-1}$ scan range has however been noted around 3.3$\mu$m.

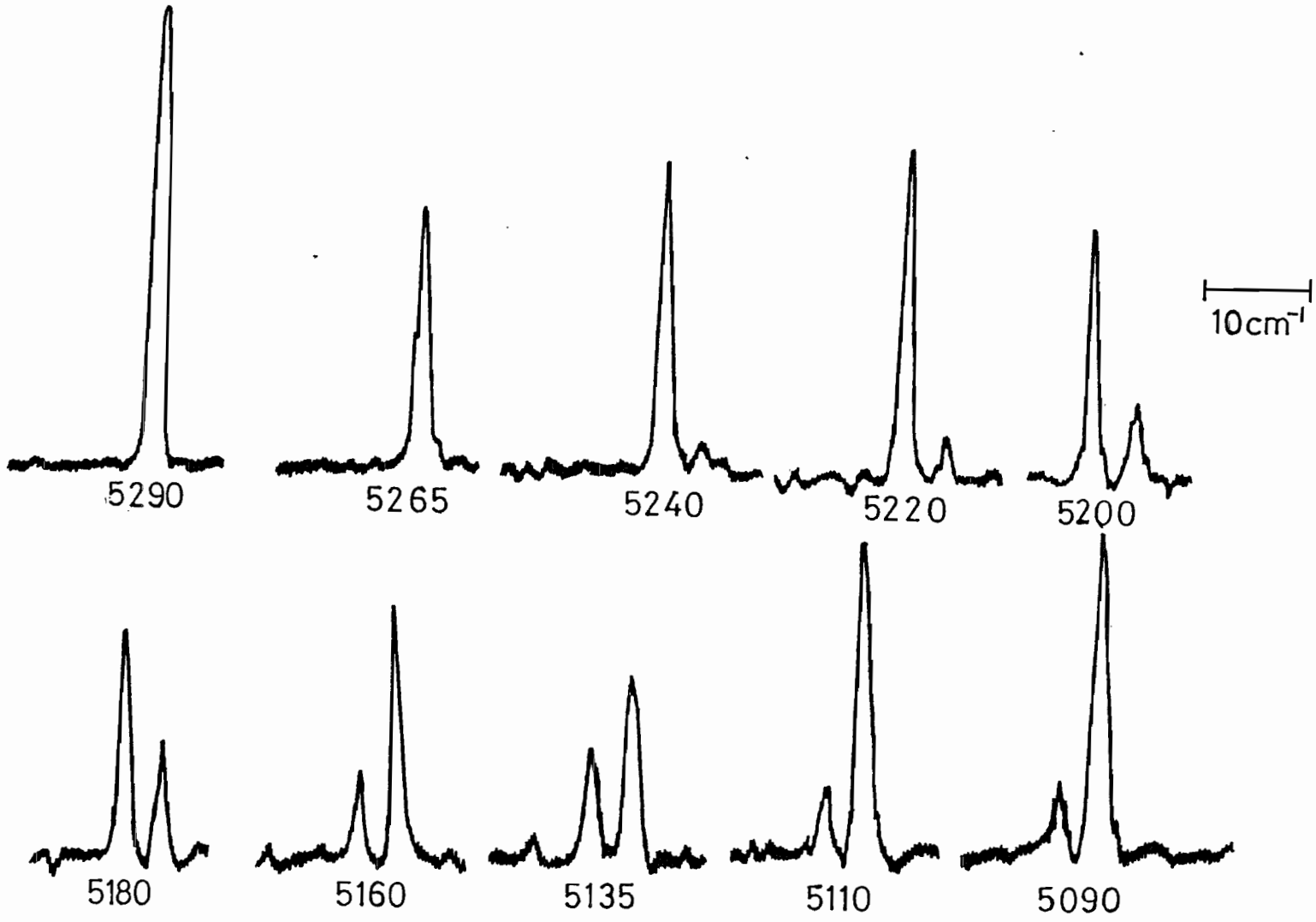


FIGURE 4.7

Spectral output of the OPO signal, with the intracavity etalon scanning in frequency about 1% slower than the grating and crystal. In each trace, the OPO was scanned across a fixed frequency monochrometer of $2cm^{-1}$ resolution. No fine adjustments were made to the etalon between runs. The figures refer to the monochrometer setting ($cm^{-1}$).

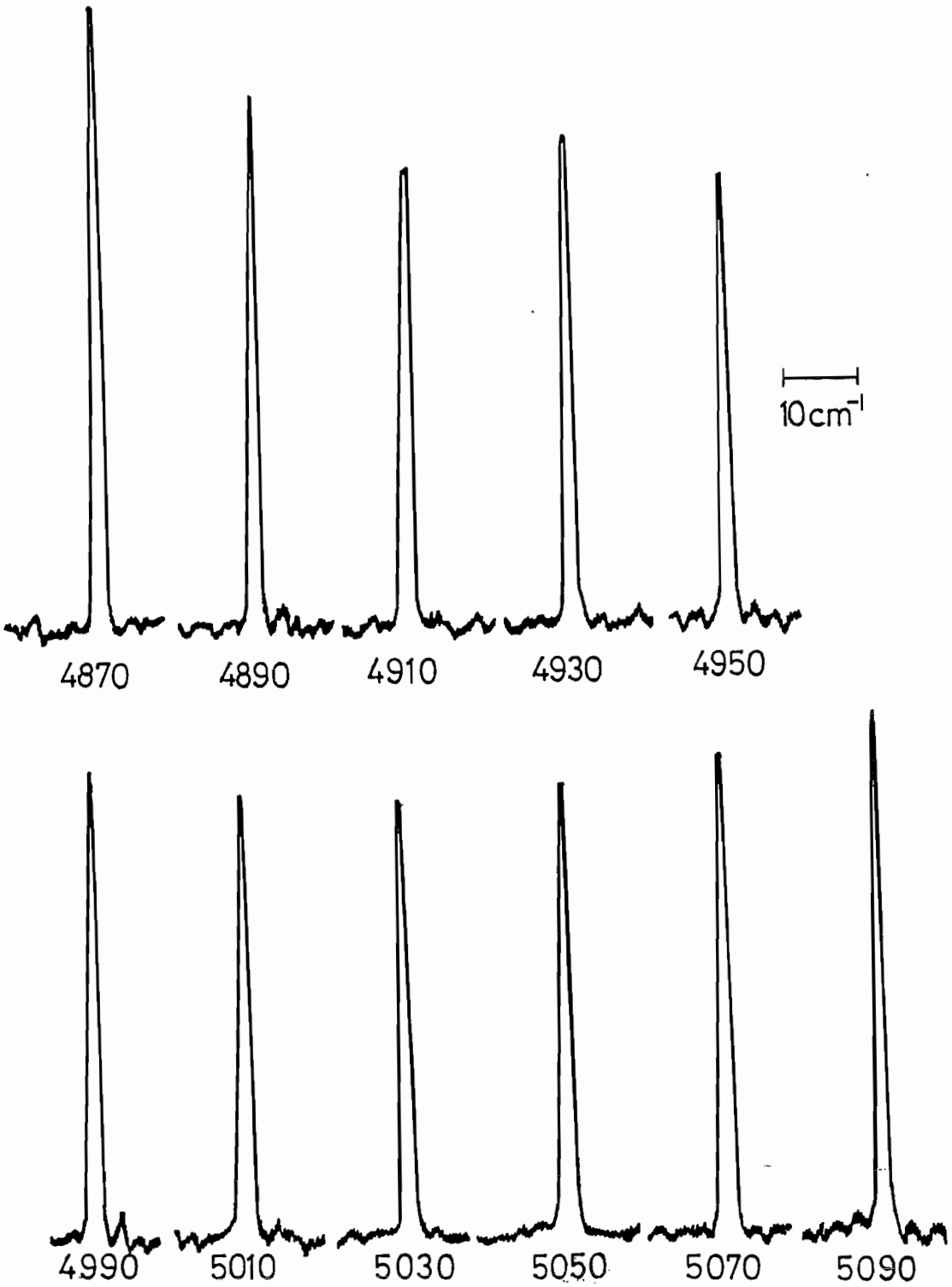


FIGURE 4.8

Spectral characteristics of the signal of the intracavity etalon narrowed OPO, showing good tracking between the etalon and grating. The traces were obtained by scanning the OPO over a fixed frequency monochrometer. No fine adjustments were made to the etalon between runs. The measurement at 4970 $cm^{-1}$ was missed because of an interuption to the experiment.

The dead reckoning between the stepper motors and computer has proved satisfactory during both normal operation, and also during normal interruptions of the power supply. The motor positions have only been lost following carelessness by the system user, or long unexpected power failures.

The maximum tuning rate is determined by the need to run the common stepper motor oscillator at a frequency within the start-stop range of each of the motors, and to be away from motor resonances. Access times can be particularly slow when the CdSe down-converter is in use, because of the wide angular range of the crystal, and the fine step size of the motor used. On the CERL OPO, where the stepper motors are each run from independent oscillators with acceleration to the highest possible speed, the longest access time is of the order of 12 seconds.

## 4.4 Experimental use of the OPO System

The outputs of the OPO and down-converter have been used as the source in a number of spectroscopic experiments. These were performed mainly to gain further information on the performance and shortcomings of the system. The results of some of these experiments are given below.

The absorption spectrum, shown in figure 4.9 is of the water content of the atmosphere at normal pressure, around 1.9$\mu$m, taken using an optoacoustic detector. The signal linewidth was 0.1cm$^{-1}$, although the time constant of the data acquisition electronics was such that the effective resolution was 0.2cm$^{-1}$. The scan, in which the etalon, grating and $LiNbO_3$ were under the complete control of the tuning computer, took 20 minutes to complete, but with a 20 pps laser, as against the 3 pps one used, would have been reduced to 3 minutes.

The detector used in the water vapour trace (figure 4.9) was an enclosed optoacoustic cell, but the strength of the acoustic signal arising from the high OPO output permits the simple use of an open microphone, placed near to the beam. Figure 4.10 shows the absorption, around 3.4$\mu$m, of methane, detected in a natural gas flame by a small microphone positioned to the side of the flame. The noise on the trace is probably a function of the signal processing rather than just fundamental acoustic or electrical noise. Dual beam ratioed scans of the infra-red transmission of the flame were also made (figure 4.11), demonstrating the use of the system in spectroscopically difficult samples.

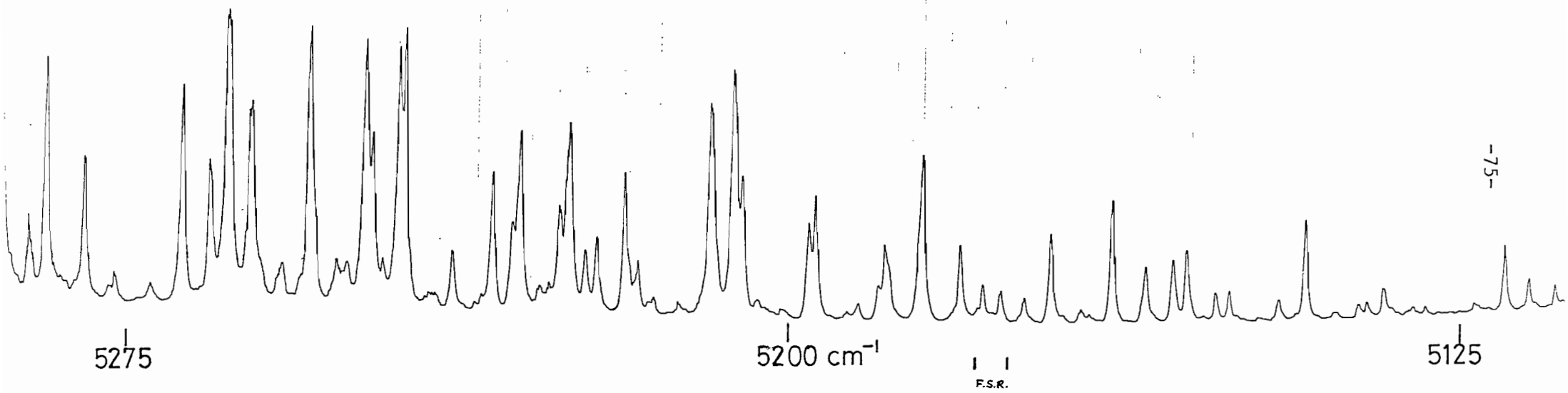




FIGURE 4.9

0.2 $cm^{-1}$ resolution opto-acoustic spectrum of atmospheric $H_2O$ vapour, around 5200 $cm^{-1}$, taken using the signal of the $LiNbO_3$ OPO.

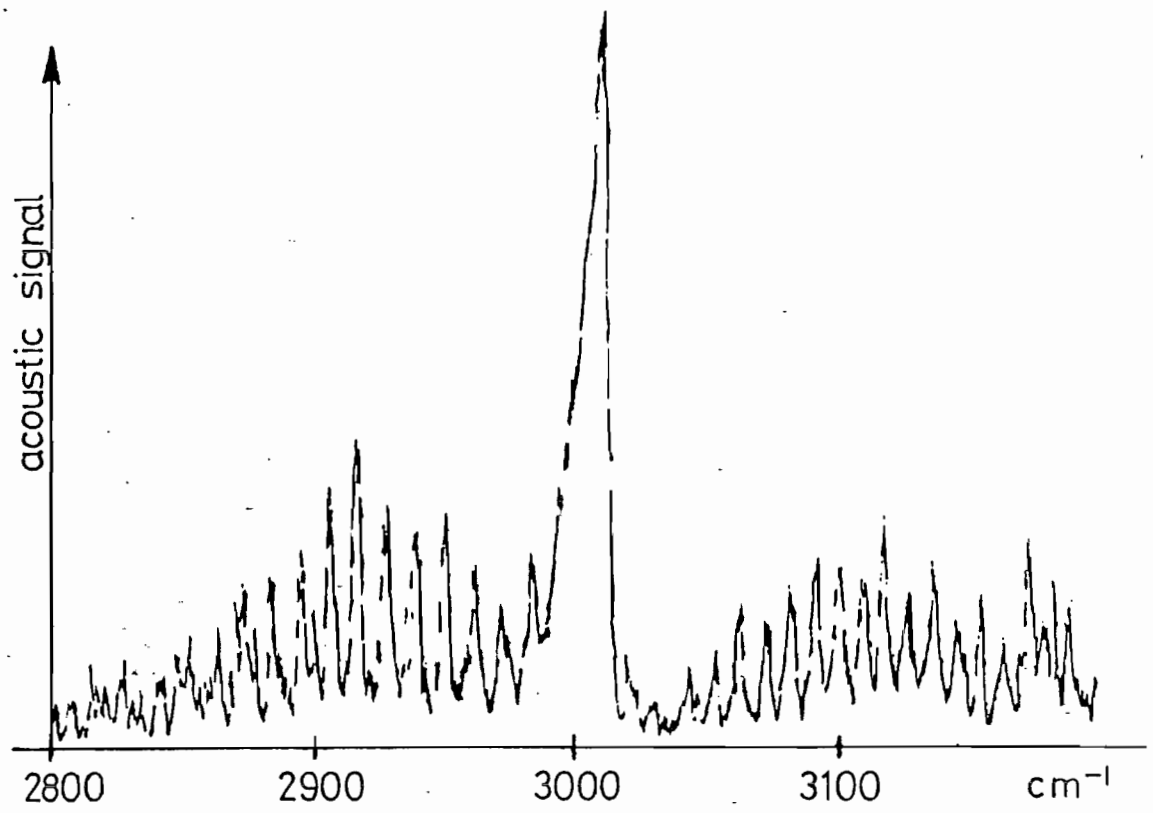


FIGURE 4.10

Optoacoustic spectrum around 3.3μm of a natural gas flame.

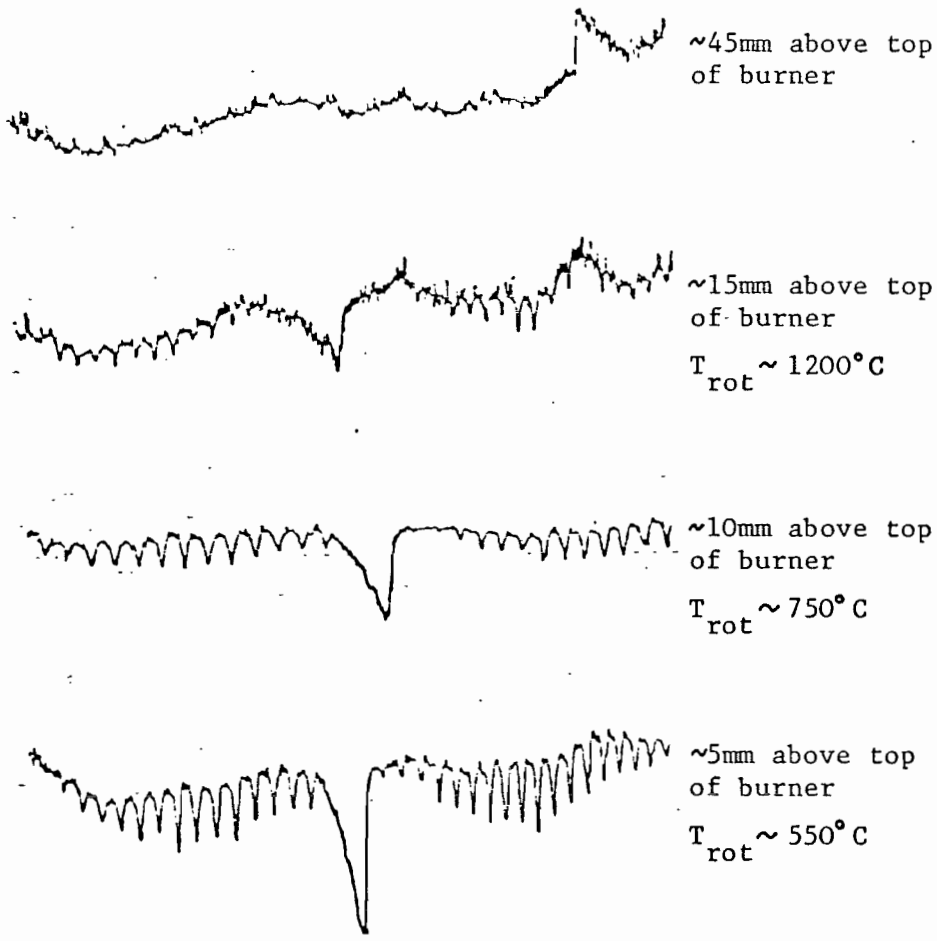


FIGURE 4.11

Dual beam spectra of a natural gas flame.

## 4.5 Optical Damage and Other Effects

The main danger while operating the system is that of optically induced damage to components. A series of measurements established that pump intensities of $2J/cm^2$ (at the centre of the beam) could be safely handled in double-pass by the OPO crystal and good quality mirrors. A pump beam of good spatial quality, and with a peak intensity of $2J/cm^2$ pumps the OPO efficiently, without risk of damage to components. In two years of operation, surface damage has occurred occasionally on the OPO crystal, but has been attributed to excessive pumping levels, or to hot spots in the pump beam. The OPO mirrors have been similarly damaged.

When the OPO is tuned to a strong atmospheric absorption line, such as water vapour at $1.9\mu m$, absorption of the signal or idler leads to an audible "ticking", emanating from both the OPO cavity and the path of the output beam. The effect can be particularly impressive while scanning, with a quiet pump laser operating at 20 pps. The absorption does not appear to significantly affect the output generated by the OPO, but attenuation is noticeable in the output over a path length in air of greater than 1 metre. One strong water vapour absorption line lies close in wavelength to three times that of the visible He-Ne laser, and has on occasions caused confusion when the OPO has been aligned and optimised at this wavelength.

In addition to the 3-wave parametric coupling between pump, signal and idler, two other NLO processes can be observed in the $LiNbO_3$ crystal. At about $1.85\mu m$, the $LiNbO_3$ is phase-matched for type I second harmonic generation of the signal, giving rise to an additional, e-polarised output at $\sim 0.925\mu m$ (35). This effect does not noticeably reduce the signal and idler outputs. Low efficiency S.H.G. of the pump also occurs, this being independent of the frequency to which the OPO is tuned, and results in a low intensity green beam propagating along with the OPO outputs. This S.H.G. is mainly due to an unphase-matched coupling between the e-ray $1.06\mu m$ beam and the e-ray second harmonic. Although the coherence length of this interaction is only about $1\mu m$, the d-coefficient is four times greater than that responsible for parametric oscillation and o-ray S.H.G.

CHAPTER 5

# Further Development

## 5.1 Continuation of Development

The tunable infra-red system described in this thesis, and currently in use at Southampton University, has shown the capability offered by the Nd:YAG pumped $LiNbO_3$ optical parametric oscillator and down-converter as a source, in the areas of difficult I.R. spectroscopy and photochemical excitation, and it has shown the additional versatility given to such a system by digital processor based electronic control. Several spectroscopic and photo-excitation experiments using the system are described by Tupper (10).

Now that the various components of the system have been working together for some time, several short-comings in the design and system integration are apparent. Some of these have arisen from the somewhat piecemeal way in which the system was developed, while others are due to components behaving differently from what was expected. The system would gain considerably from the input of a few new ideas, and complete redesign and reconstruction, with the advantage now that reference can be made to a working system.

A major redesign was done for the OPO built and supplied to CERL. However, most of the changes were made to rectify 'individual' weaknesses in the Southampton design, and no fundamental changes in overall design philosophy were made. The CERL device still therefore lacks complete harmony between the optics, mechanics and electronics. The CERL OPO has been at the Laboratories at Leatherhead since March 1978, and in the ensuing period, the general behaviour of the device while in operation has been observed, and several parameters measured. The most noticeable improvement over the Southampton OPO is that of the divergence of the output beam, which has been measured as being a factor of two smaller in both vertical and horizontal planes than the Southampton OPO. This can probably be attributed to the improvement in the quality of the beam from the pump laser (J K System 2000). However, some problems, not previously encountered on the Southampton device, remain to be overcome, particularly in connection with $0.1cm^{-1}$ idler operation. Operation of the CERL OPO, including the full minicomputer control, is easier that that of

the original, in part due to the higher repetition rate of the pump laser, and also the use of a V.D.U. for communication.

The final engineering of the system must be the responsibility of a commercial manufacturer rather than that of a university research group. Following an order for an OPO from Cambridge University's Department of Physical Chemistry, J K Lasers Ltd have executed much of the necessary design and engineering work on the device, based on the designs of the CERL and Southampton OPOs. The company has produced and delivered a device considerably simpler in concept and design than that at Southampton, by the introduction of a new optical and mechanical layout, while maintaining the same level of performance. In this device, the pump is introduced into the cavity by reflection from the 45° beam-splitting dielectric mirror, thus eliminating the need for a wide-band dichroic reflector. At present, this OPO is manually tuned, but provision exists for incorporation of stepper motors, driven by electronic control.

As an additional part of the design effort for the JK OPO, a microprocessor-based control system was developed at Southampton, using the same software concepts as are used in the minicomputer system. However, the use of a special function keyboard and display simplifies communication with the operator, and the use of read-only memory for program and data table storage turns the microprocessor into a compact dedicated OPO controller. One of the features of this controller is the front panel 'digital knob', connected to a rotary shaft encoder, which allows fine tuning of the system frequency or motor position in a manner similar to the fine tuning of a radio. The microprocessor at present lacks control of the etalon, memory retention in the event of power failures, and several other refinements, but it still represents a considerable step forward, removing the need for specialised knowledge to operate the minicomputer, as well as reducing the physical size, cost and complexity of the controller.

## 5.2 Future Improvement

One feature which could be added to the two computer controlled systems is the addition of accurately positioned sensors on the stepper motor drive mechanisms. These would allow automatic calibration when the system is switched on, thus removing the need for non-volatile memory. They would also remove any uncertainty regarding the use of motor dead reckoning over a long period of time. Microswitches or optical sensors monitoring both linear and rotary movement of the leadscrews could be used to obtain adequate accuracy in calibration. Alternatively, linear or rotary position encoders could be used to give an absolute read-out of the actual drive positions at all times. The motor drive electronics could be redesigned to reduce power dissipation while the motors are static.

The two most significant parameters of the output beams of the $LiNbO_3$ OPO and down-converter which are capable of considerable improvement are the linewidth, which is still a factor of $\sim$100 greater than the Fourier Transform of the pulse length, and the divergence of the output beams, which is about five times greater than diffraction limited. Single longitudinal mode operation of a Nd:YAG pumped $LiNbO_3$ OPO has been reported in the USA (36), with a linewidth of approximately $0.01cm^{-1}$. Such a device has the additional complexity of requiring, for fine tuning, adjustment of the cavity length, although pressure tuning could be used in this connection.

The present large beam divergence is due to the lack of transverse mode control within the cavity. The divergence and transverse mode structure are determined by the effects of phase-matching and beam overlap within the crystal. One method which was tried for control of the transverse modes was the insertion of circular apertures of varying sizes in front of the grating. These appear to have had little effect on the beam divergence, but narrowed the linewidth of the OPO slightly.

The grating tuned L-shaped cavity has been used for most of the $1.06\mu m$ pumped $LiNbO_3$ OPOs constructed world-wide. However, other cavity configurations are possible, and may offer some advantages, particularly in assisting improvement of the linewidth or mode structure of the output. One interesting configuration is the ring-cavity OPO, in which the return path through the crystal is eliminated. Ring cavities can have the peculiar property of having a shorter cavity transit time than

that of the shortest two mirror cavity formed around the same crystal, since the physically longer return path is in air. With angle tuning, there is a problem of beam shift and overlap (figure 5.1(a) ), although the cavity can remain in parallel alignment as the crystal is rotated. Reflective diffraction gratings cannot be easily used as line narrowing elements in a ring cavity, but there is a large amount of space available in the return path for the insertion of transmission tuning elements, such as birefringent filters and etalons, and also for mode control apertures, which could be used in conjunction with focusing elements (figure 5.1(b) ). Angle tuned ring-cavity oscillators have been demonstrated using proustite and $LiNbO_3$ as the non-linear materials (37).

An alternative approach to transverse mode control of the OPO which may prove of value is the use of a geometrically coupled unstable resonator cavity. The use of a dichroic output coupler reflecting only the signal would result in the idler emerging without the hole, which is a characteristic of the output of most unstable resonator devices.

The $LiNbO_3$ crystals currently available are potentially capable of handling pump energies of a few joules provided the pump beam diameter is suitably large. It is unlikely that all this energy can be used successfully in the pumping of an OPO of the current design, without severe degradation of the output beam. One technique for increasing the energy of the tunable output is to follow a well-behaved $LiNbO_3$ OPO similar to the present design by one or more high energy stages of optical parametric amplification, using 1.06 $\mu$m pumped $LiNbO_3$. This has been done in the USA (38). It may also be possible to use the high energy O.P.A. in conjunction with many other kinds of infra-red tunable source covering the range 1.4 $\mu$m to 2.1 $\mu$m (or 2.1 $\mu$m to 4 $\mu$m). Likely candidates are the CW colour centre laser, and down-conversion from tunable dye lasers. In both these cases, the initial tunable source is better developed than the 1.06 $\mu$m pumped OPO in terms of beam divergence and linewidth. To maintain a narrow linewidth during amplification, a frequency narrowed pump is required, otherwise both the signal and idler outputs of the O.P.A. may acquire linewidths of the same order as that of the pump*. The $LiNbO_3$ optical parametric amplifier can be used in a predictable way to generate high energy pulses from the 1.06 $\mu$m pump, and the outputs can be mixed in a down-conversion stage to generate outputs of wavelength longer than can be generated in $LiNbO_3$.

* The assumption that a broadband pump will not broaden the linewidth of the signal is only valid in the low gain limit of an OPA.

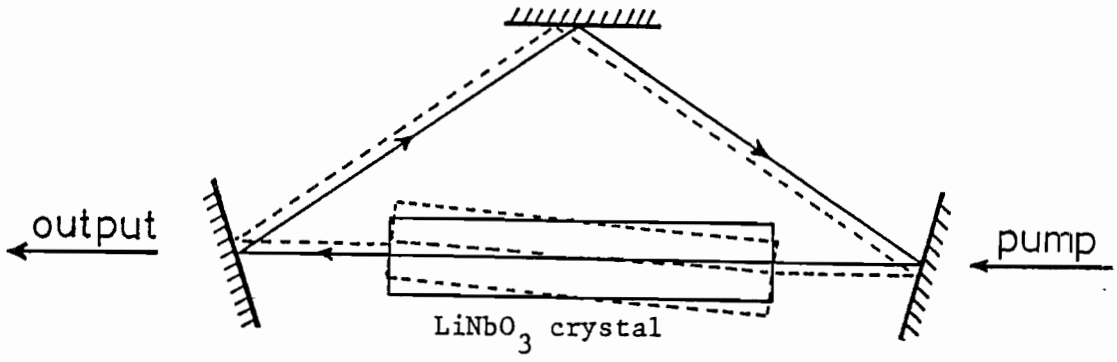


a

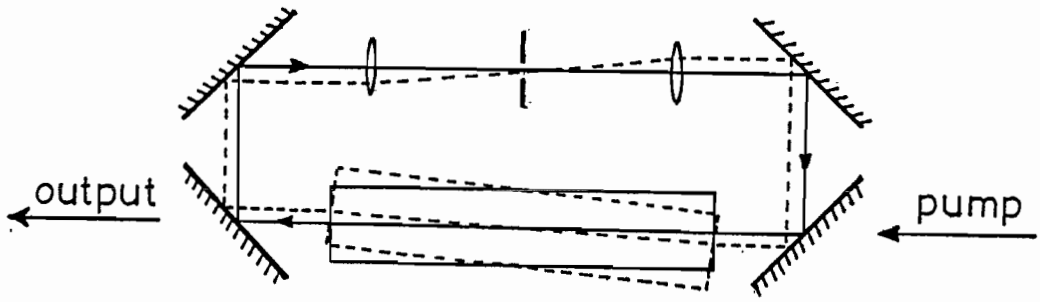


b

FIGURE 5.1

Ring cavity configurations

a - basic 3-mirror cavity, showing effects of crystal rotation.

b - 4-mirror cavity, with spatial filter.

APPENDIX 1

## OPO Alignment Procedure

### A1.1 Alignment without Etalon

The OPO and down-converter have to be positioned so that the pump beam passes through the mirrors and non-linear crystals, for all possible angles of the crystals. Both the $LiNbO_3$ and down-converter crystals have limited centering facilities to allow fine adjustments of their positions to be made. Allowance has to be made for beam walk-off in the crystals.

The main reason for using collinear operation of the OPO is simply that the signal and idler otherwise emerge at differing angles, with the angle of the idler being wavelength dependent. The angle of emergence of any output generated in a subsequent down-conversion stage is even more strongly affected. The threshold of oscillation of the OPO increases for misalignments greater than a few milliradians. This appears to be due to the reduction in signal acceptance angle and hence effectively to an increase in diffraction loss rather than to a reduction in beam overlap within the crystal. The one occasion on which non-collinear working of the OPO has been found useful was when the OPO was pumped by the far field of an unstable resonator laser without an isolator (19), in which case the slight vertical tilting of the OPO cavity prevented the 1.06 $\mu$m radiation reflected from the OPO mirrors re-entering the Nd:YAG oscillator and causing instability of the laser.

For collinear operation, both the output mirror and the 1.06 $\mu$m total reflector are required to be aligned exactly perpendicular to the pump beam. This is easily done by tracing the return path of the 1.06 $\mu$m beam, or in the case of a simple oscillator-amplifier pump configuration, by optimising the output of the free running laser cavity formed around the amplifier Nd:YAG rod by the OPO mirrors and the laser oscillator mirrors, with the isolator temporarily switched off.

For the grating to remain in perfect alignment with the rest of the cavity as it is tuned, the grooves of the grating must be angled so that they are exactly parallel to the axis of rotation of the grating, and perpendicular to the cavity axis. Only one adjustment is however provided for the grating. The grating and the 45° mirror must therefore be adjusted to obtain best tracking between the incident and reflected

beams. One method to do this is to align a 633nm helium-neon laser to the OPO output mirror (which has already been aligned to the Nd:YAG pump beam) and compare the horizontal angles of the second, third and fourth reflected orders of the 633nm beam from the grating as the grating, disconnected from its drive, is rotated.

Alignment is achieved by observation of the relative positions of these three orders as adjustments are made simultaneously to the grating and $45^{o}$ mirror angles, until all three reflections indicate good horizontal alignment. This procedure takes time and patience but is only required when the grating or the pump beam direction has been changed.

The second stage of alignment involves the setting of the stepper motors and the computer to a common starting point, so that dead reckoning can subsequently be used. In the case of the grating, this can be set by using one of the appropriate computer commands to independently rotate the grating to the position at which the 3rd order of the 633nm line of a helium-neon alignment laser is reflected, this corresponding to an OPO signal wavelength of 1.899 $\mu$m. The computer is informed of the wavelength setting of the grating by the use of an 'Origin' command. A similar procedure can be followed for initial setting of the $LiNbO_3$ and down-converter crystals, by rotating the crystals to their face normal angles and entering the corresponding frequency or wavelength, or an estimate if these are not known exactly.

## A1.2 Initial Operation of the OPO

With the alignment of the OPO carried out properly, little difficulty is usually encountered in obtaining efficient parametric oscillation with the OPO tuned to about 2$\mu$m and the pump intensity set to about 1.5J/cm$^2$. The most usual cause of no or weak oscillation is that the $LiNbO_3$ is slightly off angle, and this can be finely tuned by using an appropriate computer command. If such fine tuning of the $LiNbO_3$ improves the performance of the OPO, the computer requires to be informed of the corrected position of the $LiNbO_3$ crystal.

The output energy of the OPO can sometimes be enhanced by fine adjustment of the angle of the 1.06$\mu$m total reflector, so as to obtain exact phase-matching in both directions in the $LiNbO_3$. This mirror is the most critical of the OPO mirrors in terms of alignment. Some improvement can sometimes also be had by adjustment of the 45$^o$ mirror angle, but adjustment of the output mirror is likely to affect tuning and collinearity.

The alignment procedure outlined above will at best calibrate the OPO at 1.899$\mu$m to an accuracy of a few wavenumbers. A more accurate calibration can be obtained by tuning the OPO to correspond to an absorption line or optical filter of known frequency, and informing the computer of the exact frequency by the use of the 'Origin' command.

A1.3 Etalon Alignment

Initial installation of the etalon requires that the electrical zero, as determined by the computer, is set to be equivalent to normal incidence of the etalon. This is ideally also set close to the mechanical centre position of the galvanometer. This definition of the optical and electrical zero is required because of the square root relation between the etalon angle and detuning. The adjustment of the etalon zero angle can be made either on the drive amplifier, or by use of the appropriate computer command.

The second adjustment required of the galvanometer and drive is that of internal loop gain. The calculations in the lookup section of the computer program and the programs used to generate the tables assume a value of $2^{13}$ bits/radian of etalon angle. Basic measurement of the angle of the etalon against numerical drive can be used in setting the drive amplifier gain. More accurate setting of the gain can be achieved by tuning the OPO onto a narrow gas absorption line and noting the drive positions of the etalon, on both sides of face normal, for which different modes give an output corresponding in frequency to that of the absorption line. These values obtained can be compared with the expected values, and the percentage error noted and corrected.

When setting the OPO to a particular frequency or frequency range, the etalon usually requires to be fine tuned so that one of its modes is central to the frequency defined by the grating and $LiNbO_3$. Fine tuning of the etalon is achieved through computer commands which vary a frequency offset, used during calculation of the etalon angle. Establishing whether the OPO output is centred in frequency on one etalon mode, or spread between 2 modes, is not particularly simple, because the total OPO output varies in amplitude by less than 10% while the etalon is fine tuned from mode to mode. This change in amplitude is of the same order as the normal medium term power fluctuations in output, and is therefore difficult to identify.

One method of aligning the OPO etalon is to observe the spectral output of the OPO directly, using a detection system such as a scanning Fabry-Perot etalon or monochrometer with a fixed detector, while adjusting the etalon angle until a single mode output is obtained. An alternative, quicker method involves the tuning of the OPO (including the etalon) so that some of the output corresponds to a gas absorption line or narrow

band filter close to the centre of the required frequency range. The grating and $LiNbO_3$ crystal can then be tuned together using a special command which leaves the etalon angle fixed. The frequencies at which power is transferred to adjacent etalon modes and therefore away from the absorption line frequency can then be used to determine the correct frequency to which the grating and $LiNbO_3$ crystal should be set. If the OPO is to be used in the 1.9$\mu$m region, water vapour absorption in the atmosphere can be used to provide the absorption line, using the audible optoacoustic "tick" to determine the energy at the absorption lines frequency, providing there is little atmospheric absorption $3.5cm^{-1}$ either side of the absorption line used.

APPENDIX 2

## Computer Commands

Listed below are descriptions of the commands accepted by the tuning control minicomputer. The following abbreviations are used throughout:

| | |
|---|---|
| $\nu$ | Frequency (in $cm^{-1}$)<br>Usually, wavelength (in $\mu m$) is also accepted. |
| n | Integer (usually of either sign). |
| + + - - | The command is followed by a sequence of + and - signs. Each '+' increments the appropriate parameter by the stated amount, while each '-' similarly decrements it. |

## A MOTOR MOVE COMMANDS

In this group,

1 refers to the grating motor
2 refers to the $LiNbO_3$ motor
3 refers to the down-converter motor

| | | |
|---|---|---|
| MOVE1 | n ) | The appropriate motor is moved by the stated number of steps. Subsequent tuning commands are unaffected. |
| MOVE2 | n ) | |
| MOVE3 | n ) | |
| M1 | n ) | Shortened forms of above. |
| M2 | n ) | |
| M3 | n ) | |

| | | |
|---|---|---|
| IMOVE1 | n + + - - ) | Incremental move of specified motor by the stated number of steps for each + and -. |
| IMOVE2 | n + + - - ) | |
| IMOVE3 | n + + - - ) | |
| IM1 | n + + - - ) | Shortened form of above. |
| IM2 | n + + - - ) | |
| IM3 | n + + - - ) | |

## B TUNING COMMANDS

| | |
|---|---|
| SET $\nu$ | The motors and etalon are set to positions corresponding to the specified frequency. |
| SCAN $\nu_1$ $\nu_2$ $\nu_3$ | The OPO is set in frequency to $\nu_1$, then is incremented in frequency by $\nu_2$ every laser pulse (unless altered by WAIT command) until $\nu_3$ is exceeded. $\nu_2$ can be negative (reverse scan). |
| SC $\nu_1$ $\nu_2$ $\nu_3$ | Shortened form of scan. |
| RESCAN | Initiates a scan using the last defined values of $\nu_1$ $\nu_2$ $\nu_3$. |
| RE | Shortened form of RESCAN. |
| ISCAN $\nu$ + + - - | Incremental scan for rapid fine tuning. |
| IS $\nu$ + + - - | Shortened form of ISCAN. |
| SWITCH $\nu_1$ $\nu_2$ | Tunes the OPO alternatively to $\nu_1$ and $\nu_2$ on each laser pulse (unless modified by WAIT) |
| WAIT n | This determines the number of laser pulses for each point in a SCAN or SWITCH sequence. |

C ORIGIN COMMANDS

In this group

1 refers to the grating motor
2 refers to the $LiNbO_3$ motor
3 refers to the down-converter motor

ORIGIN1 ν )
ORIGIN2 ν )
ORIGIN3 ν )

These inform the computer of the frequency corresponding to the physical setting of the specified motor. This position is used as the reference for further tuning.

ORIG1 ν )
ORIG2 ν )
ORIG3 ν )

Shortened forms of above.

ORIGIN ν

This informs the computer of the frequency corresponding to the physical settings of the three stepper motors. These positions are used as the references for further tuning.

ORIG ν

Shortened form of above.

## D ETALON COMMANDS

| | |
|---|---|
| EBIAS n | Sets the etalon angle offset to a new value, and moves the etalon by an amount corresponding to this change. |
| FN | Sets the etalon to the nominal face normal angle (as defined by previous EBIAS command) |
| FBIAS $\nu$ | Sets the etalon frequency offset (in $cm^{-1}$) to a new value, and tunes the etalon by an amount corresponding to the change. |
| IFB $\nu$ + + - - | Incremental change in etalon frequency offset ($cm^{-1}$). The etalon is also moved by an amount corresponding to the change. |
| ISNE $\nu$ + + - - | Incremental scan with etalon angle fixed. The stepper motors are tuned as normal, but the etalon frequency offset is adjusted to maintain the etalon at a fixed angle. |

'E STATUS COMMANDS

| | |
|---|---|
| LOOKUP ↵ | Prints the motor and etalon positions corresponding to the specified frequency on the teletype. The motors remain static. |
| LOOK ↵ | Shortened form of above. |
| STATUS | Prints current frequency, motor positions and etalon parameters on the teletypewriter. |
| STAT | Shortened form of above. |
| PSTAT | Punches status information onto paper tape (for permanent storage). |
| RSTAT | Reads status information from paper tape. |

## F INPUT / OUTPUT COMMANDS

In this group

- m = 1 refers to the grating data table
- m = 2 refers to the $LiNbO_3$ data table
- m = 3 refers to the down-conv. data table
- m = 4 refers to the FSR data table
- m = 5 refers to the frequency offset data table
- m = 6 refers to the slope data table

| | |
|---|---|
| LIST $\nu_1$ $\nu_2$ | Lists all the table entries between $\nu_1$ and $\nu_2$ |
| LI $\nu_1$ $\nu_2$ | Shortened form of LIST. |
| CHANGE m $\nu$ | Allows examination and change of entry-table m at frequency $\nu$ . |
| OUTPUT m | Dumps table m onto paper tape. |
| INPUT m | Loads table m from paper tape. |

REFERENCES


1 J.A.Giordmaine, R.C.Miller, Physics Review Letters 14, p973 (1965)

2 R.W.Wallace, Applied Physics Letters 17, p497-499 (1970)

3 A.Ashkin et al, Applied Physics Letters 9, p72 (1966)

4 R.L.Byer, in Treatise in Quantum Electronics (H.Rabin, C.L.Tang, editors), Academic Press, New York (1975)

5 R.W.Wallace, IEEE Journal of Quantum Electronics 8, p819 (1972)

6 R.L.Byer, R.L.Herbst, R.S.Feigelson, Optics Communications 12, p427 (1975)

7 R.L.Herbst, R.N.Fleming, R.L.Byer, Applied Physics Letters 25, p520 (1974)

8 B.Luther-Davies, PhD Thesis, University of Southampton (1974)

9 R.A.Baumgartner, R.L.Byer, Journal of the Optical Society of America 17, p3555 (1978)

10 G.D.Tupper, PhD Thesis, University of Southampton (1980)

11 S.E.Harris, Procedings of the IEEE 57, p2096-2113 (1969)

12 R.L.Byer, in Nonlinear Optics (P.G.Harper, B.S.Wherret, editors) Academic Press, London (1977)

13 J.Falk, IEEE Journal of Quantum Electronics 7, p230 (1971)

14 D.C.Hanna, B.Luther-Davies, R.C.Smith, Optoelectronics 4, p249-256 (1972)

15 R.W.Wallace, Optics Communications 4, p316 (1971)

16 D.C.Hanna, B.Luther-Davies, R.C.Smith, R.Wyatt, Applied Physics Letters 25, p142-144 (1974)

17 R.Wyatt, unpublished

18 S.J.Brosnan, R.N.Fleming, R.L.Herbst, R.L.Byer, Applied Physics Letters 30, p330-332 (1977)

19 D.C.Hanna, L.C.Laycock, Optical and Quantum Electronics 11, p153-160 (1979)

20 L.B.Kreuzer, Applied Physics Letters 15, p263 (1969)

21 P.H.Sarkies, private communication

22 J.E.Bjorkholm, A.Ashkin, R.G.Smith, IEEE Journal of Quantum Electronics 6, p797 (1970)

23 M.V.Hobden, J.Warner, Physics Letters 22, p243 (1966)

24 D.F.Nelson, R.M.Mikulyak, Journal of Applied Physics 45, p3688 (1974)

25 D.A.Humphrys, undergraduate project, University of Southampton (1978)

26 D.C.Hanna, P.A.Karkkainer, R.Wyatt, Optical and Quantum Electronics 7, p115-119 (1974)

27 D.C.Hanna, A.J.Turner, Optical and Quantum Electronics 8, p213-217, (1976)

28 G.C.Bhar, PhD Thesis, University of Southampton (1973)

29 G.C.Bhar, D.C.Hanna, B.Luther-Davies, R.C.Smith, Optics Communications 6, p323-326 (1972)

30 B.Luther-Davies, R.C.Smith, R.Wyatt, Applied Physics 7, p215 (1975)

31 M.V.Hobden, Optoelectronics 1, p159 (1969)

32 R.Wyatt, A.J.Turner, R.C.Smith, to be published

33 L.W.Casperson, Applied Optics 14, p299-305 (1975)

34 D.J.Brassington, private communication

35 E.O.Amman, J.M.Yarborough, J.Falk, Journal of Applied Physics 42, p5618 (1971)

36 S.J.Brosnan, R.L.Byer, IEEE Journal of Quantum Electronics 15, p415-431 (1979)

37 A.J.Turner, unpublished

38 R.A.Baumgartner, R.L.Byer, IEEE Journal of Quantum Electronics 15, p432-444 (1979)

ACKNOWLEDGEMENTS

I would like to offer thanks to the many people who have helped during the course of this work. Included are my supervisor, Professor R.C.Smith, whose guidance and organisation of finance made the project possible, Dr D.C.Hanna, who supervised the early phases of the work, and Dr T.Wilmshurst, for his help during the initial stages of the computer side. Thanks also go to Dr R.Wyatt, who did many of the systematic measurements of OPO and pump performance, and to Mr G.Tupper, who is responsible for obtaining some of the spectra included in this thesis, and to Mr D Hearn and Mr C.Sawyers, both of whom helped for a period. The useful discussion and help given by other members of the Quantum Electronics Group and the technical staff of the Electronics Department is also acknowledged.

The project was financed by grants from the Science Research Council, by the Central Electricity Research Laboratories and by J K Lasers Ltd. Perkin-Elmer Ltd covered the cost of typing and copying this thesis.